

University of Bradford eThesis

This thesis is hosted in [Bradford Scholars](#) – The University of Bradford Open Access repository. Visit the repository for full metadata or to contact the repository team



© University of Bradford. This work is licenced for reuse under a [Creative Commons Licence](#).

DEVELOPMENT OF A CURRENT TO PRESSURE (I/P) CONVERTER

J.T.SANEECHARAUN

MPhil

2014

DEVELOPMENT OF A CURRENT TO PRESSURE (I/P) CONVERTER

System analysis of a current to pressure (I/P) converter through physical modelling and experimental investigation, leading to a design for improved linearity and temperature independence.

Jeet Tarik SANEECHARAUN

submitted for the degree
of Master of Philosophy

Department of Engineering, Design and Technology
University of Bradford

2014

Abstract

Current-to-pressure (I/P) converters are pneumatic devices which provide precise control of pressure in various industries – for example these devices are often used in valve positioner systems (typically found in the oil and gas industry) and tensioning systems (typically used in the packaging industry). With an increasing demand for such devices to operate in harsh environments all by delivering acceptable performance means that Current-to-pressure converters need to be carefully designed such that environmental factors have no or minimal effects on its performance. This work presents an investigation of the principles of operation of an existing I/P converter through mathematical modelling. A simulation model has been created and which allows prediction of performance of the I/P converter. This tool has been used to identify areas of poor performances through theoretical analysis and consequently led to optimisation of certain areas of the I/P converter through a design change to deliver improved performances, for instance the average percentage shift in gain at 1mA input signal (over the temperature range of -40°C to 85°C) on the new I/P converter is 2.13% compared to the average gain of 4.24% on the existing I/P converter, which represents an improvement of almost two fold. Experimental tests on prototypes have been carried out and tests results showed that improved linearity and temperature sensitivity can be expected from the new design.

Keywords: Current to Pressure converter (I/P converter), modelling and simulation, electromagnetic, compressible flows, heat transfer, non-linearity, temperature sensitivity, vibration sensitivity, balance beam

Acknowledgements

I would like to thank Dr. Peter Olley for providing supervision and support throughout this project. I would like to thank Dave Thompson and Marc Robertson for providing support and motivation.

Thanks also go to Professor Andrew Day, John Clayton, Andrew Spivey, Melanie Powell, IMI Norgren and the TSB for facilitating the Knowledge Transfer Partnership (KTP008693).

Special thanks go to my parents and brother for their unconditional support and encouragement.

Table of Contents

Abstract.....	i
Acknowledgements.....	ii
Table of contents.....	iii
Nomenclature.....	vi
1. INTRODUCTION.....	1
1.1. Background.....	1
1.2. Aims and Objectives	3
1.3. Outline of Thesis.....	3
2. LITERATURE REVIEW	6
2.1. Power Transmission and Pneumatic Controllers	6
2.2. Actuators.....	9
2.3. Regulators, valve control devices and Current-to-Pressure converters.....	10
2.3.1. Types of I/P converters	11
2.4. Electronic Feedback	16
2.5. General Physics applied in electropneumatics	17
2.5.1. Electromagnetics.....	17
2.5.2. Permanent magnets	19
2.5.3. Fluid Dynamics.....	22
2.5.4. Compressible and Incompressible flows	24
2.5.5. Laminar, turbulent flow and Reynolds' number	25
2.5.6. Coefficient of Discharge	25
2.5.7. Thermodynamics.....	26
2.5.8. Heat Transfer	27
2.6. Modelling and Simulation.....	28
3. INVESTIGATION OF THE OPERATION OF THE TR140 I/P CONVERTER	31
3.1. Introduction	31
3.2. The System and its components.....	31
3.3. Interaction of forces	37
3.4. Operating Mode	40
3.4.1. Flow to the system with no electrical power	40

3.4.2.	Flow to the system with electrical power on	40
3.4.3.	Steady state	41
3.5.	Temperature cycles	41
4.	DETERMINATION OF PARAMETERS	43
4.1.	Introduction	43
4.2.	Determination of parameters	43
4.2.1.	Stiffness of the flexure	43
4.2.2.	Coil Strength and magnet strength.....	51
4.2.3.	Magnet	54
4.2.4.	Movement of Rubber diaphragm with Control spring	55
4.2.5.	Volumes measurement	58
4.2.6.	Coefficient of discharge and other dimensions.....	60
4.2.7.	Nozzle Diameter.....	61
4.2.8.	Effective circumference of pintle valve opening ('a' used in simulation)	61
4.2.9.	Area of hole in orifice disc ('Ah' used in simulation)	62
4.2.10.	Distance pintle valve can travel ('x' used in simulation)	62
5.	MODELLING AND SIMULATION.....	63
5.1.	Introduction	63
5.2.	Initial modelling of flow.....	63
5.2.1.	Net mass flow-rate into the Booster chamber	63
5.2.2.	Net mass flow-rate into the Control chamber & through the nozzle-flexure gap	65
5.2.3.	Opening of the flexure-nozzle gap.....	66
5.3.	Initial simulation results.....	67
5.4.	Modelling of flow – Compressible flow effects	68
5.5.	Modelling of thermal effects	70
5.5.1.	Heat transfer due to compressible effects and convection	70
5.5.2.	Heat transfer through conduction	72
5.6.	Simulation of complete model with compressible effects and heat transfer	75
6.	IDENTIFICATION OF CAUSES OF UNWANTED VARIATION	83
6.1.	Introduction	83
6.2.	Non-linearity at Low current & variation with temperature change..	83

6.3.	Theoretical explanation of pressure variations.....	90
6.4.	Orientation and Vibration effects.....	93
6.5.	Summary	95
7.	OPTIMISATION.....	96
7.1.	Introduction	96
7.2.	Potential improvements	96
7.3.	Mechanical compensator – New Flexure Design.....	100
7.4.	Balance Beam	101
7.4.1.	Design and Component sizing	103
7.4.2.	Prototype I.....	106
7.4.3.	Prototype II.....	109
7.4.4.	Prototype III.....	115
7.5.	Testing and performance comparison.....	116
7.5.1.	Testing to investigate the overall gain of the I/P converters ...	117
7.5.2.	Temperature variation	119
7.5.3.	Vibration test	121
7.6.	Summary	124
7.7.	Discussion	126
8.	CONCLUSION AND RECOMMENDATION	130
8.1.	Conclusion.....	130
8.2.	Recommendations for further work.....	132
	Appendix I – Coil drawing	135
	Appendix II – Initial Matlab simulation model	136
	Appendix III – Heat transfer by conduction	140
	REFERENCES	141

Nomenclature

<i>Symbol</i>	<i>Definition</i>
A_{ij}	Area of component i in contact with component j
d	Measured electromagnetic force from coil in magnet assembly
F_e	Electromagnetic force
F_f	Fluidic force
F_x	Elastic force
h	Overall heat coefficient
k	Thermal conductivity
P_b	Booster chamber pressure
P_c	Control chamber pressure
q	Heat current
Q	Heat energy transfer
Q_i	Initial heat energy
Q_{inew}	New heat energy
Q_j	Heat energy transferred from preceding compartment
r_{eff}	Effective radius of nozzle
T_a	Temperature of atmosphere
T_b	Temperature of booster chamber
T_c	Temperature of control chamber
T_g	Temperature of flexure
T_i	Initial temperature in compartment
T_{inew}	New temperature in compartment
T_j	Temperature in preceding compartment
T_n	Temperature of component
V_b	Volume of booster chamber
V_c	Volume of control chamber

x_0	<i>Gap between flexure and nozzle</i>
ρ	<i>Density</i>
$\frac{dT_i}{dt}$	<i>Rate of change of temperature of component i</i>
$\left. \frac{dT_i}{dt} \right _{HT}$	<i>Rate of change of temperature of component i due to heat conduction</i>
$\frac{dT}{dx}$	<i>Temperature gradient</i>
ΔP	<i>Pressure difference</i>
ΔT	<i>Temperature difference</i>
ΔT_{ij}	<i>Temperature difference between component i and j</i>
Δt	<i>Time difference</i>

1. INTRODUCTION

This chapter presents the main concepts of Watson Smith's current-to-Pressure converters and highlights the importance of such devices in the control industry. The motivations for this research work are also described, followed by the aims and objectives. The final part contains the outline of the thesis.

1.1. Background

Current-to-Pressure converters (I/P converters) are high precision devices which are commonly used in pneumatic systems to control pressure. Current-to-Pressure converters are also referred to as electro-pneumatic converters. They use a low current supply, generally between 4 to 20mA as input and the standard output pressure ranges between 3 to 15psi gauge. The relation of input signal to output signal tends to be linearly proportional. Such devices are used in various industries ranging from oil and gas to industrial process control. In many applications, I/P converters are subjected to operate in harsh environments such as extreme temperatures, corrosive atmospheres or even in places where there is constant vibration. Most of these environmental factors will have an effect on the performance of the I/P converters and, potentially, any weak performance of the I/P converter could result in failure in subsequent systems and/or components. Hence it is desirable that I/P converters deliver reliable performance even under the influence of varying environmental factors (within specified criteria).

Watson Smith, part of IMI Norgren, has specialised in the manufacture of I/P converters since the early 1980s. There are various types of I/P converters which are marketed by the company, however all of these are based around a core technology – the voice-coil system, which principally consists of a flexure, nozzle, coil and permanent magnet. This technology was patented by Dave Carey in 1999 [1]. The following figure shows the common components used in Watson Smith I/P converters.

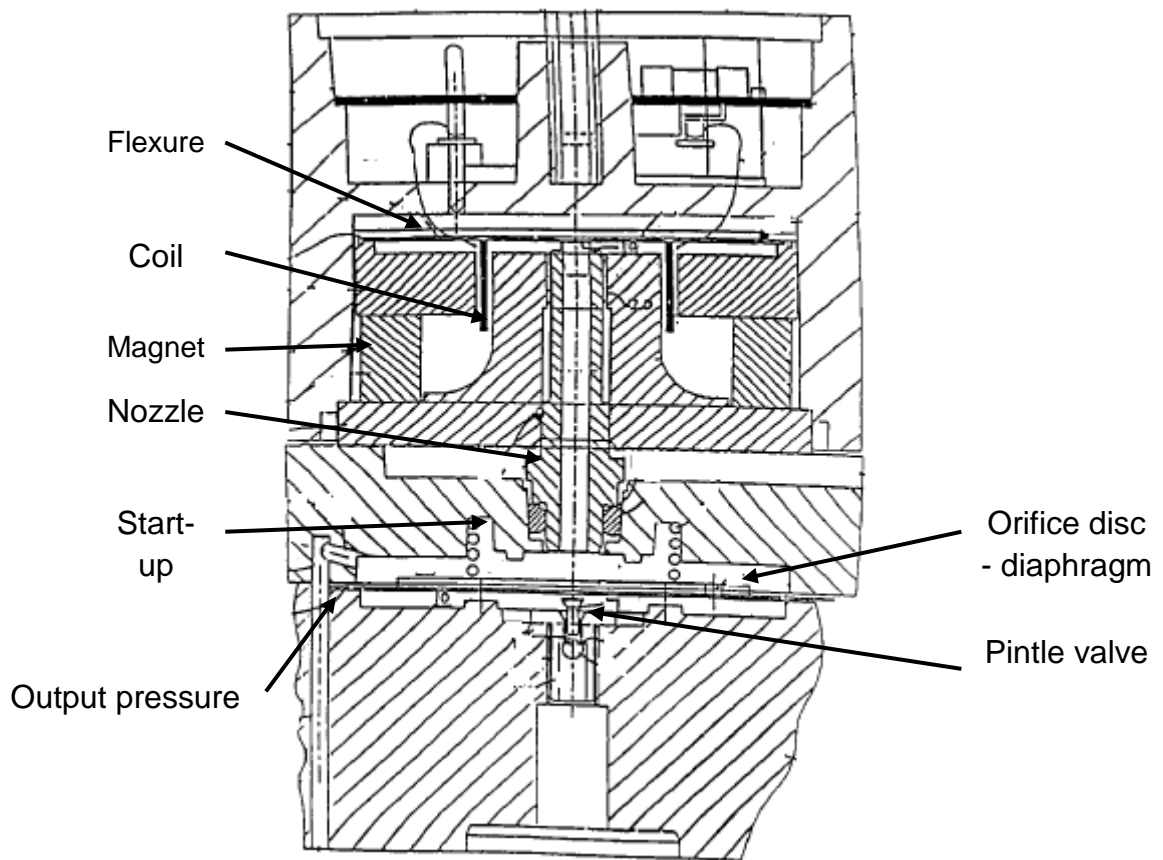


Figure 1-1: Common components in a Watson Smith I/P converter [1]

This current technology is known to be broadly reliable but to give inadequate and often unpredictable performance under certain conditions; 1) through temperature change tests, it was found that the output pressures tend to shift in an unpredictable manner, especially the zero current output pressures; 2) at low current inputs, there is a non-linear behaviour of the output pressure with respect to input signal; 3) under vibrations, the output pressure of the I/P converter is affected – through tests carried out, it was

found that a frequency between 200-250Hz at a 2g acceleration causes a major drop in output pressure; 4) under orientation conditions, the output pressure from the I/P converter varies quite significantly – for a 180° rotation (single plane) the output pressure can vary by 150mbar [2].

1.2. Aims and Objectives

The main aims of this work were to develop a better understanding of the principles of operation of the existing technology and to develop an optimised design for the I/P converter which will have better performance in the following areas: *linearity at low current, thermal stability, vibration stability and orientation stability.*

To achieve these aims the following objectives were set:

- Investigation of principles of operation of existing I/P converter through mathematical modeling and experiment
- Development and verification of a detailed simulation which should allow the prediction of performance of the I/P converter
- Identification of the root causes of poor performance
- Optimisation of the system to improve on the identified poor performances
- Verification and validation of optimized design through prototyping and testing

1.3. Outline of Thesis

This thesis is structured as follows:

Chapter 2 (Literature review) contains a brief evaluation of the types of power transmission systems and it introduces actuating systems. An extensive review of different types of technology used in I/P converters was carried out followed by a presentation of general physics commonly present in I/P converters (e.g. electromagnetism, fluid dynamics and heat transfer). The final part of this chapter is focused on modelling and simulation methods.

Chapter 3 (Investigation of the operation of the TR140 I/P converter) introduces the product which this work will be focused on. The interactions of components under normal operation are described and the governing forces and how they relate to the output pressure of the I/P converter were derived.

Chapter 4 (Determination of parameters) contains the various experimental investigations carried out to determine the values of key parameters such as stiffness of flexure, magnetic forces and volumes of chambers in the I/P converter.

Chapter 5 (Modelling and simulation) presents the mathematical representation of components within the I/P converter. An initial modelling and simulation of the overall system was carried out – this simulation contains a wide range of general physics. A more advanced simulation was then developed, whereby flow compressibility and heat transfer were also included.

In chapter 6 (Identification of root causes of problems) the observed non-linearity at low currents, pressure variations with temperature and orientation sensitivity of the I/P converter were investigated. A theoretical explanation is presented and it is shown that very good correlation exists between theoretical values and experimental values.

Chapter 7 (Optimisation) presents a number of potential changes which could be made to existing components. Following a SWOT analysis it was found that changing any one parameter would improve performance in a certain area to the detriment of performance in another area. Unless (for example) a lower gain is acceptable, in which case a larger nozzle would give improved linearity and thermal stability. This chapter also presents the balance beam technology and how it allows meeting the desired performance of the controlled pressure (P_c) – this is discussed in more detail in a later section of this report. Furthermore, experimental investigations to evaluate the performance of the prototypes were carried out in a later section of this chapter. The final section is focused on the comparison of

performance of the balance beam I/P converter with the original I/P converter.

Chapter 8 (Discussion, Conclusion and Recommendation for further work) – this chapter contains a review of the main findings in this thesis; especially the results and conclusions obtained from tests carried out on the prototypes.

2. LITERATURE REVIEW

This chapter contains a review of power transmission techniques, actuators and especially I/P converters. A review of general physics ideas which are often applied in electropneumatics; including electromagnetics, fluid dynamics and thermodynamics has been carried out. The last section of this chapter is focused on modelling and simulation techniques.

2.1. Power Transmission and Pneumatic Controllers

There are various types of power transmission systems which can be used to control and to actuate overall systems. Mechanical power transmission systems often rely on devices such as shafts, universal joints, belts and chains to transmit energy. In general the energy transfer is from one form into another, for example potential energy is transferred into kinetic energy. The best-in-class of actuator types can be measured as the one which transfers the energies in the most efficient way possible although for many applications size or safety are of greater importance. Fluid power systems (hydraulic and pneumatic) are recognized for their flexibility and control although they are less energy efficient than electrical systems [3]. The following table provides a comparison of electrical, hydraulic and pneumatic systems.

	Electrical	Hydraulic	Pneumatic
Energy source	Usually from outside supply or battery	Electric motor or diesel driven	Electric motor or diesel driven
Energy storage	Limited (batteries)	Limited (accumulator)	Good (reservoir)
Distribution system	Excellent, with minimal loss	Limited, basically a local facility	Good, can be treated as a plant wide service
Energy cost	Lowest	Medium	Highest
Rotary actuators	AC and DC motors Good control on DC motors, AC motors cheap	Low speed good control; can be stalled	Wide speed range; accurate speed control is difficult
Linear actuator	Short motion via solenoid, otherwise via mechanical conversion	Cylinders; very high force	Cylinders; medium force
Controllable force	Possible with solenoid and DC motors Complicated by need for cooling	Controllable, high force	Controllable medium force
Points to note	Danger from electric shock	Leakage dangerous and unsightly; fire hazard	Noise

Table 2-1: Comparison of electrical, hydraulic and pneumatic systems [4]

Pneumatic controllers use variable air pressure as an input signal to operate in an automatic manner. Generally, pneumatic controllers are design to provide output pressures within the range of 0.2 to 1.0 bar (3 to 15 psig). They tend to be very reliable and offer good performance when operated on clean, dry plant air. However, when operated on a poor quality air supply (unclean or not dry) the performance of pneumatic controllers is downgraded [5,6].

Development of pneumatic control elements was reported as early as the 1930s and it was only in the early 1940s that pneumatic controllers were first available [1]. Pre 1940, the main method of design control systems was by trial-and-error, but soon after that period, with advances in mathematical and analytical methods, development in the field of control engineering was much improved due to the use of feedback control and time domain in applications such as telephone system and radar antenna control systems [7,8,9,10,11,12].

There is a lack of flexibility from pneumatic controllers when compared to modern electronic controller designs – an electronic controller offers a wider range of adjustability, control algorithms, better communication links to the control system and additional features/ services. The performance of pneumatic systems is often affected by a time delay which is generally induced by capacitance due to the size of tubing [1].

Pneumatic controllers continue to be used in areas where it would be hazardous to use electronic equipment, such as environments with flammable or explosive atmospheres or other locations where compressed air is available but where access to electrical services is limited or restricted [1].

2.2. Actuators

An actuator can be defined as a device or a mechanism which provides driving force and motion in a controllable manner. Naturally occurring actuators include muscles of animals and plants, whilst man-made actuators can be classified under two main categories: mechanical and solid state. Actuators which are based around shape changing materials (e.g. shape memory alloys, piezoelectric) are increasingly used in novel applications. The following figure shows the various types of actuators under set categories [13].

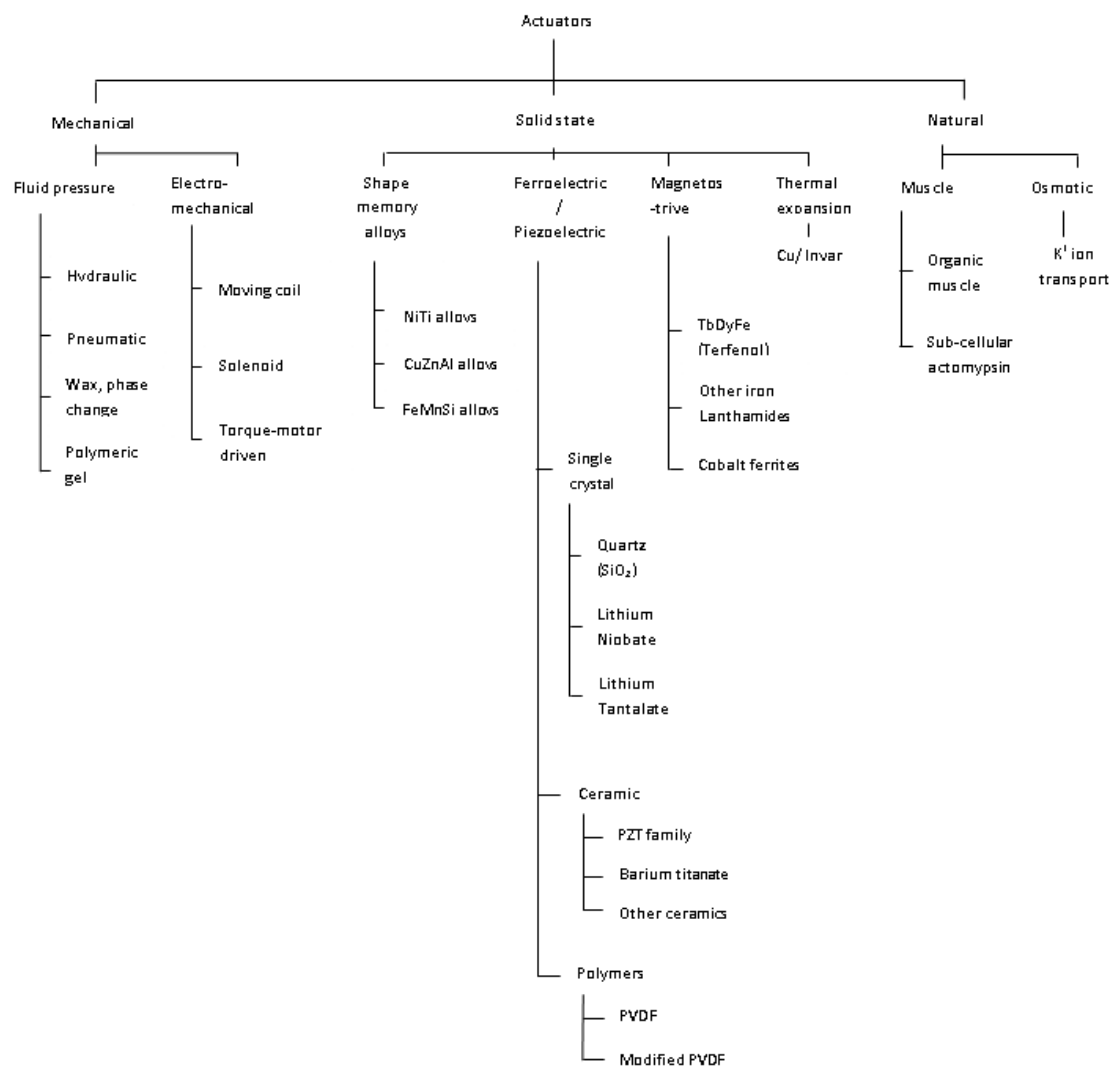


Figure 2-1: Hierachy of actuators [13]

Pneumatic actuators are very popular in industrial applications for their ease of maintenance, fast action, installation flexibility and relatively low cost. The

speed of hydraulic actuators is much lower than pneumatic actuators due to the viscous nature of the fluid typically used in hydraulic systems [14,15].

Use of piezoelectric actuators varies from positioning devices such as reading heads in compact disc players, adjustable aerodynamic surfaces [16] and vibration damping [17]. Shape memory alloys are normally used in applications where there is a requirement for a single contracting stroke, e.g. pipe couplings [13].

2.3. Regulators, valve control devices and Current-to-Pressure converters

A regulator is a device which allows maintenance of process output at a constant level despite the presence of disturbances in the load flow. These are very important devices in the process industry; they can be used to control pressure, temperature, flow and other process variables. Regulators usually have a fast dynamic response and sophisticated systems can include sensor, controller and final control elements in a single device (such a system can allow for fast corrective actions) [5].

Valve control devices are mechanisms which are mounted on a control valve and these provide interface platforms for input signals, monitoring functions and changing position or response of the valve [5]. Typical valve control devices are traditional valves, positioners, electropneumatic converters (Current-to-Pressure converters), limit switches, booster relays and manual actuator overrides. These devices ensure that the performances of the control valves help to meet stringent specifications which are present in some industrial applications [5,18,19].

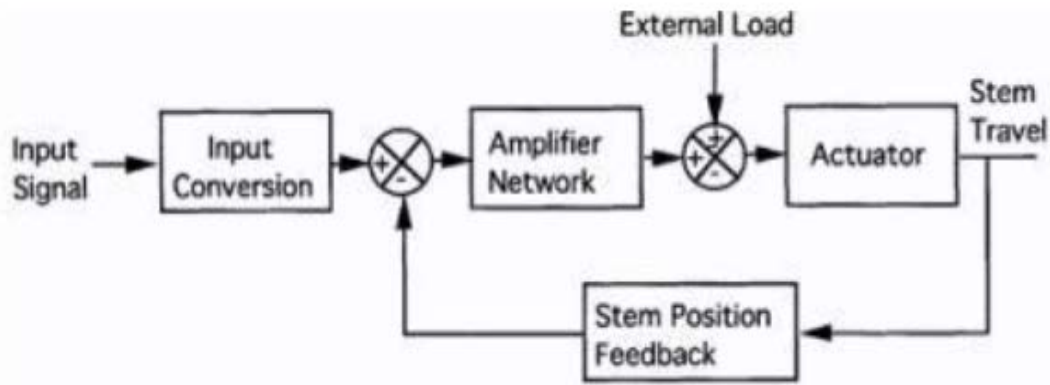


Figure 2-2: Generic block diagram representing a positioner/ actuator system with feedback control [5]

Current-to-Pressure (I/P) converters are devices which convert an electrical input signal (normally currents between 4mA and 20mA) to a proportional pneumatic output signal [20]. Generally the pneumatic output is between 3 to 15psig (0.2 – 1.0bar g) although 6- to 30psig versions can be obtained [5, 18]. Current-to-pressure converters are also referred to as I/P transducers or electropneumatic converters.

The output from an I/P converter is often used to actuate a piston or diaphragm, which in turn directs a valve. I/P converters can provide precise and fast control. Current-to-Pressure devices must be able to provide adequate performance under various operating conditions which are often encountered in industrial or process applications and these include vibration, dirty air supply, extreme temperatures and corrosion [15, 21].

2.3.1. Types of I/P converters

Since the mid-1960s, the most common type of technology which has been used in current-to-pressure converters is based around the flapper-nozzle concept. In the late 1980s, new technologies were introduced by manufacturers in an attempt to address the weaknesses around the traditional flapper-nozzle design [18]. The following diagram illustrates a traditional flapper-nozzle concept.

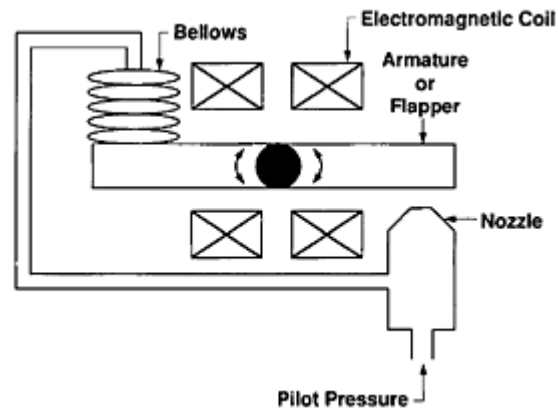


Figure 2-3: Traditional flapper - nozzle design [22]

The flapper is made to move between a set region when an input current (4 to 20mA) is applied to the coil and by doing so, the gap between the flapper and the nozzle consequently controls how much air can flow through. By restricting the flow, a backpressure is created (also known as pilot pressure) in the nozzle. To help balance the forces on the armature-flapper, a bellows is used. The pilot pressure is usually used to control other mechanisms, e.g. a pneumatic booster or relay [18,22].

This traditional arrangement of flapper-nozzle is known to be affected by environmental factors like external vibration, temperature changes or aging of the magnetic coil. Hence there is often a requirement for periodic calibrations of the I/P converters in order to maintain the performance within acceptable range [18].

The following diagram shows variation of the flapper-nozzle arrangement.

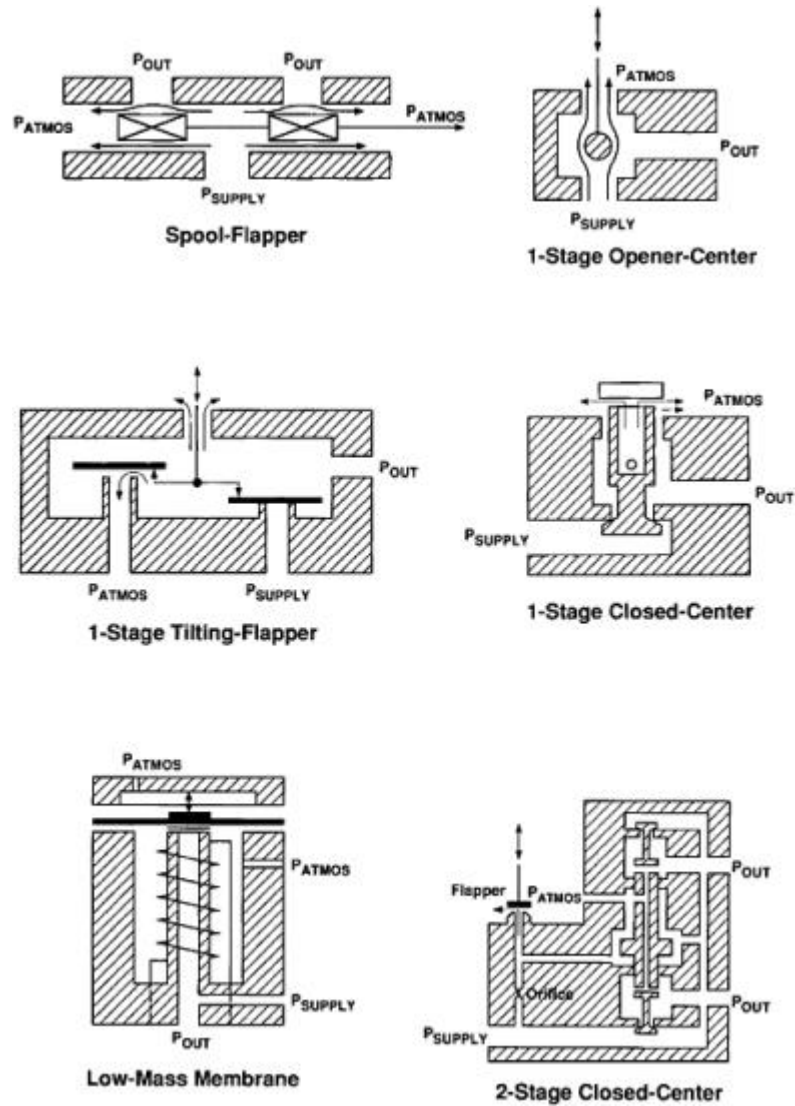


Figure 2-4: Variation in flapper nozzle arrangement [22]

2.3.1.1. Piezoceramic Bender-Nozzle

In this device, there is no coil or electromagnet used to move the flapper – the flapper is made to bend when a voltage is applied across its layer. Generally a voltage in the range of 20 to 30 V DC is required and this means that the standard 4- to 20-mA needs to be converted into a voltage. Figure 2-5 shows the main components in a piezoceramic bender nozzle device [18,23].

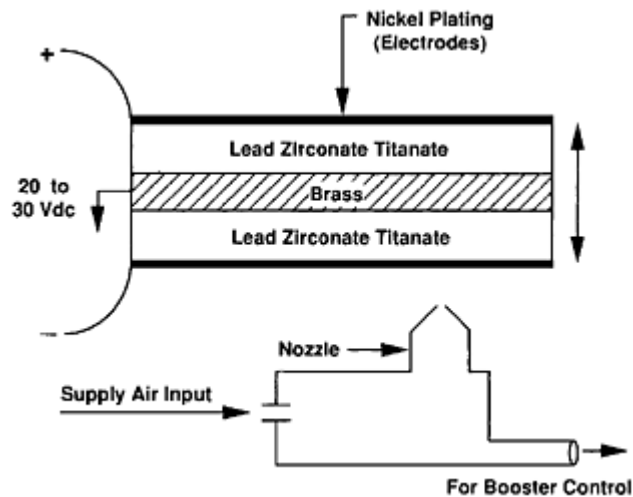


Figure 2-5: Piezoceramic bender nozzle arrangement [22]

The piezoceramic bender suffers from poor repeatability when it comes to positioning for the same input signal, this error can be compensated by combining an electronic feedback sensor [18]. The inherent hysteresis characteristics of piezoactuators can impact on the accuracy in pressure control devices [23].

2.3.1.2. Deflector bar design

In this configuration, a deflector bar is used as the main moving component in the system rather than a flapper; this is shown in the following diagram. A Coanda effect is generated by the deflector bar – this effect can be defined as the tendency of a fluid stream to attach itself to a surface with which it makes oblique contact. It uses two nozzles; one which guides the high-velocity fluid stream and the other one (spaced at a set distance) which recaptures the fluid stream. The deflector bar is susceptible to vibration stability since it is of low mass [18,22].

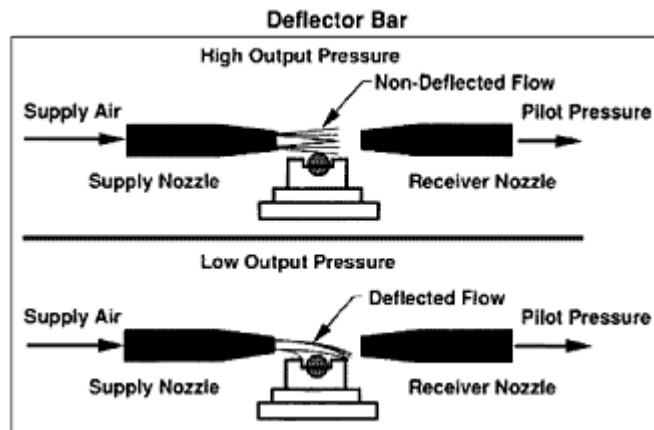


Figure 2-6: Deflector bar concept [18]

2.3.1.3. Electrostrictive element

This concept is quite similar to the piezoceramic bender design, except that a bimorph-type electrostrictive element is used as the moving component [24]. The bimorph plate deflects proportionally to the applied voltage [25].

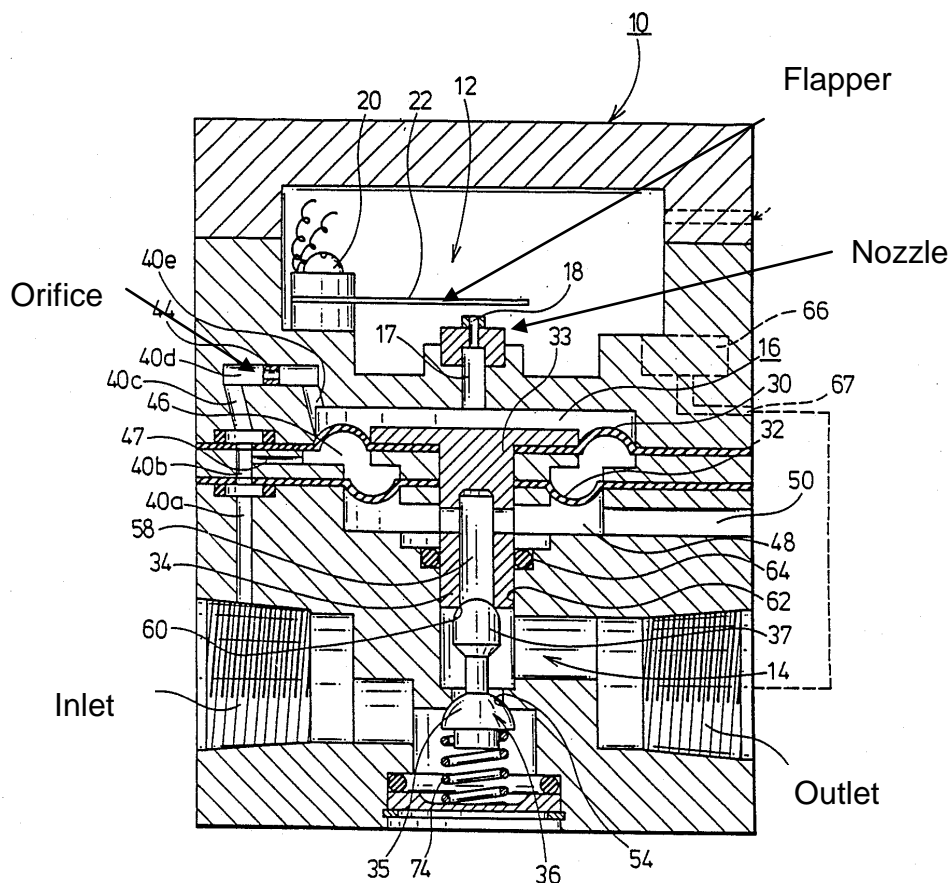


Figure 2-7: Bimorph electroresistive element used in the flapper-nozzle electropneumatic device [24]

2.3.1.4. Pivotal beam – Torque system

This system consists of two telescopic coils attached onto the two opposing ends of a 'Z-shaped' beam. At one end of the beam is located the nozzle which provides the path for the fluid, the beam is mounted onto a flexural pivot about its centre. When the fluid flows from the nozzle a torque is created on the beam, by passing a current through the coils, this torque is counteracted and the gap between the nozzle and the beam is altered accordingly, thus resulting in a back pressure. This pressure is claimed to be proportional to the electrical current supplied [26].

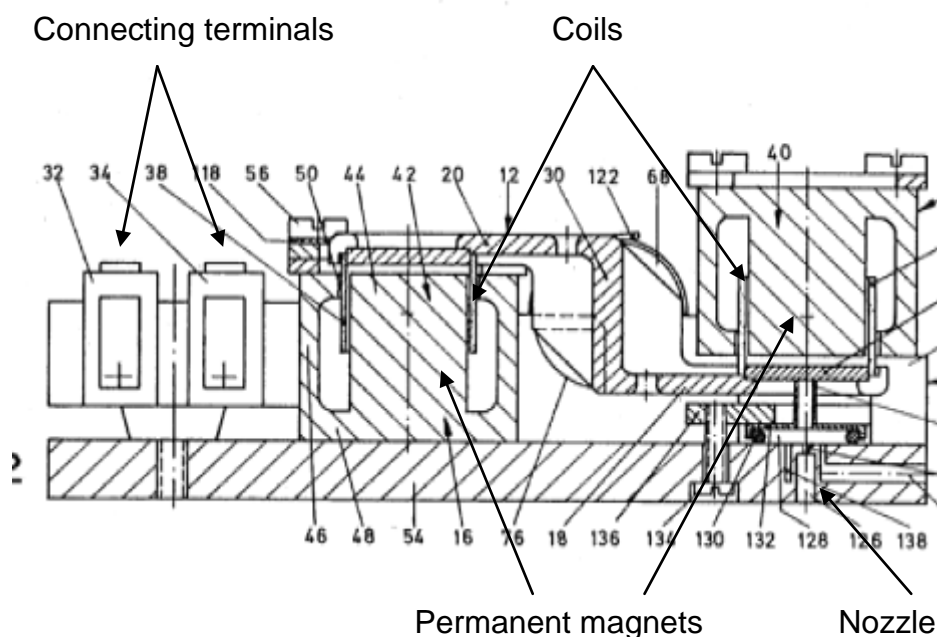


Figure 2-8: Z-shape flapper nozzle with two coils system [26]

2.4. Electronic Feedback

Many current-to-pressure converters have incorporated pressure sensors and electronic feedback control since the late 1980s. The electronic feedback circuit corrects for any error in the system; this is achieved by comparison of the output sensor signal with the input signal and the electronics then adjust the current signal accordingly to get the required output in pressure [18]. Figure 2-9 shows the schematic of a feedback control in an I/P converter.

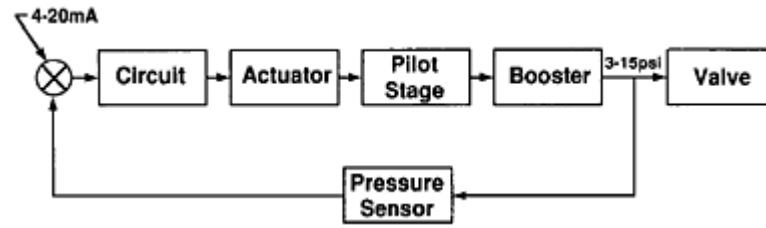


Figure 2-9: Electronic feedback control in an I/P converter [18]

Electronic feedback control has brought several advantages to the performance of I/P converters, namely vibration immunity, calibration stability, repeatability, quick dynamic response and reduced downtime [18]. It should be noted that the accuracy of the overall device is limited by the accuracy of the pressure sensor, which is often not very high for low power sensors.

2.5. General Physics applied in electropneumatics

2.5.1. Electromagnetics

One of the most commonly used methods of energy conversion for electromechanical actuators is electromagnetic force. The main reason for utilising magnetic fields rather than electric fields is due to the higher energy density in magnetic fields. There is an air gap which separates the stationary component and the moving component within the system, this air gap is where the electromechanical energy conversion takes place. The magnitude of energy per unit volume of air gap in a magnetic field can be five times more than in an electric field [28].

The main physical laws which govern electromagnetic forces and electromagnetic induction are Lorentz's law and Faraday's law.

Lorentz's law of electromagnetic forces states that when a current carrying conductor is placed in a magnetic field, it will experience an induced force. This force can be expressed as:

$$\vec{F} = \vec{i} \times \vec{B} \quad (2-1)$$

Where \vec{F} is the electromagnetic force vector per unit length, \vec{i} is the current vector and \vec{B} is the magnetic flux density vector.

For a current carrying conductor of length, L (as shown in Figure 2-10-10), the electromagnetic force can be written as:

$$F = BiL \quad (2-2)$$

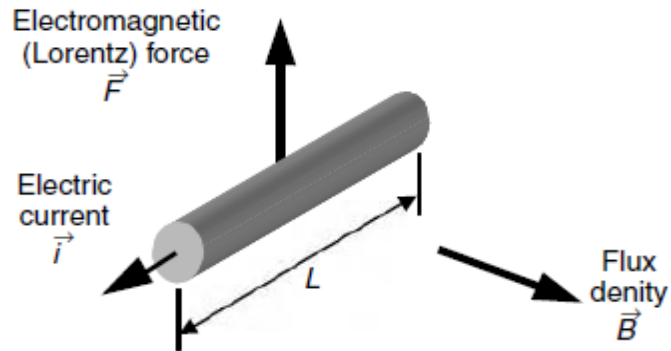


Figure 2-10: Force on a current carrying conductor [28]

Magnetic field strength and magnetic field density are related by the permeability of the material or medium through which the field is made to pass through, in a vacuum the magnetic flux density is directly proportional to the magnetic field strength and is expressed by the following equation [27]:

$$B = \mu_o H \quad (2-3)$$

Where B is the magnetic flux density measured in Tesla (T), μ_o is the permeability constant and H is magnetic field strength measured in A/m.

A helical coil (solenoid) with N turns will induce a magnetic field when a current is passed through. The induced magnetic field across a typical solenoid is illustrated in Figure 2-11.

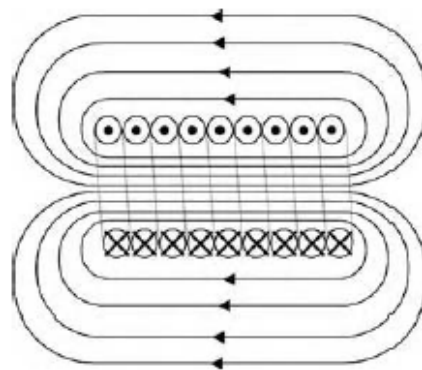


Figure 2-11: Induced magnetic field across a coil/ solenoid [28]

The flux density inside the coil can be approximated as follows:

$$B = \mu \frac{N}{L} i \quad (2-4)$$

Where μ is the magnetic permeability of the material inside the coil, i is the current flowing through the coil and N is the number of turns of the coil.

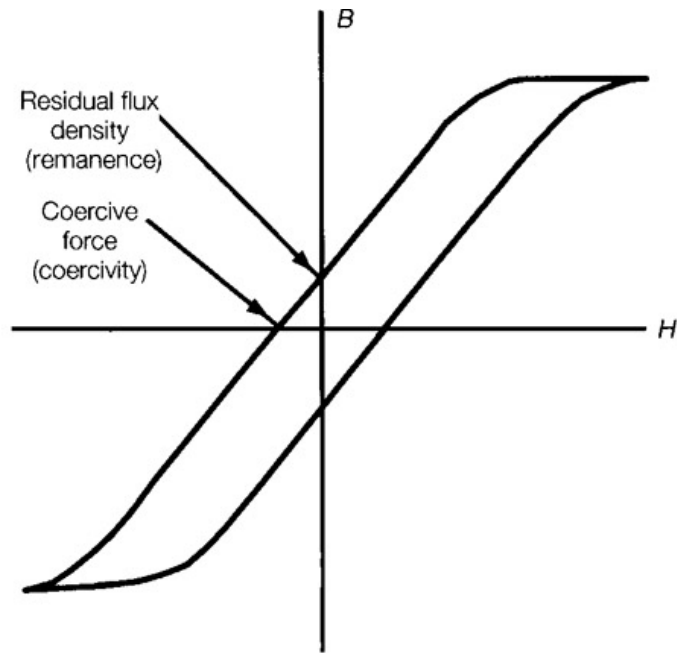
Solenoids can be considered as the simplest electromagnetic actuators which are used in linear and rotary actuations commonly found in valves, switches and relays. Voice-coil motors (VCMs) consist of a moving coil (often in an air gap) and a permanent magnet which generates a magnetic field in the gap. When a current is made to pass through the coil, the coil experiences an electromagnetic force as described by Lorentz's law [27, 28].

$$F_{vcm} = BiLN \quad (2-5)$$

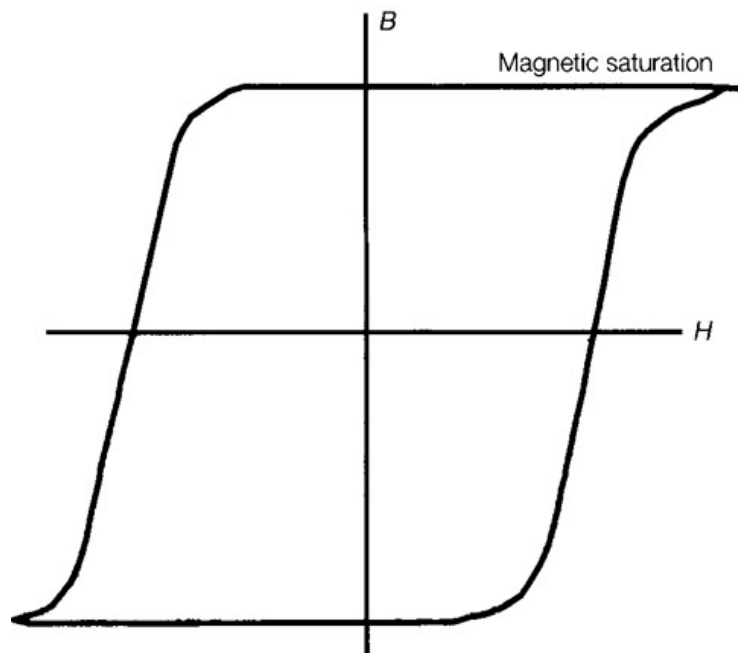
The force (F_{vcm}) is proportional to the applied current (i). This force depends on the flux density and the amount of wires in the gap. This force can be increased in magnitude by increasing the flux density (by using a stronger magnetic material) or by coil size (number of turns and/or using larger diameter coil, thus increasing the total length of wire). It should be noted that using thinner wire for the coil will allow to pack more turns in the air gap, however thinner wires have larger resistance and this limits the allowable current [27].

2.5.2. Permanent magnets

A permanent magnet is a material which can retain its magnetism indefinitely when subjected to magnetisation. Permanent magnets are commonly used in sensing devices and speakers [29]. Different types of magnetic material respond differently to being magnetised – some easily retain their magnetism while others are difficult to magnetise. A way to examine the properties of magnetic materials is measure the flux density (B) of the material with increasing and decreasing values of magnetic field strength (H). The following graphs show the relationship of these two measures and this characteristic is often referred to as the magnetic hysteresis loop.



(a)



(b)

Figure 2-12: Magnetic hysteresis loops of a) an electromagnetic material, (b) permanent magnetic material [30]

The observed hysteresis effect causes the magnetic material to preserve some of its magnetism after the magnetic field strength has been removed. Then flux density (B) when the magnetic field strength (H) is zero is known

as the *residual flux density*. Applying a negative magnetic field strength ($-H$) can reduce the residual flux density to zero and this demagnetising force is known as *coercive force* [30].

Hard ferrite and rare-earth magnets can generate high flux densities which are comparable to when they were initially magnetised. The following table shows a list of permanent magnets with their typical properties and approximate year of development [31].

Type	Residual flux density B_r (T)	Approximate year of development
Carbon steel (quenched)	0.9	1600
Cobalt steel (quenched)	0.96	1916
Alnico3	0.68	1931
Alnico5	1.03	1948
Ceramic5 (ferrite)	0.38	1952
Ceramic8 (ferrite)	0.39	1955
Samarium cobalt	0.88	1970
Neodymium iron (early)	1.08	1990
Neodymium iron (latest)	1.43	2004

Table 2-2: Types of permanent magnets with corresponding properties and approximate year of development

2.5.3. Fluid Dynamics

Since the principle medium used in a pneumatic system is compressed air, it is essential to understand the characteristics of this fluid and the gas laws which are related are discussed in this section.

Air (clean and dry) is a mixture of approximately 78% nitrogen, 21% oxygen and the remaining 1% is made up with of small quantities of an additional 14 gases. Typically in pneumatic systems, the opening of valves causes air to expand according to one of the gas laws, depending on the rate of expansion and temperature conditions [32]. The ideal gas law is the basic law for gas equations and is often expressed in the following form [33]:

$$PV = nRT \quad (2-6)$$

Where P is the pressure of the gas (Pa), V is the volume of the gas (m^3), n is the number of moles of gas present, R is the universal gas constant and T is the temperature of the gas (K).

There are different types of forces which control the behaviour of fluids and not every type of force is involved in every problem, the following lists are the possible types of forces involved [34]:

- Pressure forces, which can be described as the forces due to piezometric pressure (arising due to difference of piezometric pressure between different points in a fluid)
- Forces resulting from the action of viscosity
- External forces acting on the fluid, e.g. gravity
- Forces due to surface tension
- Elastic forces due to compressibility of the fluid

For the purpose of this thesis, a brief review of forces resulting from action of viscosity and elastic forces in fluid will be carried out. These are considered to be significant in the electropneumatic system under study.

Viscosity can be described as a measure of resistance to the deformation rate of a fluid when it is subjected to a shearing force [35]. The following

figure illustrates the concept of continuous deformation of fluid when subjected to a shear stress.

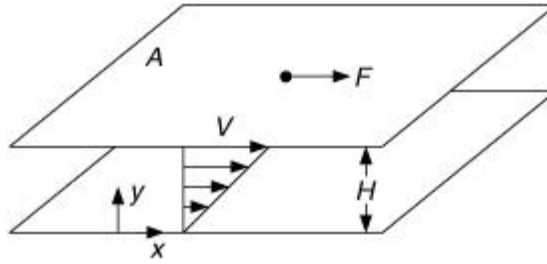


Figure 2-13: Shear stress causing deformation in a fluid [5]

In the above figure, two large parallel plates of area A bound a fluid over a small distance H . Keeping the bottom plate in a fixed position and applying a force, F to the upper plate will cause it to move at a velocity U . This overall action will result in a continuous deformation of the fluid, as long as the force is applied. The force can be considered to be directly proportional to the area of the plate, hence the shear stress is expressed as $\tau = F/A$. Within the fluid, there is a velocity gradient ($\frac{dU}{dy}$) which develops and is often called the shear rate.

Combining the shear stress and the velocity gradient of the fluid, formulation of the Newton's law of viscosity is obtained [5]:

$$\tau = \mu \frac{dU}{dy} \quad (2-7)$$

Where μ is the viscosity and is measured in poise (or Pa.s).

Gases are generally Newtonian fluids. For a Newtonian fluid, the viscosity is dependent only on temperature and possibly pressure [5]. Examples of non-Newtonian fluids are ketchup, blood and paint [33]. The following table shows the viscosity for different gases at various temperatures.

Gas	Viscosity in 10^{-6} Pa.s
Air at 100K	7.1
Air at 300K	18.6
Air at 400K	23.1
Hydrogen at 300K	9.0
Helium at 300K	20.0
Oxygen at 300K	20.8
Nitrogen at 300K	17.9
Xenon at 300K	23.2

Table 2-3: Viscosity of gases at various temperatures [36]

2.5.4. Compressible and Incompressible flows

Incompressible flows refer to fluids whose density remains constant or nearly constant. Liquids flows are generally considered as incompressible. Compressibility effects become important if there is a density variation by more than 5 to 10 percent [5, 33]. If the pressure and/or temperature changes have negligible effects on the density, the fluid may undergo incompressible flow. This case is often applied in flows where the speeds are low compared to the speed of sound [37]. Gases are generally considered as being compressible.

The flow of a gas results in changes of density and temperature from point to point as well as changes in pressure, velocity and elevation. A balance equation for the sum of kinetic energy and potential energy can be obtained from physical principles which are based on i) conservation of mass and ii) Newton's second law of motion and is expressed as Bernouilli's equation. Bernouilli's equation for incompressible flow is

$$\frac{p_1}{\rho} + \frac{v_1^2}{2} + gz_1 = \frac{p_2}{\rho} + \frac{v_2^2}{2} + gz_2 \quad (2-8)$$

Where p_1 , v_1 and z_1 are pressure, velocity and elevation at the entrance respectively, and p_2 , v_2 and z_2 are the pressure, velocity and elevation at the exit point respectively.

For compressible gas, Bernouilli's equation needs to be modified to take into account the variation in density with pressure [38].

$$gz + \frac{1}{2} v^2 + \int_{p_1}^{p_2} \frac{dp}{\rho} = constant \quad (2-9)$$

Where the integral is evaluated according to the flow condition (adiabatic or constant temperature).

2.5.5. Laminar, turbulent flow and Reynolds' number

In laminar flow, the 'layers' within the fluid move past one another without generating cross currents. Such flows occur when the fluid viscosity is large enough to damp out any perturbations which may occur due to boundary imperfections or other irregularities. In turbulent flows there are large and random fluctuations in velocity and pressure in both space and time [39].

For a Newtonian fluid, a dimensionless parameter known as Reynolds' number is used to characterise the type of flow. A range of values define whether a flow is laminar, transition or turbulent. This geometry dependent parameter is determined experimentally and the following formula gives the Reynolds' number [5]:

$$Re = LU \frac{\rho}{\mu} \quad (2-10)$$

Where L is a characteristic length, U is the velocity of the flow, ρ is the fluid density and μ is the viscosity.

2.5.6. Coefficient of Discharge

The mass flow rate m , through an aperture can be estimated from the continuity equation:

$$m = \rho Au \quad (2-11)$$

Where A is the cross sectional area through which the fluid flows and u is the velocity.

In real life, the flow area through which the fluid passes is usually less than area, A . This is mainly due to the effects of vena contracta and boundary layers. For this reason, to get a good approximation of the flow rate, a discharge coefficient is used in calculations. The discharge coefficient can be described as the ratio of actual flow rate to ideal flow rate [34, 40].

The equation for discharge coefficient (C_d) is as follows:

$$C_d = \frac{\dot{m}}{A\sqrt{2\rho\Delta P}} \quad (2-12)$$

Where \dot{m} is the mass flow rate (kg/s), A is the cross sectional area through which the fluid flows (m^2), ρ is density (kg/m^3) and ΔP is differential pressure (Pa).

There are readily available information on the discharge coefficient of various orifices and nozzles since these are commonly used in flow measurements. The following graph shows how the discharge coefficient of a typical orifice plate varies with Reynolds' number.

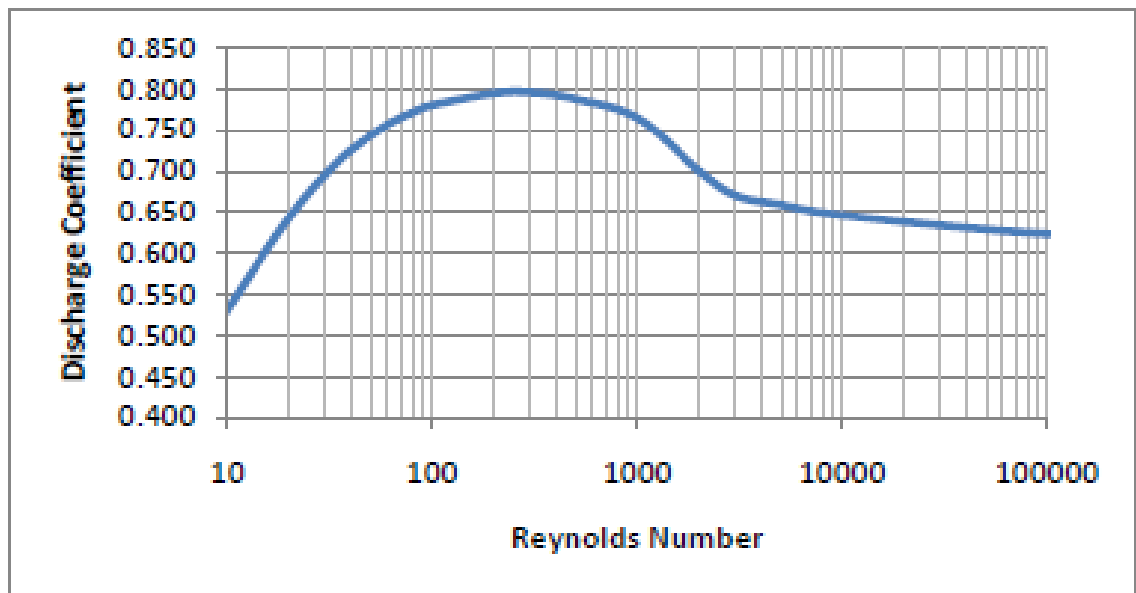


Figure 2-14: Discharge coefficient of a typical orifice plate with varying Reynolds' number [41]

2.5.7. Thermodynamics

Thermodynamics is the study of equilibrium states of matter, assuming the properties are constant both in space and time [42]. A particularly important aspect of thermodynamics for this work is heat transfer as I/P converters are sometime used in environments where temperature can vary quickly.

2.5.8. Heat Transfer

There are four basic thermal transfer modes:

- Conduction
- Convection
- Phase change
- Radiation

The main modes which are generally encountered in operation of electropneumatics are heat conduction and heat convection. Heat conduction is where the heat is transferred through a solid or stationary fluid by means of contact. Heat convection is where the motion of a fluid transfers the heat energy [43].

Heat conduction is governed by Fourier's law and is expressed as follows:

$$q = -kA \frac{dT}{dx} \quad (2-123)$$

Where q is the heat current, k is the thermal conductivity of the material, A is the cross sectional area through which the heat flows and dT/dx is the temperature gradient (insertion of a negative sign in this equation is required since when dT/dx is negative, this ensures that heat flow q is positive).

The above analysis assumes perfect contact at the interface between the two materials, however in reality the mating surfaces are rough and actual contact only occurs at discrete points [44], as illustrated in the following figure.

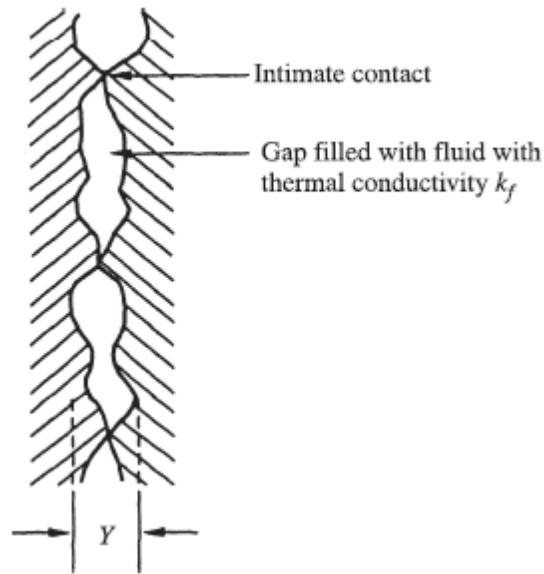


Figure 2-15: Physical contact between two imperfect surfaces [43]

Combined convective and conductive heat transfer is much more practical for such situations, it uses an overall heat transfer coefficient between adjacent materials, and this is generally obtained from experiments [45].

$$Q = h A \Delta T \quad (2-14)$$

Where Q is the heat energy transferred, h is the overall heat transfer coefficient and ΔT is the temperature difference between the two bodies.

2.6. Modelling and Simulation

Modelling and simulation has allowed a reduction in development cycle times and costs of many products. Simulations providing high accuracy (<5% error) are often achieved, however other less accurate simulations can still provide important information [46,47]. There are many dynamic simulation packages which are commonly used such as LabVIEW, SimulationModule and Simulink [46- 48].

There is a limited amount of reported work relating to modelling and simulation of electropneumatic converters. A published paper on mathematical and intelligent modelling of electropneumatic servo actuator systems [49] describes various methodologies used for deriving and simulating models of a pneumatic actuator controlled by a proportional valve.

It includes non-linear mathematical modelling of mass flow rate, determination of pressures, volumes, temperatures and determination of dynamics of the loads. Furthermore this paper describes how the non-linear equation governing mass flow rate can be linearised by using a Taylor series expansion. The final part of the paper is dedicated to intelligent modelling using neural networks; this is based on a system which has the ability to learn. Additional work relating to neural network modelling in pneumatic applications have been given in other works [50].

The force and flow rate across a poppet valve was described in the following paper: *A direct solution for flowrate and force along a cone seated poppet valve for laminar flow conditions* [51]. This study was solely based on laminar flow and no consideration to a non-unity discharge coefficient was given. The derived theories were verified through CFD simulation and experimental tests were carried out. It was shown that there is good agreement between the results obtained from simulation and experiment.

A comparison study between some linear and non-linear laws in control of an electropneumatic actuator was presented in a paper [52]. The actuator model was based on two physical aspects: 1) Pressure dynamics in a chamber with variable volume and 2) Fundamental mechanics relationships. Some assumptions were made with regards to the pressure evolution law in the chamber with variable volume: 1) Fluid is a perfect gas and its kinetic energy is negligible in the chamber, 2) pressure and temperature are homogeneous in each chamber and 3) process is polytropic.

A study of the dynamic analysis of double acting actuator was carried out and the simulation was carried out in MATLAB-Simulink [53]. This study included the thermodynamic transformation taking place in the system – energy equations were used to model the thermal energy exchange between the chambers and external environment.

There are a few papers which focus on the mathematical modelling of nozzle-flapper systems one of which focuses on the dynamic response characteristics and comparison of results from the mathematical model with the experimental results indicate good agreement although assumptions were made[23,49,54].

3. INVESTIGATION OF THE OPERATION OF THE TR140 I/P CONVERTER

3.1. Introduction

A current to pressure converter, as its names suggests, is a device which converts an electrical signal into a pneumatic output, ideally a proportional and linear output. The current technology employed by Watson Smith electro-pneumatic regulators is based around a Voice-coil actuator.

In this section a review is given of the components used in the current product and their function in the normal operation of the I/P converter.

3.2. The System and its components

The following diagram illustrates the various components found in the Watson Smith TR140 I/P converter. The section in lime green encapsulates the critical components of the converter and on its own can be used as an I/P converter. For pneumatic amplification (large flow rates), a booster chamber is used.

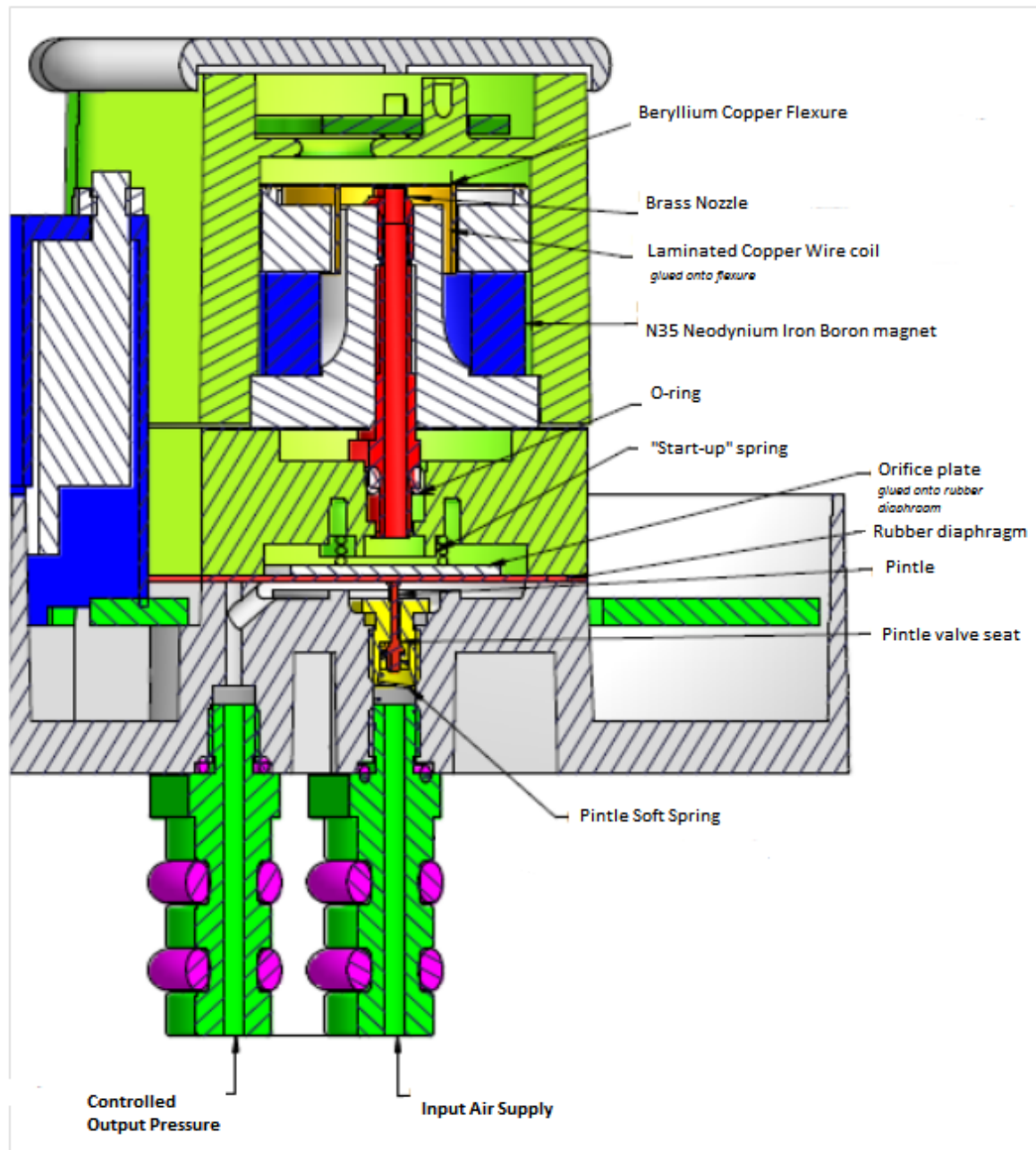


Figure 3-1: Cross Section view of TR140 I/P Converter [55]

The pintle valve (as shown in Figure 3-2) controls how much fluid gets into the booster chamber and eventually into the whole system. This component sits on a small conical spring which can be considered to have negligible spring rate; the main purpose of this spring is to keep the pintle in position.

Movement of the pintle is dependent upon the booster mechanism, supply pressure and is limited by its own design. The maximum deflection in normal operation is about 0.2mm.

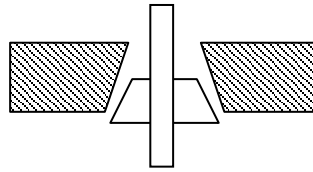


Figure 3-2: Actual
Pintle valve

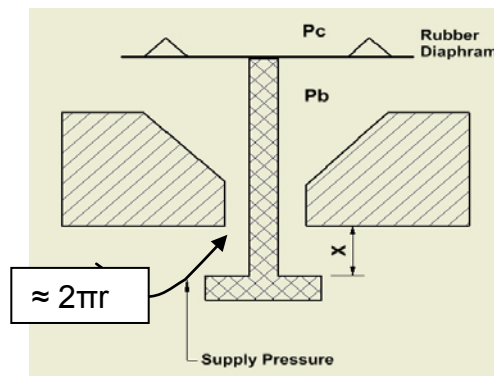


Figure 3-3: Simplified representation of Pintle valve for effective
circumference approximation

The booster mechanism consists of an orifice plate glued onto a rubber diaphragm and a spring of known force on the other side of the diaphragm. The rubber diaphragm and orifice plate creates the separation between the booster chamber and the control volume chamber. One of the main functions of this mechanism is to create the differential pressure between the pressure in the control chamber (P_c) and the pressure in the booster chamber (P_b) which in turn controls how far the pintle valve deflects. The spring known as the control start-up spring is used to initiate the operation of the whole system; when the system is not in operation and no air is being supplied to the system, the control spring exerts enough force to open the pintle valve and keeps it in open state. The spring rate of this component affects the minimum pressure needed to close the pintle valve (this will be explained further in this chapter). An initial estimate for an equation representing the

pintle valve opening (x), neglecting the effects of the control start-up spring is shown by the following

$$x = b(P_c - P_b) + x_0, \quad (3-1)$$

where b is the opening (m) per Pascal difference in the control and booster pressures (which is consistent with the pressure acting against the elastic rubber diaphragm), x_0 is the initial clearance between the pintle valve and the seat.

A more detailed model which includes the effect of the elastic force of the start-up spring and the rubber diaphragm is described below:

A pressure difference (ΔP) across the diaphragm is created due to the force from the booster control spring and considering the system in equilibrium:

$$\Delta P \cdot A_{diaphragm} = F_{spring}, \quad (3-2)$$

where $A_{diaphragm}$ is the area of the diaphragm on which the fluid pressure is acting, and F_{spring} is the resisting force of the diaphragm and booster control spring.

The resisting force of the diaphragm and the booster spring has been measured from a few samples of the booster mechanism (including booster spring, rubber diaphragm and the booster body). The behaviour of this force is quite distinctive as the control spring is in a compressed position within the booster mechanism. Figure 3-4 show the characteristics of the four samples.

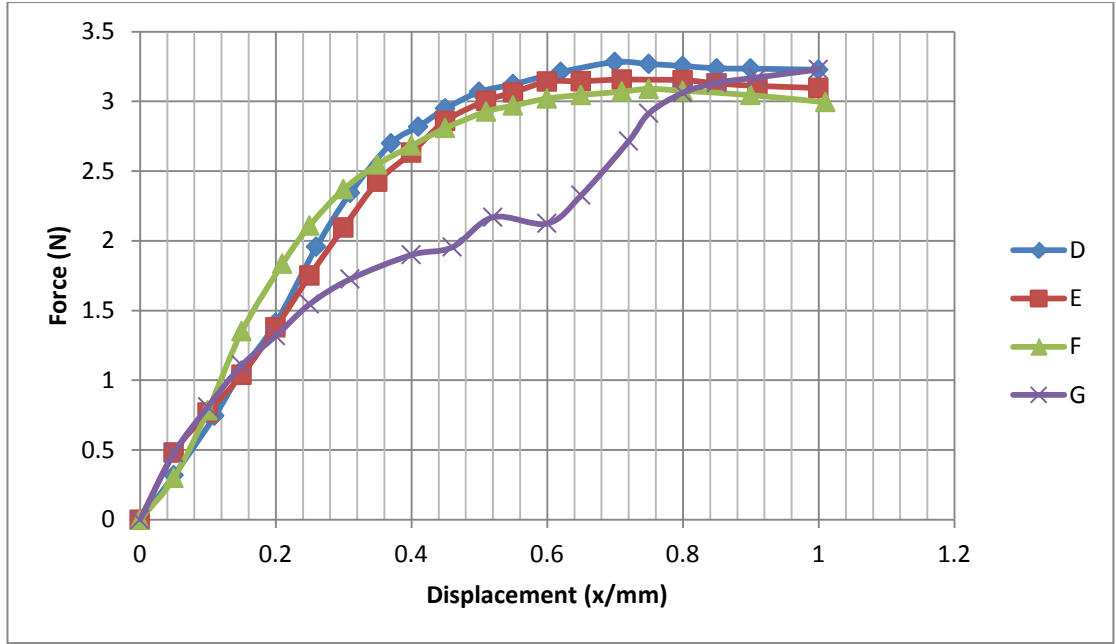


Figure 3-4: Control spring and rubber diaphragm displacement per unit force

Under operating condition, drag force on the rubber diaphragm could have an effect on the dynamics of the overall mechanism. The drag force arises due to the damping force exerted from the fluid acting over the diaphragm; based on Newton's third law of motion the diaphragm will exert an equal and opposite force.

Based on the common assumption that drag force is proportional to velocity and estimating that the rubber diaphragm cannot move 1mm in less than 1ms [56, 57] gives

$$Force_{drag} \propto v, \quad (3-3)$$

v is the velocity of the diaphragm.

Hence the overall force on the pintle valve is given by

$$F_{drag} = cv, \quad (3-4)$$

where F_{drag} is the drag force on the ball-valve and c is the drag coefficient.

At constant velocity (no acceleration) this will be equal to the net force due to spring and pressure difference across the diaphragm

$$F_{drag} = (P_b - P_c) \times \text{Area of rubber diaphragm} - F_{spring} \quad (3-5)$$

The velocity of the rubber diaphragm can then be related to c by the following,

$$v = \frac{[(P_b - P_c) \times \text{Area of rubber diaphragm} - F_{spring}]}{c}, \quad (3-6)$$

where c can be estimated from the maximum force of 3N (see from Force vs displacement graph) and based on the estimation that the maximum velocity the rubber diaphragm can reach is given by 1mm travel in 1ms (0.001/0.001 ms⁻¹) and can be expressed as follows:

$$c = \frac{F_{max}}{v_{max}} = \frac{3.0 \text{ N}}{1 \text{ ms}^{-1}} = 3 \text{ Nsm}^{-1}$$

The change in opening (dx) of the pintle valve can hence be derived as follows:

$$dx = v \Delta t \quad (3-7)$$

To fully close the pintle valve requires a force to counter the maximum force of 3N exerted by the rubber diaphragm and booster control spring mechanism. From a simple calculation ($\text{Force} = \text{Pressure} \times \text{Area}$), a 60mbar pressure drop was obtained.

This pressure drop is very similar to what was observed from actual test (as illustrated by the following graph).

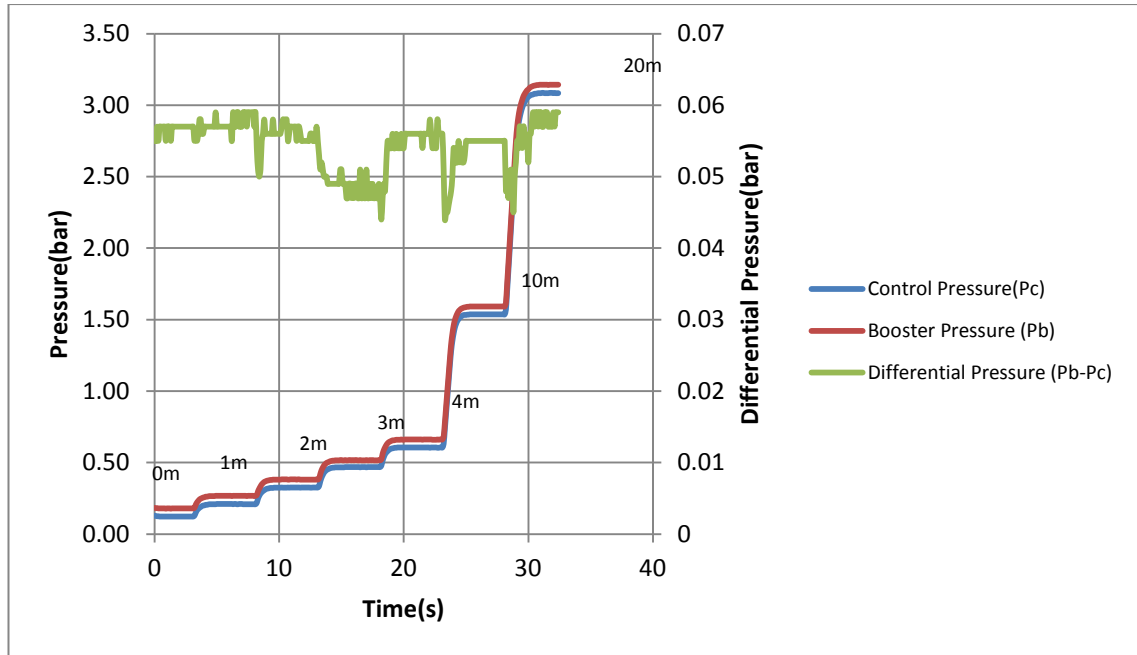


Figure 3-5: Test on actual I/P Converter showing the differential pressure across orifice disc

The mass of the pintle valve can be considered negligible considering the pressures involved.

The control section of the I/P converter is one of the most critical parts of the whole system; it consists of a control volume chamber, nozzle, flexure, coil and a permanent magnet. The coil, being attached to the flexible flexure and positioned within the permanent assembly, is made to deflect onto a brass nozzle by application of a control current in the coil. This deflection creates a variable restriction which is essentially dependent upon the input current to the coil and the fluid pressure.

3.3. Interaction of forces

The nozzle, flexure and coil are arranged (as shown in Figure 3-6) such that they create a force balancing mechanism where the electromagnetic force (F_e), fluidic force (F_f) and the elastic force (F_x) originating from the flexure springiness (k). Gravitational force arising from the mass of the coil and flexure can be considered unvarying provided that the deflection is perfectly vertical.

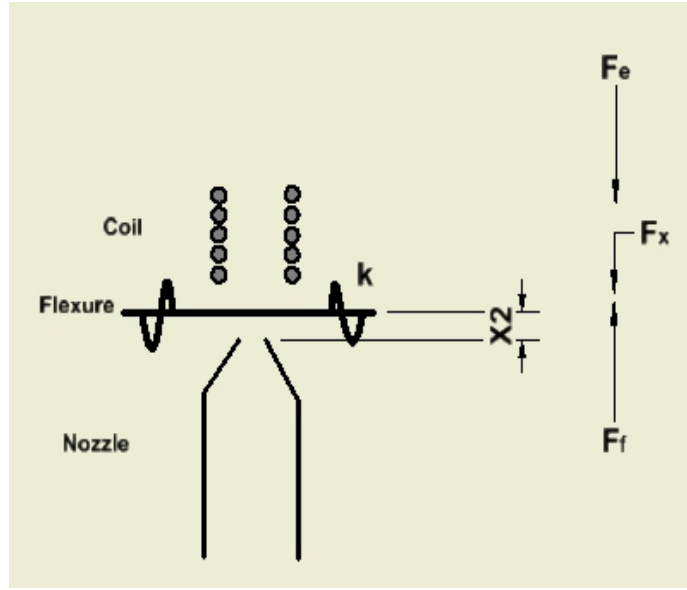


Figure 3-6: Components and interacting of forces, for illustration purpose, the coil has been placed on top of the flexure as contrary to actual arrangement

The electromagnetic force (F_e) created by the interaction of the coil in the magnet assembly is used based on the principle of electromagnetism which shows that a current carrying conductor experiences a force when placed in a magnetic field and for the case where the current carrying conductor is a coil with N number of turns this force is given by:

$$F_e = B.I.L.N, \quad (3-8)$$

where B is the magnetic field strength (Tesla), I is current (A) and L is the length of one turn of the coil (m).

From this equation, it can be seen that the electromagnetic force (F_e) is strictly proportional to the current (I) provided that the magnetic field strength (B) does not change.

Considering the current arrangement of the coil in the magnet assembly it is not definite that the magnetic field strength is perfectly uniform around the coil, hence a more appropriate representation of this force is given by the following equation:

$$F_e = d.I, \quad (3-9)$$

where d is the force per unit current (N/A) of the coil and is measured by passing a reverse current through the coil and taking the magnitude of the force at centre of the flexure.

The fluidic force from the nozzle acting on the flexure is derived from “force = pressure x area” and given by

$$F_f = (P_c - P_0) \pi r_p^2, \quad (3-10)$$

where P_0 is the atmospheric pressure and r_p is nozzle tip radius.

This fluidic force acts on the flexure to open a gap x_2 . There is an initial clearance of x_{20} between the flexure and the nozzle tip.

The flexure has a spring rate (k) which acts as a restoring force per unit displacement. This restoring force (F_x) can be considered to obey Hooke's law as the displacement of the flexure is fairly small and within the range of elastic limit of the structure of the flexure. Hence the force from the flexure spring rate is given by:

$$F_x = k(x_2 - x_{20}) \quad (3-11)$$

The resultant force acting on the flexure taking into account the electromagnetic force, the fluidic force and the restoring force from the flexure is given by

$$(P_c - P_0) \pi r_p^2 - d.I - k(x_2 - x_{20}) - mg = 0 \quad (3-12)$$

where, m is the mass of the flexure and coil combined and g is gravity. When in equilibrium this equates to zero, hence a more useful representation of this equation is

$$(P_c - P_0) = \frac{d.I + k(x_2 - x_{20}) + mg}{\pi r_p^2} \quad (3-13)$$

3.4. Operating Mode

The various components along with the interaction of forces on the system varies under different operating modes.

3.4.1. Flow to the system with no electrical power

Booster Chamber - The control spring in the booster mechanism initiates the operation by fully deflecting the pintle valve and allowing the air to flow into the booster chamber. As the pressure in the booster chamber builds up it allows some air into the control chamber through the orifice disc. At this point since the flexure is not closed onto the nozzle, the pressure in the control chamber remains at zero (atmospheric pressure), and the booster pressure rises a small amount until the net force on the diaphragm causes the pintle valve to close.

Control Chamber - In a state of no current supply to the I/P converter, the only forces acting on the flexure are gravitational (as a result of its own weight and that of the attached coil) and the pressure from the fluid. As there is not much restriction to the air path, the fluid escapes quite easily through the flexure.

The flow booster pintle is almost closed, due to a weak pintle spring pushing it up and a strong larger control spring pushing it down. This creates a slightly higher pressure in the booster chamber than the control chamber (which is slightly higher than atmospheric pressure).

3.4.2. Flow to the system with electrical power on

Control Chamber - Depending on how much current is input to the coil, the flexure is made to deflect onto the nozzle tip and thus creating a reduced aperture. When the input current is enough to overcome the spring force of the flexure and eventually pulls it down onto the nozzle tip, the pressure in the control chamber builds up quite quickly as the gap through which the air escapes is considerably much narrower. This rise continues until a steady state is reached, when the pressure in the control chamber is sufficient to open the flexure gap against the force from the coil. This results in a control chamber pressure as given by equation 3-13.

Booster Chamber - This pressure build-up creates a force onto the rubber diaphragm and depending on its magnitude; the diaphragm will cause the pintle valve to deflect accordingly and eventually restrict the flow into the system. The result is that the booster pressure, P_b , is then equal to the control pressure P_c , with an offset added (approximately 60mbar) caused by the valve spring (start-up spring).

3.4.3. Steady state

Control Chamber - As the input current to the system is constant the gap between the flexure and the nozzle is fixed assuming the pressures in the control chamber and the booster chamber are constant. Any increase in air consumption from the control chamber will cause a reduction in pressure and this eventually will cause the flexure to close until the pressure (P_c) rises again for the system to be in equilibrium. Any reduction in air consumption from this chamber will cause the pressure (P_c) to increase and eventually this force will push open the flexure until the pressure falls again such that the system is in equilibrium. The net result is that the pressure in the control chamber remains roughly constant for a given input current.

Booster Chamber - Under steady state condition, that is constant input current and constant flow supply, the flow into the booster chamber is equivalent to the air consumed by the outlet of the flow booster. An increase in consumption of air at the outlet results in a reduction of pressure and leads the pintle valve to open up which in turn leads to an increase in flow to the booster chamber until the system is in balance. A decrease in consumption will cause the pressure to increase and the pintle valve to close and eventually leads to the pressure in the booster chamber to fall until the system is in balance again.

3.5. Temperature cycles

The current I/P converters are used in products which are often used in harsh environments, notably where the temperature can be as low as -40°C and as high as +85°C. Considering this temperature range, the behaviour of the different components can significantly change and in addition the flow behaviours can also be substantially different.

Tests were carried on few samples of the actual I/P converter in a temperature controlled environment and output pressures, input currents and temperatures were recorded.

A typical result showing the gain (which is a measure of linearity of output pressure with respect to input current) is shown in the Figure 3-7.

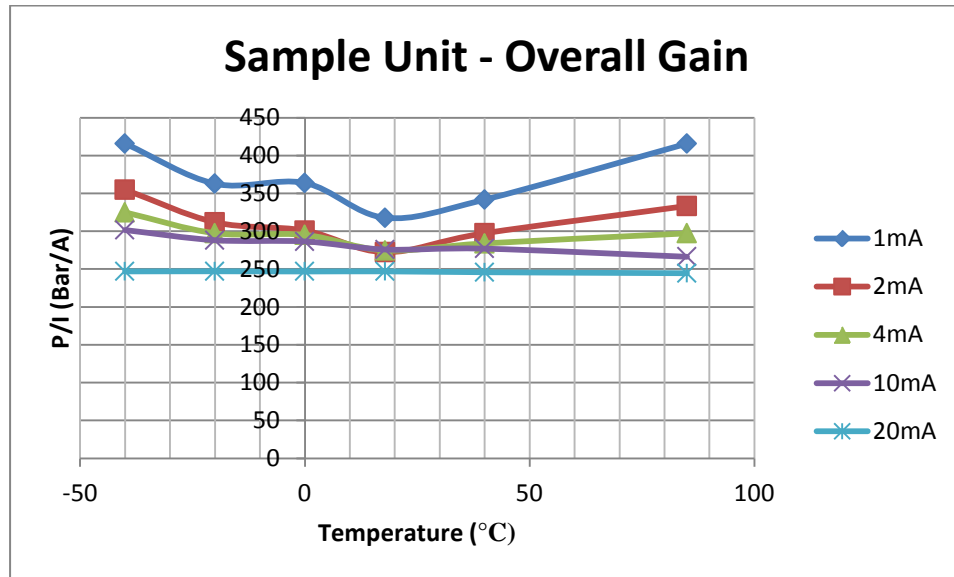


Figure 3-7: Overall gain variation with temperature change

From the graph in Figure 3-7, the variations at low currents (1mA and 2mA) are quite significant.

Ideally the overall gain with any temperature variations should be uniform over the complete range of input current. Only at high input current (as shown by the 20mA line) is a fairly constant overall gain seen.

Investigation into the cause of this trend has been carried out and further explanation can be found in Chapter 6: Identification of root causes of problem.

4. DETERMINATION OF PARAMETERS

4.1. Introduction

This section investigates how parameters, which are essential for the simulation, have been measured. In some cases reasonable approximations have been made due to the difficulty in achieving precise measurements.

The measured parameters were fed into the simulation model to predict the response of the output pressure under set conditions. Experimental tests were carried out on samples of the TR140 I/P converters and the actual responses of the output pressure were recorded. The results from the simulation were compared to the experimental results to evaluate the accuracy.

4.2. Determination of parameters

To get an accurate simulation of the I/P converter mathematical model it is crucial that the data are as accurate as possible. The parameters of the identified components were measured through experiments wherever possible. Dimensions of components were mainly obtained through measurements or through drawings, or through inspection through CAD software.

4.2.1. Stiffness of the flexure

The flexure plays a very important role in the pressure regulating of the actual I/P converter and is one of the most critical parts in the force balance mechanism. Ideally, the flexure would be an interface which floats on the nozzle but due to practicality this is not feasible as it will fall out when tilted, moved or vibrated. The actual flexure consists of a central plate which is connected by five arms held by an outer ring. The outer ring or the circumferential edge is constrained onto the magnet body by means of glue, thus limiting any lateral movement of this component. The five arms act as cantilevers allowing the central plate to move up and down, bearing similar characteristics to a spring.

This means that the flexure obeys Hooke's law (*"Elastic Force = Spring Constant \times Displacement"*). When the coil is glued onto this component, the five holes around the middle act as escape path for the fluid.

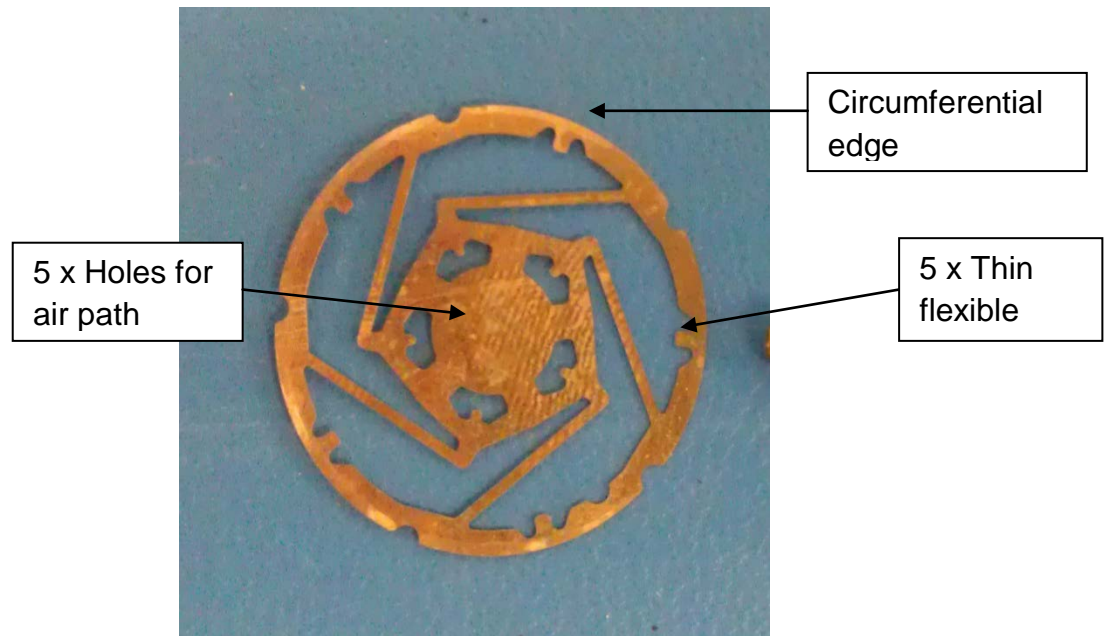


Figure 4-1: Flexure

The stiffness of the flexure was measured by means of a force gauge and the following photo shows the test setup.

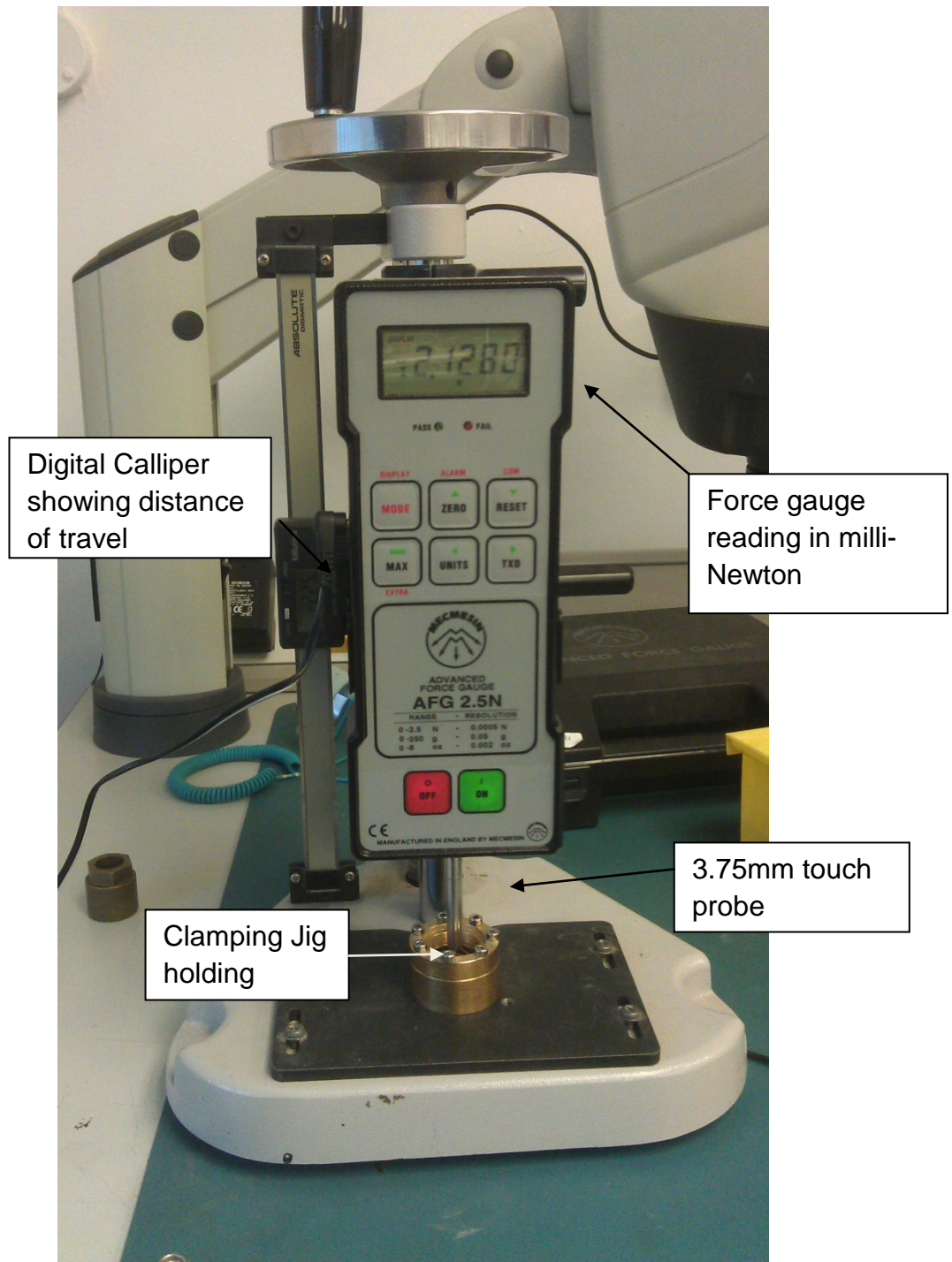


Figure 4-2: Apparatus setup to measure the stiffness of the flexure

Test equipments:

- Manual force gauge with an precision of 0.0001N (model Mecmesin AFG2.5N)
- Vernier calliper with an accuracy of 0.01mm
- Clamping jig for flexure
- 3.75mm flat head touch probe

The 3.75mm touch probe was aligned such that it was in contact with the centre of the flexure. This procedure ensured that the deformation was consistent.

The following table list the results obtained from the test carried on a sample of 5 flexures.

Displacement	Force/ N				
x/mm	Unit 1	Unit 2	Unit 3	Unit 4	Unit 5
0	0.0000	0.0000	0.0000	0.0000	0.0000
0.01	0.0143	0.0055	-	0.004	0.0089
0.02	0.0177	0.0108	0.0197	0.0103	0.0143
0.03	0.0226	0.0177	0.0275	0.0148	0.0182
0.04	0.0285	0.0265	0.0349	0.0211	0.0241
0.05	0.0329	0.0359	0.0388	0.0251	0.03
0.06	0.0393	0.0432	-	0.03	0.0343
0.07	0.0434	0.0481	0.0481	0.0359	0.0413
0.08	0.0491	0.055	0.054	0.0398	0.0442
0.09	0.0511	0.0599	0.0638	-	0.0496
0.10	0.0579	0.0668	-	-	0.0535
Temperature	21.7°C	20.4°C	20.4°C	21°C	22.2°C

Table 4-1: Table of force vs displacement for 5 flexures

Note: some of the readings are missing (at some listed displacement) due to the sudden movement of the flexure.

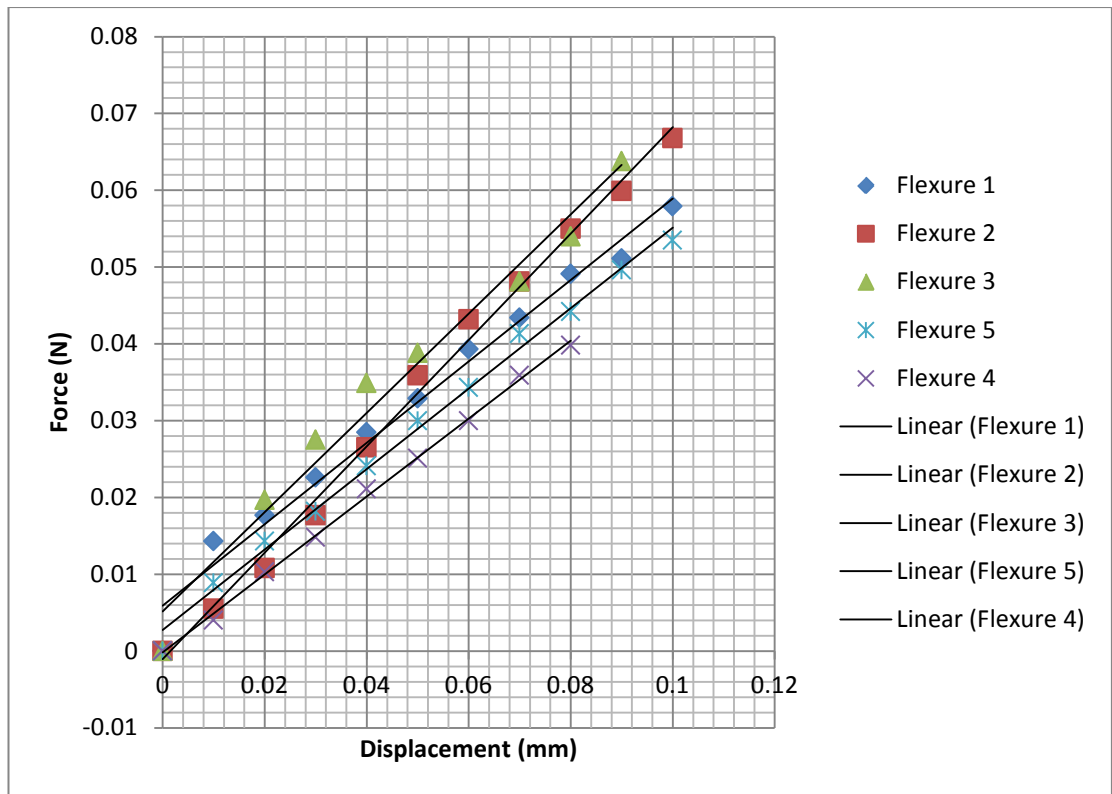


Figure 4-3: Graph of force vs displacement for 5 tested flexures

From the above graph it can be seen that although the trend is quite similar for all the five tested units, the deformation in terms of displacement per unit force is different. The following table shows the calculated stiffness of the flexure based on the test carried out.

Flexure	Stiffness (N/m)	R-squared value
1	0.6149	0.9462
2	0.6776	0.9943
3	0.7252	0.9562
4	0.5042	0.9982
5	0.5632	0.9865

Table 4-2: Calculated stiffness for the tested flexures

The observed variations in the stiffness values represent an uncertainty and could be attributed to the flexure structure or the instrument used in measuring this parameter. The force gauge used could have contributed to errors which are likely to arise from backlash in the winding mechanism.

A separate test was carried out whereby a microscope was used to measure the displacement of the flexure when a reverse current was passed through the coil.

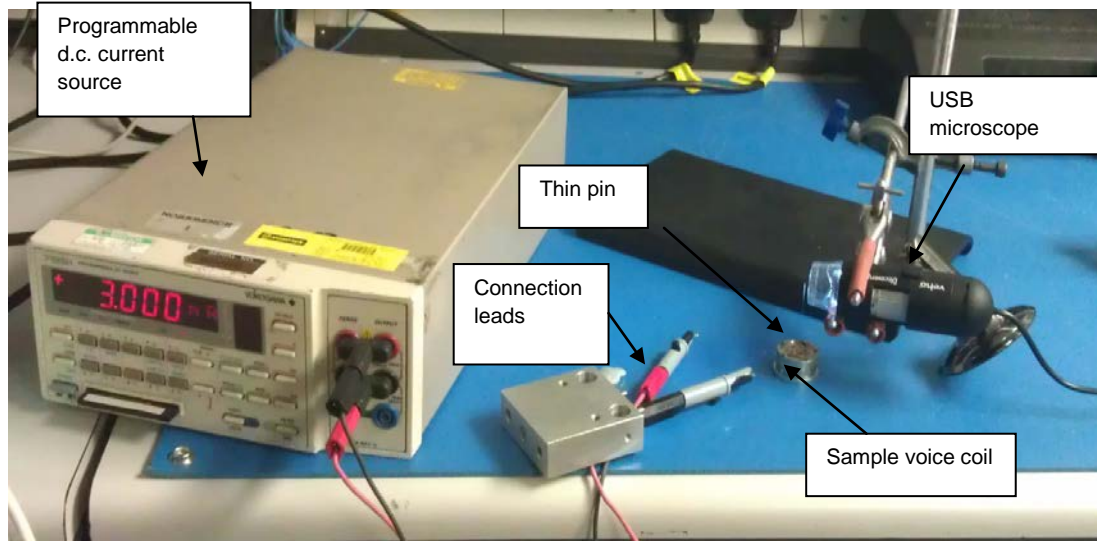


Figure 4-4: Test configuration using USB microscope

A thin light pin was glued onto the flexure, the microscope was made to focus on the pin tip and by means of a computer the movement of the pin was monitored and recorded. A programmable *d.c.* current source was used to drive a current through the coil and eventually making the flexure (with the pin) to shift in a downward direction.

The movement of the pin was measured by means of a graphic processing software (GIMP); first the magnification was calculated from the apparent diameter of the pin image and from the actual measured diameter. For each set of input currents, the displacement of the pin was measured from the software and recorded accordingly. The following figure shows the sequence of the pin displacements with regards to input current.

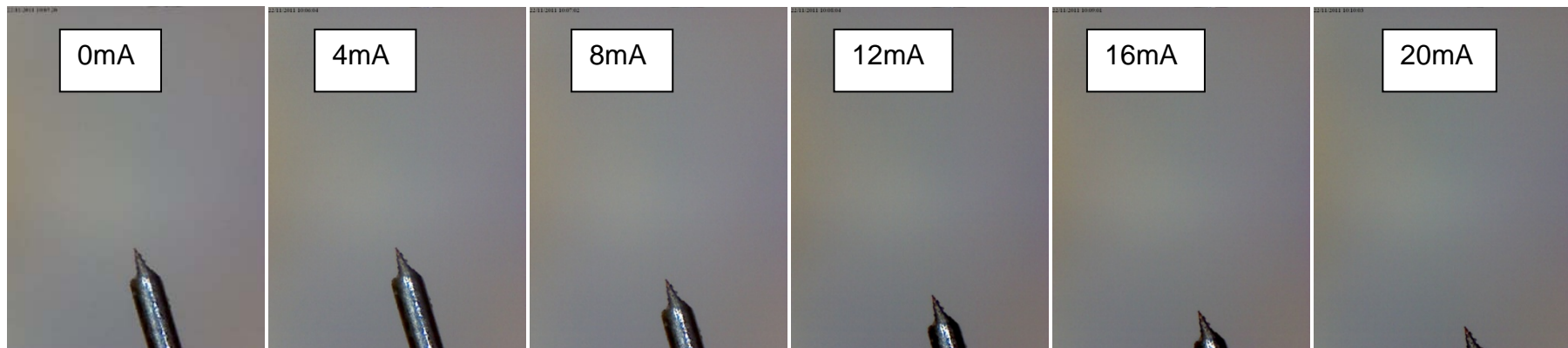


Figure 4-5: Movement of pin with varied input signal

This test was carried out on 3 units; with a known value of the force per unit current (d) exerted by the magnet onto the coil when a current is flowing through (see later section) it was possible to plot the results of force against displacement, this relationship is shown in the following figure.

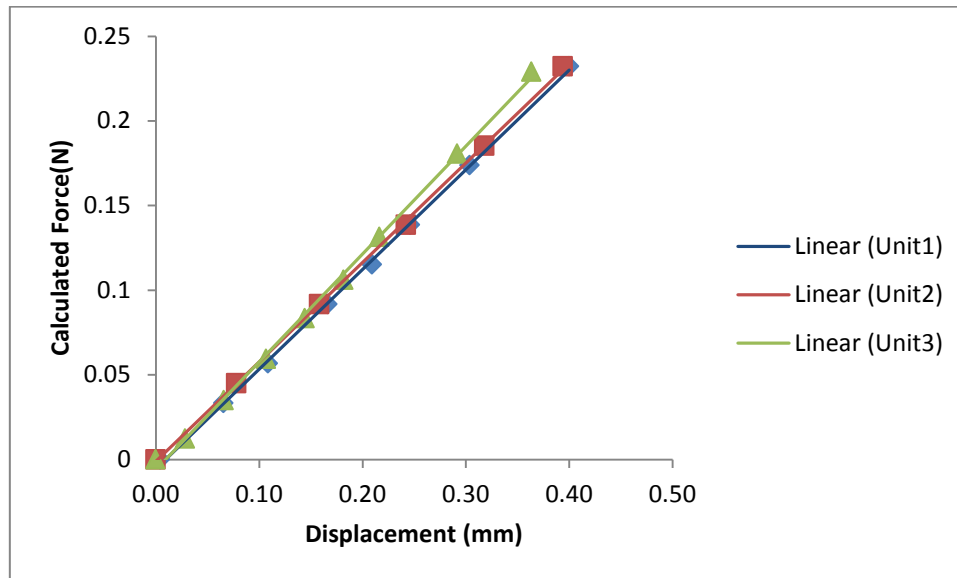


Figure 4-6: Force vs Displacement graph - using microscope test

Flexure	Stiffness (N/m)	R-squared value
1	0.5886	0.9994
2	0.5871	0.9997
3	0.6369	0.9984

Table 4-3: Calculated stiffness through measurements with USB microscope

From this test it can be seen that the stiffness of the flexures varies, but an average value can be considered for modelling purposes, within the range of 0.55N/m to 0.65N/m. The lines in figure 4-6 have R^2 values closer to 1 than the lines in figure 4-5, based on this a stronger confidence level can be put on the latter test results.

4.2.2. Coil Strength and magnet strength

The coil strength is another essential parameter which controls how much the flexure can move when applying a signal current to the coil. This movement is only possible when it is under the influence of a magnetic field. For modelling convenience, the magnetic force from the solenoid when under influence of the magnetic field is referred to as the 'Force per unit current, d' '. This parameter was measured by passing a reverse current through the coil and by using a force gauge to determine the magnitude of the force. The 1mm touch probe of the force gauge was made to be in contact with the flexure (no distortion caused) as shown in the following photo.

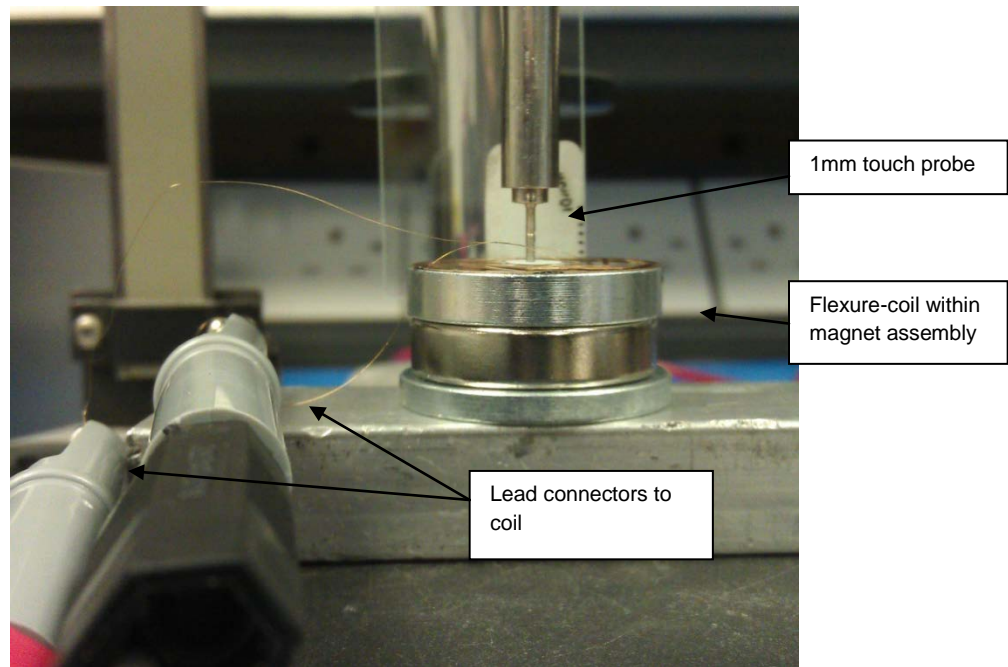


Figure 4-7: Test configuration showing the magnet-flexure-coil arrangement and the force gauge

The following table and graph show the result obtained from the test on four samples.

I/mA	Force/ N			
	A	B	C	D
0	0.0004	0.0014	0.0004	0.0009
2	0.0127	0.021	0.0103	0.0019
4	0.0353	0.0441	0.0333	0.022
6	0.0598	0.0677	0.0573	0.0451
8	0.0838	0.0912	0.0814	0.0677
10	0.1064	0.1152	0.1044	0.0912
12	0.1319	0.1378	0.129	0.1152
14	0.155	0.1618	0.1535	0.1391
16	0.181	0.1854	0.177	0.1623
18	0.2045	0.2084	0.2016	0.1864
20	0.2295	0.2325	0.2251	0.2094

Table 4-4: Readings of test - Force per unit Current

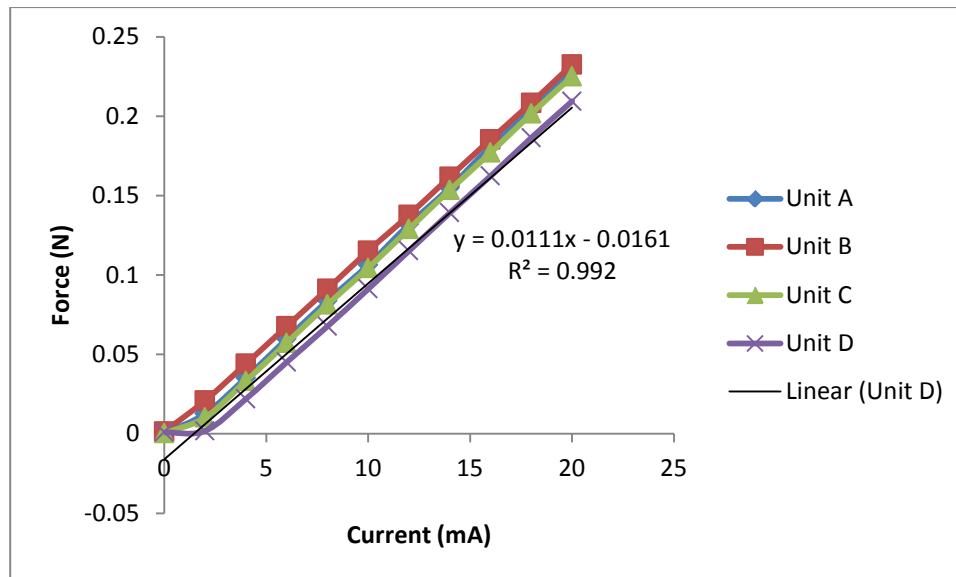


Figure 4-8: Graphs of Force per unit current for tested units

The following table shows the calculated values of the force per unit current for each tested unit, the force per unit current is obtained from the gradient of the lines.

Unit	Force per unit current, d (N/A)	R-squared
A	11.8	0.998
B	11.7	0.9998
C	11.6	0.9975
D	11.1	0.992

Table 4-5: Force per unit current formulated from the graphs of tested units

From the graph and above table it can be seen that the force is relatively linear and the force per unit current is within acceptable range, i.e. 11.2N/A – 11.7N/A. The R^2 values obtained are very close to unity indicating the readings are very close to the lines of best fit. Furthermore, the magnet drawing specification states that a force of 0.230N (+0.020/ - 0.010) should be expected when a reversed current of 20mA is passed through the coil, this equates to a force of 11.5N/A which is in good agreement with the above measurements.

The magnetic field strength can also be calculated from this parameter by using the relationship of '*Force from solenoid = Magnetic field strength x Current x Coil length per turn x number of turns*'

Using the following data from the coil specification (See Appendix I for coil specification):

Number of turns in coil – 680

Total length of wire (m) – 22.43m

The magnetic field strength = $11.5 / 22.43 = 0.51 \text{ T}$

4.2.3. Magnet

The current magnet used is a permanent magnet made out of Neodymium Iron Boron (Nd-Fe-B) of N35 grade. The excellent magnetic properties in Nd-Fe-B are mainly due to the tetragonal structure of $\text{Nd}_2\text{Fe}_{14}\text{B}$ phase [58].

It is built in an assembly which intensifies the magnetic field strength and also improves the field strength stability with temperature. The following schematic shows the magnetic field distribution within this magnetic circuit and main useful magnetic field is located in the air gap whereby the coil operates. It should be noted that the Curie temperature of the N35 grade magnet on its own, is around $+80^\circ\text{C}$ and a reversible temperature losses coefficient of $-0.12\%/^\circ\text{C}$ [59]. The Curie temperature is the point at which the magnet permanently loses its strength.

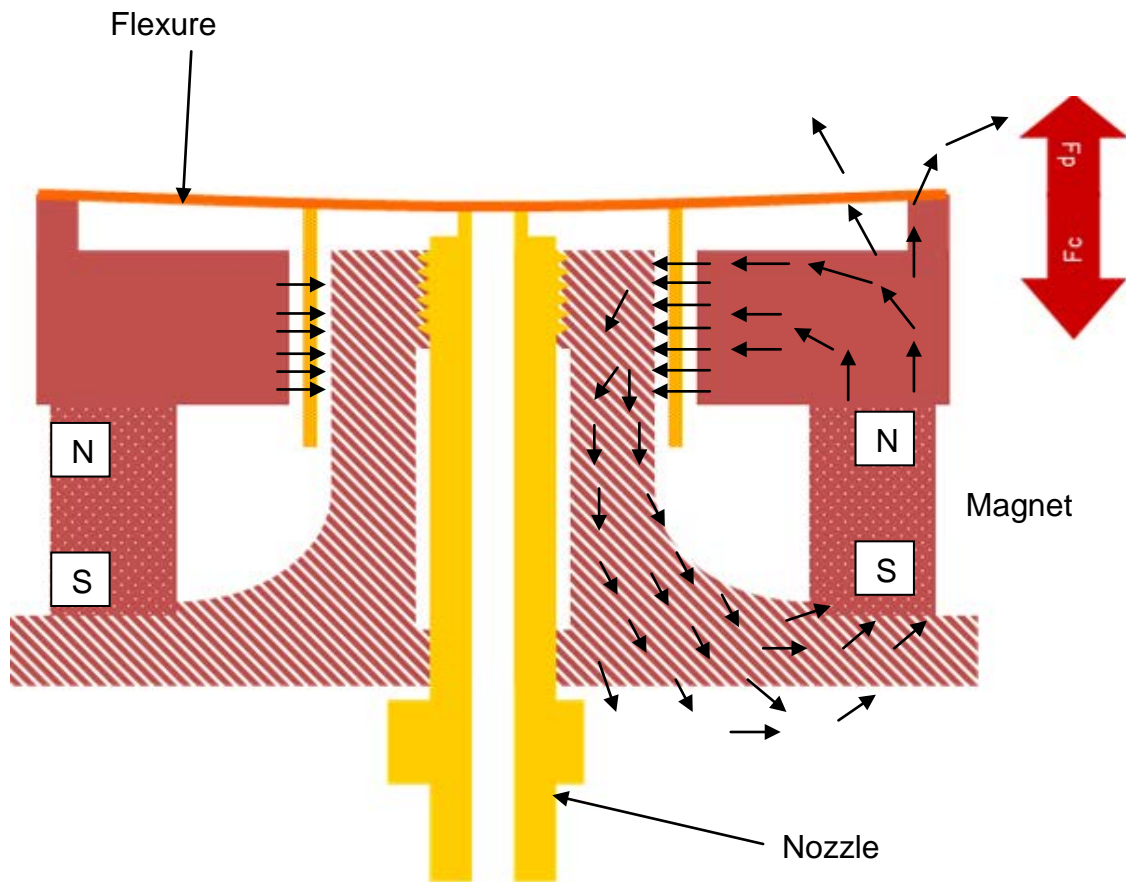


Figure 4-9: Distribution of magnetic field through the magnet assembly [60]

4.2.4. Movement of Rubber diaphragm with Control spring

The control spring is in compressed state within the control chamber assembly and its movement range is mainly restricted by the rubber diaphragm. The movement of the diaphragm controls how much the pintle valve can deflect. This parameter has been measured on assemblies of the control chamber, which included the control spring and the rubber diaphragm, by mean of a force gauge as shown in the following figure.



Figure 4-10: Test arrangement showing the force gauge and the control spring - rubber diaphragm

Measurements on five samples were carried out and the results are listed in the following table.

Unit 1		Unit 2		Unit 3		Unit 4		Unit 5	
x/mm	F/N	x/mm	F/N	x/mm	F/N	x/mm	F/N	x/mm	F/N
0.00	0.000	0.00	0.000	0.00	0.000	0.00	0.000	0.00	0.000
0.05	0.290	0.05	0.319	0.05	0.480	0.05	0.300	0.05	0.478
0.10	0.565	0.11	0.745	0.10	0.769	0.10	0.784	0.10	0.810
0.15	0.786	0.15	1.069	0.15	1.039	0.15	1.351	0.15	1.108
0.20	0.998	0.20	1.410	0.20	1.379	0.21	1.836	0.20	1.318
0.25	1.285	0.26	1.958	0.25	1.750	0.25	2.109	0.25	1.546
0.30	1.634	0.31	2.344	0.30	2.095	0.30	2.370	0.31	1.726
0.37	2.100	0.37	2.699	0.35	2.423	0.35	2.548	0.40	1.899
0.40	2.303	0.41	2.819	0.40	2.633	0.40	2.682	0.46	1.954
0.45	2.560	0.45	2.948	0.45	2.860	0.45	2.809	0.52	2.169
0.50	2.815	0.50	3.068	0.51	3.005	0.51	2.927	0.60	2.124
0.55	3.003	0.55	3.123	0.55	3.064	0.55	2.970	0.65	2.326
0.60	3.168	0.62	3.210	0.60	3.141	0.60	3.021	0.72	2.715
0.65	3.288	0.70	3.282	0.65	3.145	0.65	3.046	0.75	2.915
0.70	3.328	0.75	3.268	0.71	3.156	0.71	3.070	0.80	3.062
0.75	3.339	0.80	3.254	0.8	3.152	0.75	3.090	0.85	3.133
0.80	3.300	0.85	3.237	0.85	3.129	0.80	3.076	0.91	3.172
0.85	3.250	0.90	3.235	0.91	3.111	0.90	3.045	1.00	3.229
0.90	3.205	1.00	3.227	1.00	3.096	1.01	2.994	-	-
0.95	3.170	-	-	-	-	-	-	-	-
1.00	3.100	-	-	-	-	-	-	-	-

Table 4-6: Force - displacement results of samples of the rubber diaphragms and control springs assemblies.

Graph 3-4 representing the above results has been presented in chapter 3 - INVESTIGATION OF THE OPERATION OF THE TR140 I/P CONVERTER. It can be seen from the graph that there is a slight variation in the behaviour of the

force vs displacement across the measured samples as this would probably be due to the rubber nature of the diaphragm and variation in the stiffness of the spring, however it can be assumed from this that the force required to (nearly) close the valve, as is normal in operation, is around 3N.

4.2.5. Volumes measurement

The volumes of the chambers through which the fluid flow can affect the dynamic response of the I/P converter. The booster volume (V_b) is the space below the rubber diaphragm expanding to the pintle base valve.

The control volume (V_c) consists of the space within the spacer body and the nozzle volume.

Measurements of these volumes were made through CAD software (Inventor) since the bodies are of irregular shapes and this software can deal with such geometries.

The following figures show the measurement of the specific volumes from CAD.

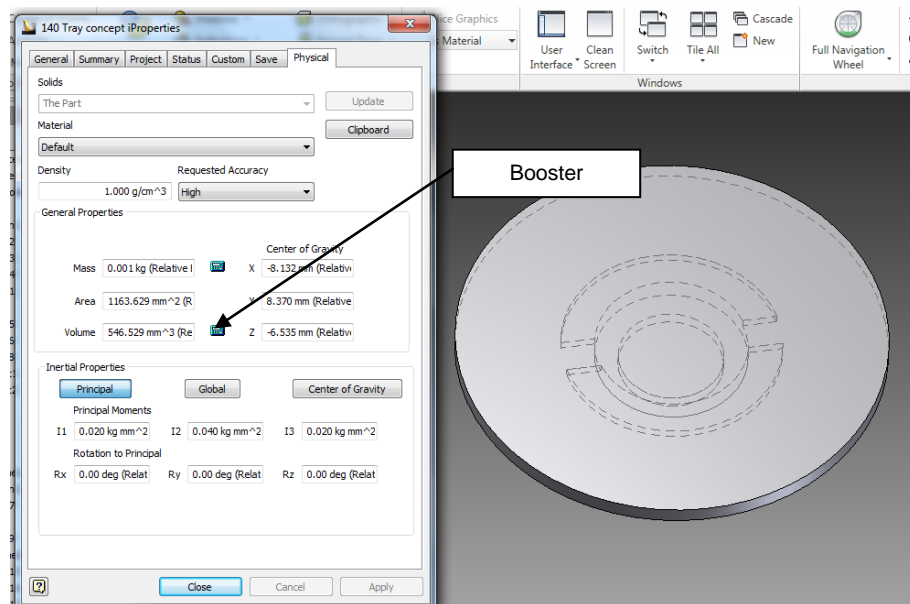


Figure 4-11: Booster chamber volume

The measured volume of the booster chamber is 546.5mm³

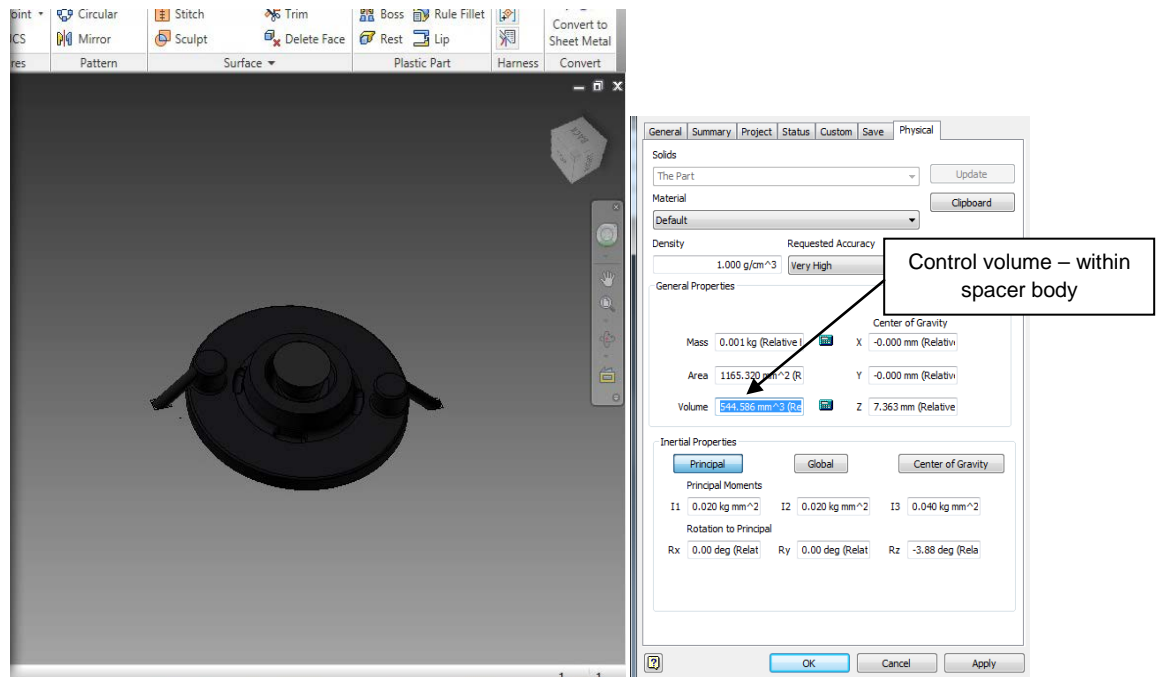


Figure 4-12: Control chamber volume

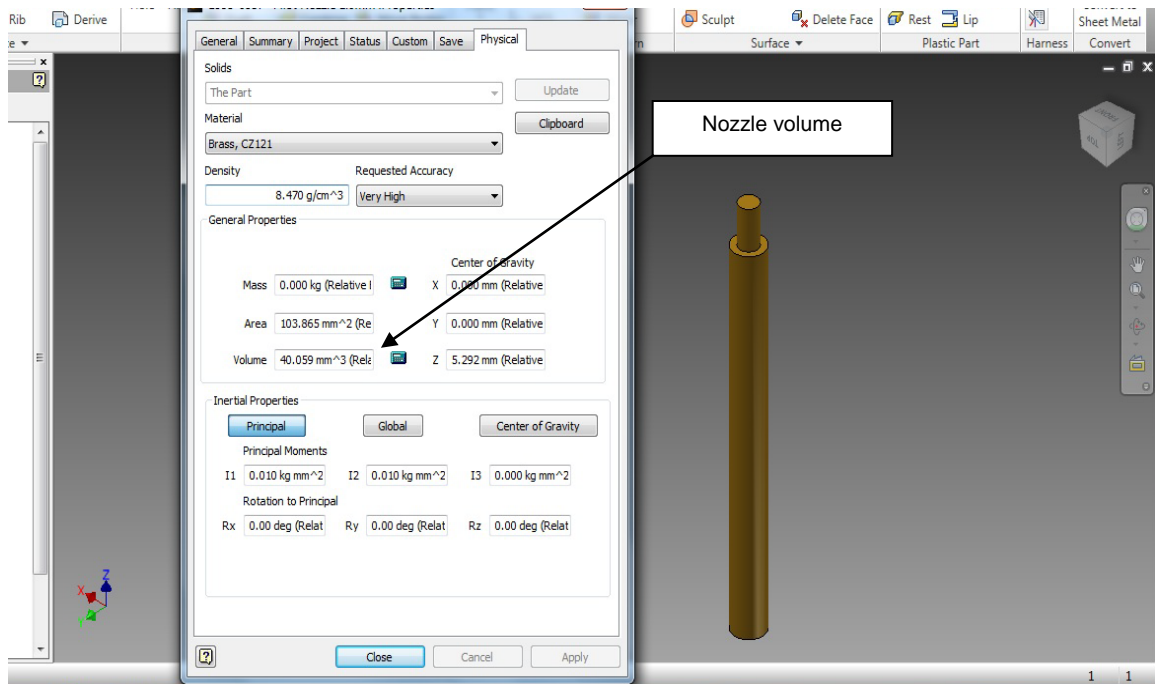


Figure 4-13: Nozzle volume

Booster volume (V_b) : 546.5 mm³

Control chamber volume: 544.6mm³

Nozzle volume: 40.1mm³

Total Control volume (V_c): 584.7mm³

4.2.6. Coefficient of discharge and other dimensions

The discharge coefficient plays an important role in determining how much flow can go through a given aperture. Discharge coefficient accounts for vena contracta which is an area less than the orifice opening through which the flow passes. As part of the modelling process there are three distinctive areas through which the flow can be significantly affected have been identified:

- Flow through the pintle valve
- Flow through the orifice disc
- Flow past the nozzle and the flexure gap

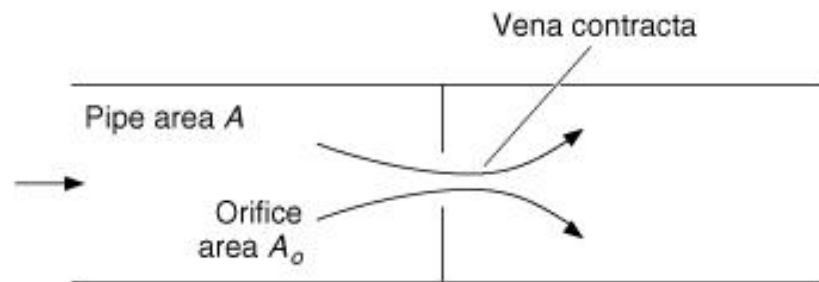


Figure 4-14: Vena contracta through orifice [61]

The discharge coefficient values are commonly assumed to be 0.6 (which is typical for large Reynolds' number flows) except for the orifice disc. Flow measurements were carried out by means of a mass flow meter (Model: Omega FMA-1620) configured to measure the flow supplied to the device under test. It was found that the flow rate through the I/P converter was 0.009g/s when the differential pressure across the orifice disc was measured as 60mbar. Using this value, the discharge coefficient for the orifice disc was calculated as follows

(effects of compressibility not considered, thus density ρ assumed to be constant at 1.2kg/m^3):

$$\dot{m} = \rho A u \quad (4-1)$$

$$\text{So } u = \frac{0.009 \times 0.001}{1.9635 \times 10^{-7}} = 38.2\text{m/s}$$

$$\text{Using } u = C d_{orifice} \sqrt{2 \frac{\Delta P}{\rho}}, \quad (4-2)$$

$$\text{then } C d_{orifice} = \frac{u}{\sqrt{2 \frac{\Delta P}{\rho}}} \quad (4-3)$$

$$\text{so } C d_{orifice} = \frac{38.2}{\sqrt{\frac{2 \times 6000}{1.2}}} = 0.382$$

4.2.7. Nozzle Diameter

The nozzle diameter was obtained from drawing specification. The internal diameter of the nozzle tip used in this particular product is 1.0mm.

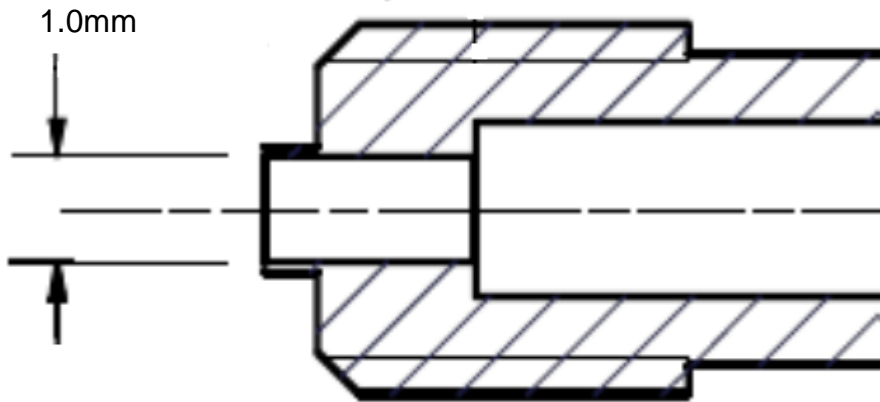


Figure 4-15: Nozzle tip feature

4.2.8. Effective circumference of pintle valve opening ('a' used in simulation)

Diameter of pintle: 1.95mm (measured using a micrometer)

$$\text{Effective circumference: } 2\pi \frac{(1.95 \times 10^{-3})}{4} = 6.13 \times 10^{-3} m$$

4.2.9. Area of hole in orifice disc ('Ah' used in simulation)

Diameter of hole: 0.05mm (measured using CMM)

$$\text{Area of hole: } \pi \frac{(0.5 \times 10^{-3})^2}{4} = 1.96 \times 10^{-7} m^2$$

4.2.10. Distance pintle valve can travel ('x' used in simulation)

Length of moveable section: 0.2mm (obtained from CAD)

5. MODELLING AND SIMULATION

5.1. Introduction

For an appropriate modelling of the TR140 I/P converter it is essential to take into account the interaction of the parts within the systems and also the effects of the environment on the overall system. The model developed for this I/P converter takes into account the major fluidic, mechanical and thermal aspects.

Simulation of the model was done using MATLAB and is capable of predicting the performance under dynamic conditions. An explicit time-stepping scheme has been employed to update the various physical conditions in the simulation.

5.2. Initial modelling of flow

The flow through the system is a very important consideration and for modelling purpose the flow into the following compartments has been taken into account:

- Flow into and out of the booster chamber
- Flow into and out of the control chamber (including the flow through the nozzle and flexure gap)

5.2.1. Net mass flow-rate into the Booster chamber

The pintle valve opening is the main component which limits the amount of flow into the booster chamber.

By considering Bernoulli's equation, the fluid velocity through the pintle valve is given by:

$$v = \sqrt{\frac{2(P_s - P_b)}{\rho_s}} \quad (5-1)$$

The effective aperture of the pintle valve is ax , where a is the effective circumference of the equivalent cylindrical gap and x is the distance the pintle valve is opened (as shown in Figure 3-3).

Considering that mass flow rate = “Velocity x Density x Area through which the fluid is passing”, the mass flow rate through the pintle valve is given by:

$$\begin{aligned}\dot{m} &= \rho_s a x \sqrt{\frac{2(P_s - P_b)}{\rho_s}} \\ &= a x \sqrt{2\rho_s(P_s - P_b)} \quad (\text{for } P_s - P_b \geq 0, \text{ else reverse direction}).\end{aligned} \quad (5-2)$$

The mass flow from the booster chamber (V_B) into the control chamber (V_C) is

$$= A_h \sqrt{2\rho_b(P_b - P_c)} \quad (\text{for } P_b - P_c \geq 0, \text{ else reverse direction}),$$

where A_h is the area of the orifice hole between the booster chamber and the control chamber.

Hence the total mass flow rate into the booster volume is

$$\dot{m}_b = a x \sqrt{2\rho_s(P_s - P_b)} - A_h \sqrt{2\rho_b(P_b - P_c)} - \dot{m}, \quad (5-3)$$

where \dot{m} is the mass flow output from the I/P converter to external devices.

The pressure, density and temperature in each compartment are linked by the ideal gas law.

For the booster pressure

$$P_b = \rho_b R T_b, \quad (5-4)$$

where R is the universal gas constant (287 J/kg.K).

The total mass flow rate in the booster volume is also equal to “Volume x Density”;

$$m_b = \rho_b V_b \quad (5-5)$$

Differentiating this with respect to time gives

$$\frac{dm_b}{dt} = \frac{d\rho_b}{dt} V_b, \quad (5-6)$$

which can be substituted in 5-3 to give

$$\dot{m}_b = \frac{d\rho_b}{dt} V_b = a \times \sqrt{2\rho_s(P_s - P_b)} - A_h \sqrt{2\rho_b(P_b - P_c)} - \dot{m} \quad (5-7)$$

Differentiating (5-4) and assuming that the temperature is constant,

$$\frac{dP_b}{dt} = \frac{d\rho_b}{dt} RT_b \quad (5-8)$$

The evolution of pressure in the booster chamber is obtained by combining equations (5-7) and (5-8) to give:

$$\frac{dP_b}{dt} = \frac{RT_b}{V_b} [a \times \sqrt{2\rho_s(P_s - P_b)} - A_h \sqrt{2\rho_b(P_b - P_c)} - \dot{m}] \quad (5-9)$$

5.2.2. Net mass flow-rate into the Control chamber & through the nozzle-flexure gap

The effective flow into the control chamber is dependent on the ‘normal flow in’ and on the ‘flow escaping through the nozzle’.

The normal flow in is given by $A_h \sqrt{2\rho_b(P_b - P_c)}$ (for $P_b - P_c \geq 0$, else reverse direction).

The flow through the nozzle-flexure gap is given by $A_p \sqrt{2\rho_c(P_c - P_0)}$,

where A_p is the effective area of the gap between the nozzle and the flexure, and P_0 is the atmospheric pressure. Effectively (assuming the nozzle tip and the flexure are perfectly parallel) $A_p = \text{“Circumference of nozzle exit} \times \text{distance between flexure and nozzle tip} (x_2)\text{”}$.

Hence the total mass flow rate into the control chamber is

$$\dot{m}_c = A_h \sqrt{2\rho_b(P_b - P_c)} - A_p \sqrt{2\rho_c(P_c - P_0)} \quad (5-10)$$

As air can be closely considered as “ideal gas”, the pressure in the control chamber is

$$P_c = \rho_c R T_c \quad (5-11)$$

where P_c , ρ_c and T_c are the pressure, density and temperature in the control chamber respectively. Similarly to the case for the booster chamber, $m_c = \rho_c V_c$, thus giving

$$\frac{dm_c}{dt} = \frac{d\rho_c}{dt} V_c , \quad (5-12)$$

where V_c is the volume in the control chamber.

The pressure evolution in the control chamber can be obtained by combining Equations (5-13), (5-14) and (5-15).

$$\frac{dP_c}{dt} = \frac{RT_c}{V_c} [A_h \sqrt{2\rho_b(P_b - P_c)} - A_p \sqrt{2\rho_c(P_c - P_0)}] \quad (5-16)$$

5.2.3. Opening of the flexure-nozzle gap

From Equation (3-12), the resultant force acting on the flexure can be readily extended to a 2nd order differential equation for the transient response of the flexure.

As a working approximation (assuming that the response of the diaphragm is so fast that the delay is insignificant), a model that neglects the mass of the flexure has been used – the velocity of the flexure is a resultant of the force which pushes against the viscosity of the fluid (this is equivalent to achieving a “terminal velocity” without having to model acceleration).

$$\frac{dx_2}{dt} = \frac{1}{\mu} [(P_c - P_0)\pi r_p^2 - d.I - k(x_2 - x_{20})], \quad (5-17)$$

where μ , is a measure of the resistance to motion (analogous to viscosity).

5.3. Initial simulation results

This initial modelling of the fluidic and mechanical behaviour was implemented in Matlab using a forward-difference time-stepping scheme.

Physical parameters of components (such as dimensions and forces – these are listed in the simulation model provided in Appendix II) were measured and included in the simulation.

An input current of 5mA was used at the start of the simulation, $t=0s$ and stepped up to 10mA after $t=0.1s$ and to 15mA at $t=0.15s$. Up to this time no flow was drawn from the I/P converter from the main regulator. After $t=0.3s$, a mass flow rate of $3 \times 10^{-6} \text{kg/s}$ was drawn from the I/P converter.

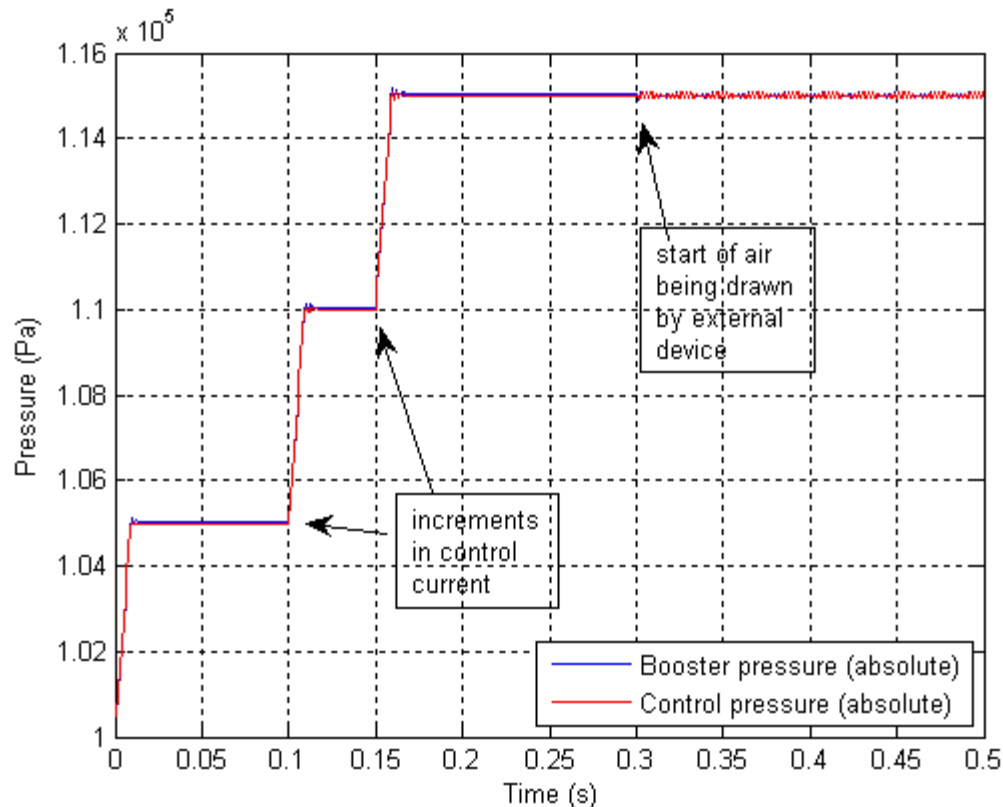


Figure 5-1: Output of numerical simulation of model for step rises in input current, followed by a step rise in air drawn out of I/P converter

Note: The pressure is absolute rather than gauge pressure, which would need $1 \times 10^5 Pa$ to be subtracted.

Both the booster chamber pressure (P_b) and the control chamber pressure (P_c) rise linearly with input current signal. If looked at closely, it can be seen that the booster chamber pressure (P_b) is slightly higher than the control chamber pressure (P_c) at steady-state condition; this is mainly because for a flow there must be pressure in the booster chamber to flow into the control chamber and past the nozzle-flexure gap. Small overshoots are seen as the device settles to steady pressures at each current step. As the regulator starts to draw flow from at $t=0.3s$, some oscillations are seen at the output pressure and very little drop in output pressure is seen. It was found that reducing the time step significantly (by a factor of 10) these oscillations and overshoots disappeared, hence they can be considered as a numerical artefact and the importance of small time steps is established.

5.4. Modelling of flow – Compressible flow effects

The flow through several sections can be considerably restricted by compressibility issues and it is essential to consider the effects of compressibility on the flow. There are three stages in the system which can restrict the flow and these are:

- Flow through the pintle valve
- Flow through the orifice disc
- Flow through the nozzle – flexure gap

The general formula for the mass flow rate of a compressible fluid is

$$\dot{m} = \frac{P_{01}}{\sqrt{RT_{01}}} A_t \left(\frac{P_t}{P_{01}} \right)^{1/\gamma} \sqrt{\frac{2\gamma}{\gamma-1} \left(1 - \left(\frac{P_t}{P_{01}} \right)^{\frac{\gamma-1}{\gamma}} \right)} \quad (5-18)$$

where P_{01} is the upstream pressure, T_{01} is the upstream temperature, A_t is the cross section area at the throat or restriction and γ is the heat capacity ratio of the fluid [62].

To account for the flow effects caused by the valve design, a discharge coefficient factor (C_d) is included in the equation:

$$\dot{m} = \frac{C_d P_{01}}{\sqrt{RT_{01}}} A_t \left(\frac{P_t}{P_{01}} \right)^{1/\gamma} \sqrt{\frac{2\gamma}{\gamma-1} \left(1 - \left(\frac{P_t}{P_{01}} \right)^{\frac{\gamma-1}{\gamma}} \right)} \quad (5-19)$$

The maximum mass flow rate is dependent on the pressure ratio $\left(\frac{P_t}{P_{01}} \right)$. When the flow reaches sonic velocity at the throat, the flow is choked and at this point the pressure ratio is known as Critical Pressure Ratio.

From definition the Critical Pressure Ratio is given by:

$$\frac{P_t}{P_{01}} = \left(\frac{2}{1+\gamma} \right)^{\frac{\gamma}{\gamma-1}}, \quad (5-20)$$

where γ is the specific heat ratio of the gas. For air $\gamma = 1.4$, this means that the Critical Pressure Ratio is 0.528.

When the Pressure Ratio increases above this point, the flow is affected and does not behave as per equation 5-16, which is for sub-critical flow.

To model the mass flow rate at condition beyond the Critical Pressure Ratio the following should be used:

$$\dot{m} = \frac{C_d P_{01}}{\sqrt{RT_{01}}} A_t \gamma^{\frac{1}{2}} \left(\frac{2}{\gamma+1} \right)^{\frac{(\gamma+1)}{2(\gamma-1)}} \quad (5-21)$$

For mass flow into booster including compressibility:

$$\dot{m}_B = \frac{C_d P_S}{\sqrt{RT_S}} ax \left(\frac{P_B}{P_S} \right)^{1/\gamma} \sqrt{\frac{2\gamma}{\gamma-1} \left(1 - \left(\frac{P_B}{P_S} \right)^{\frac{\gamma-1}{\gamma}} \right)} \text{ if } \frac{P_B}{P_S} > 0.528 \quad (5-22)$$

$$\dot{m}_B = \frac{C_d P_S}{\sqrt{RT_S}} (ax) \gamma^{\frac{1}{2}} \left(\frac{2}{\gamma+1} \right)^{\frac{(\gamma+1)}{2(\gamma-1)}} \text{ if } \frac{P_B}{P_S} \leq 0.528 \quad (5-23)$$

For mass flow into control including compressibility:

$$\dot{m}_C = \frac{C_d P_B}{\sqrt{RT_B}} A_h \left(\frac{P_C}{P_B} \right)^{1/\gamma} \sqrt{\frac{2\gamma}{\gamma-1} \left(1 - \left(\frac{P_C}{P_B} \right)^{\frac{\gamma-1}{\gamma}} \right)} \quad \text{if } \frac{P_C}{P_B} > 0.528 \quad (5-24)$$

$$\dot{m}_C = \frac{C_d P_B}{\sqrt{RT_B}} \gamma^{\frac{1}{2}} A_h \left(\frac{2}{\gamma+1} \right)^{(\gamma+1)/2(\gamma-1)} \quad \text{if } \frac{P_C}{P_B} \leq 0.528 \quad (5-25)$$

For mass flow through nozzle-flexure including compressibility:

$$\dot{m}_{out} = \frac{C_d P_C}{\sqrt{RT_C}} A_p \left(\frac{P_0}{P_C} \right)^{1/\gamma} \sqrt{\frac{2\gamma}{\gamma-1} \left(1 - \left(\frac{P_0}{P_C} \right)^{\frac{\gamma-1}{\gamma}} \right)} \quad \text{if } \frac{P_0}{P_C} > 0.528 \quad (5-26)$$

$$\dot{m}_{out} = \frac{C_d P_C}{\sqrt{RT_C}} A_p \gamma^{\frac{1}{2}} \left(\frac{2}{\gamma+1} \right)^{(\gamma+1)/2(\gamma-1)} \quad \text{if } \frac{P_0}{P_C} \leq 0.528 \quad (5-27)$$

These are used to modify the differential equations for pressure obtained using only Bernouilli's equation.

5.5. Modelling of thermal effects

As the fluid is subjected to compressible effects, it is likely that its temperature will be affected and in addition the thermal effects from the surroundings will influence the behaviour of the flow.

5.5.1. Heat transfer due to compressible effects and convection

Since the fluid follows the ideal gas law, a change in temperature means that the pressure will change. The rate of change in pressure is given by

$$\frac{dP_i}{dt} = \frac{d\rho_i}{dt} RT_i + \rho_i R \frac{dT_i}{dt} \quad (5-28)$$

where P_i, ρ_i and T_i are the Pressure, density and temperature (respectively) in the corresponding compartment i .

The rate of temperature change $\frac{dT_i}{dt}$ is caused by the moving mass of fluid and it can be obtained by considering the following which is based on the 1st Law of thermodynamics

$$Q_{inew} = Q_i + Q_j \quad (5-29)$$

where Q_{inew} is the new heat energy from the moving mass of fluid, Q_i is the initial heat energy (i.e. at time $t=0$) and Q_j is the heat energy transferred from the preceding compartment.

Rearranging this to take into account the mass flow rates, specific heat capacities and temperatures since

$\dot{Q} = \dot{m}cT$ gives

$$(m_i + \dot{m}_i \Delta t) c_{fluid} T_{i\ new} = m_i c_{fluid} T_i + \dot{m}_j \Delta t c_{fluid} T_j \quad (5-30)$$

where m_i the initial mass of fluid in the compartment is, c_{fluid} is the specific heat capacity of the fluid, \dot{m}_i is the mass flow rate into the compartment, T_i is the initial temperature in the compartment, \dot{m}_j is the mass flow rate from the previous compartment into i and T_j is the temperature in the preceding compartment.

Assuming no leakage, $\dot{m}_i = \dot{m}_j$

And from density $(\rho) = \frac{\text{mass (m)}}{\text{volume (V)}}$, $m_i = \rho_i V_i$

Hence the new temperature in the chamber due to convection is

$$T_{i\ new} = \frac{\rho_i v_i c_{fluid} T_i + \dot{m}_i \Delta t c_{fluid} T_j}{(\rho_i v_i + \dot{m}_i \Delta t) c_{fluid}} \quad (5-31)$$

Implying that the temperature difference with respect to time, $\frac{dT_i}{dt}$ is given by

$$\frac{dT_i}{dt} \approx \frac{\Delta T_i}{\Delta t} = \frac{T_{i\ new} - T_i}{\Delta t} \quad (5-32)$$

5.5.2. Heat transfer through conduction

Considering the effect of heat transfer on the system and denoting the rate of change of temperature of i from heat conduction as $\left. \frac{dT_i}{dt} \right|_{HT}$, the heat transfer is

$$\left. \frac{dT_i}{dt} \right|_{HT} = \frac{1}{m_i c_i} \sum_j h_{ij} A_{ij} \Delta T_{ij} \quad (5-33)$$

where m_i is the mass of the individual component i , c_i is the specific heat capacity of the component, h_{ij} is the overall heat transfer coefficient between the adjacent components/ fluid i and j , A_{ij} is the area of the component i in contact with j and ΔT_{ij} is the temperature difference between components/fluid i and j .

It should be noted that the heat transfer through conduction is modelled based on Newton's law rather than Fourier's law of heat conduction since the thermal conductivity is not an adequate parameter to be used as many components in the system have uneven shape and surface finish, making an analytical determination of heat transfer very difficult.

The new temperature of the individual chamber and component (T_n) taking into account heat convection and heat conduction is

$$T_n = T_i + \left(\frac{dT_i}{dt} + \frac{dT_i}{dt_2} \right) \times \Delta t \quad (5-34)$$

The following diagram shows the various components which have been considered for the heat transfer.

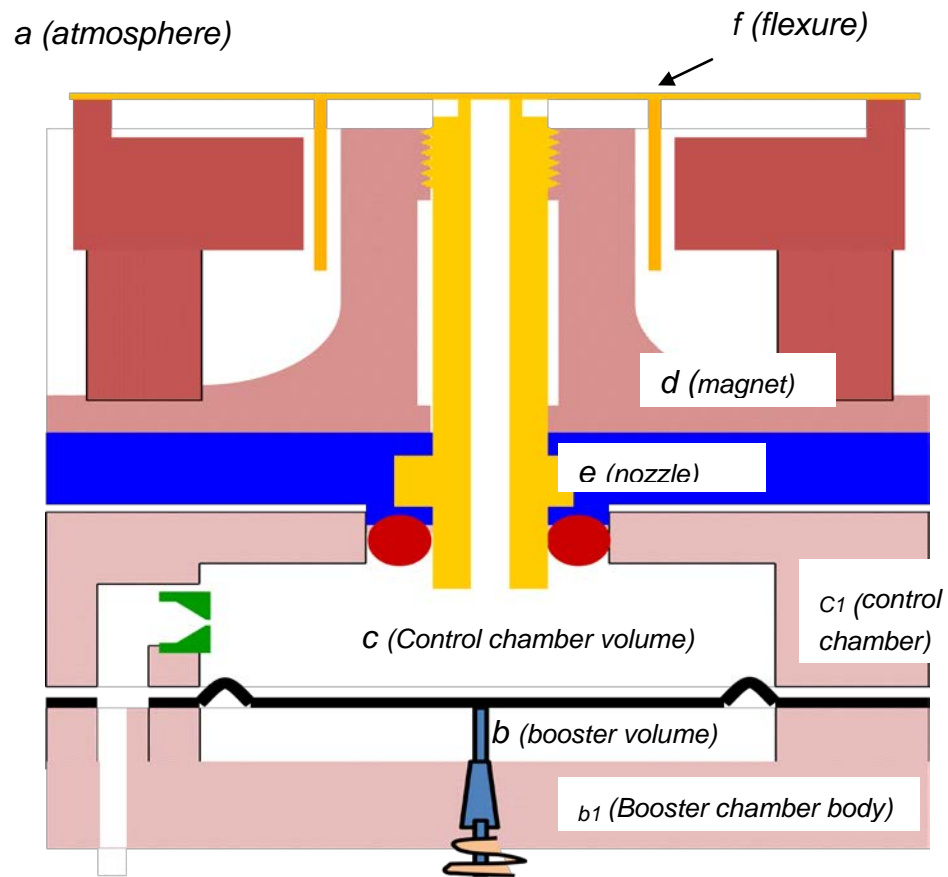


Figure 5-2 : Cross section view of I/P converter showing annotated components

For convenient representation of the heat transfer equations, the following annotations have been used to identify the various components and chambers:

Component	Annotation
Atmosphere	<i>a</i>
Booster chamber volume	<i>b</i>
Booster chamber body	<i>b1</i>
Control chamber volume	<i>c</i>
Control chamber body	<i>c1</i>
Magnet	<i>d</i>
Nozzle	<i>e</i>
Flexure	<i>f</i>

Table 5-1: Annotated elements

The heat transfers by conduction through each component/ region are listed in Appendix III:

The Overall Heat Transfer Coefficients have been classified according to the materials present in the system and according to the contact bodies.

Annotation	Contact materials	Overall Heat Transfer coefficient
H_{ag}	Copper	1
H₁	Metal – Metal	50
H₂	Still Air – Metal	0.1
H₃	Flowing Air – Metal	1
H₄	Plastic – Metal	0.1
H₅	Air – Plastic	0.01

Table 5-2: Overall heat transfer coefficient through identified materials [63]

The areas are determined by measurement and are given in the table below.

Area annotation	Body in contact	Area (m ²)
AREA_{ab1}	Atmosphere with booster body	1.05e-3
AREA_{ac1}	Atmosphere with control body	1.05e-3
AREA_{ad}	Atmosphere with magnet	0.39e-3
AREA_{ae}	Atmosphere with nozzle	9.11e-6
AREA_{af}	Atmosphere with flexure	2.60e-3
AREA_{bb1}	Booster volume with booster body	4.91e-6
AREA_{bc}	Booster volume with control volume	1.20e-5
AREA_{bc1}	Booster volume with control body	6.39e-5
AREA_{cc1}	Control volume with control body	0.93e-3
AREA_{ce}	Control volume with nozzle	1.46e-5
AREA_{c1b1}	Control body with booster body	0.96e-3
AREA_{c1d}	Control body with magnet	0.62e-3
AREA_{de}	Magnet with nozzle	0.16e-3

Table 5-3: Contact bodies with respective areas

The mass of each component with specific heat capacity (determined by measurements) are listed in the following table.

Component	Mass (kg)	Specific Heat Capacity (J/kg K)
Booster body (M_{b1})	0.045	420
Control body (M_{c1})	8.5e-3	1670
Magnet (M_d)	0.049	420
Nozzle (M_e)	1.3e-3	390
Flexure (M_f)	0.3e-3	390
Air (C_{air}) – only Sp. Heat capacity	<i>'density x volume'</i>	1000

Table 5-4: Mass of component with respective specific heat capacity

5.6. Simulation of complete model with compressible effects and heat transfer

SIMULATION 1:

Values of the measured parameters (see chapter 5) were included in the simulation model and the following conditions setup were used:

- Supply Pressure (P_s) – 6 bar absolute (5bar gauge)
- Atmospheric Pressure (P_0) – 1 bar absolute (0bar gauge)
- Atmospheric temperature (T_a) – 298K (typical)
- Temperature of supply (T_s) – 283K (typical)
- Temperatures of all components – 293K (initialised to intermediate temperature to determine change rate)

Input current sequence:

- From 0 – 1s: 0mA
- From 1s - 2s: 1mA
- From 2s – 3s: 2mA
- From 3s – 4s: 4mA
- From 4s – 5s: 10mA
- From 5s – 6s: 20mA

After 5.8s a mass flow rate of 2×10^{-6} kg/s was to be drawn from the I/P converter.

The following graph was generated from the MATLAB simulation. The data labels represent the pressures at steady input current.

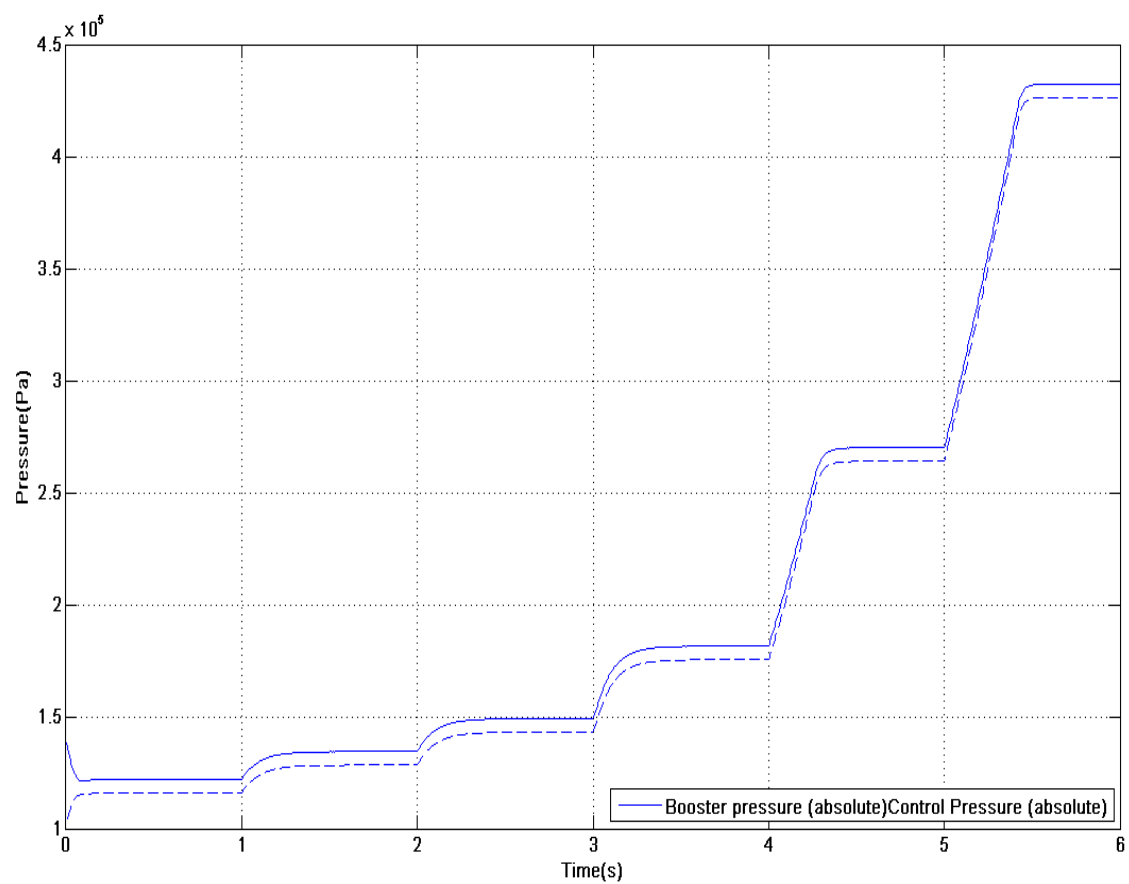


Figure 5-3: Simulation of complete model

It can be seen from the graph above that the pressures rises quite linearly and also the pressure difference between the booster and control pressures is constant at 60mbar at all steady input currents.

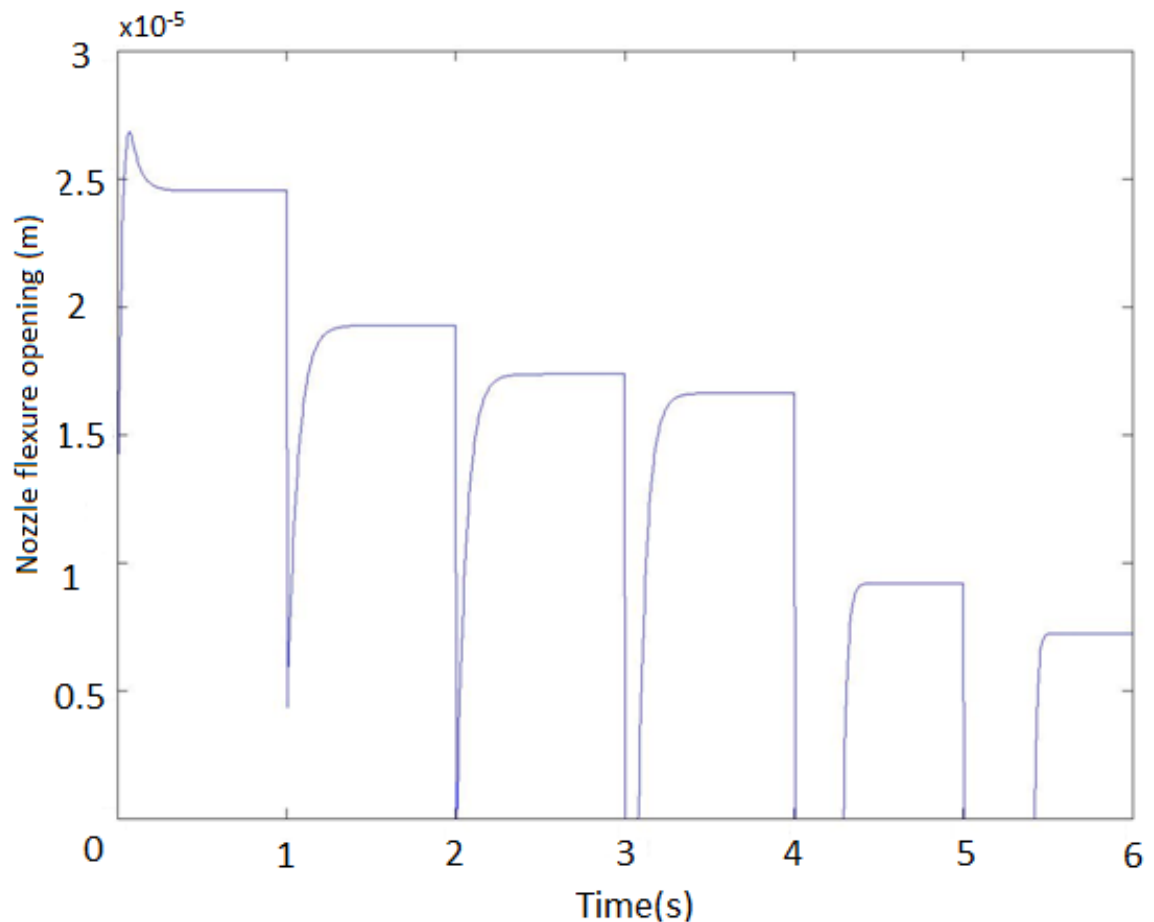


Figure 5-4: Simulation of Nozzle-flexure opening

The above figure shows the nozzle-flexure openings for the simulation. It can be seen from the graph that the operation of the flexure is predicted to be between $5\mu\text{m}$ to $30\mu\text{m}$ for the set conditions.

As the supply temperature has been set at lower value than the initial chambers' temperatures, the temperature within the booster chamber and the control chamber will take a certain amount of time to reach stability. The following graph shows how the temperature in the booster volume varies over time.

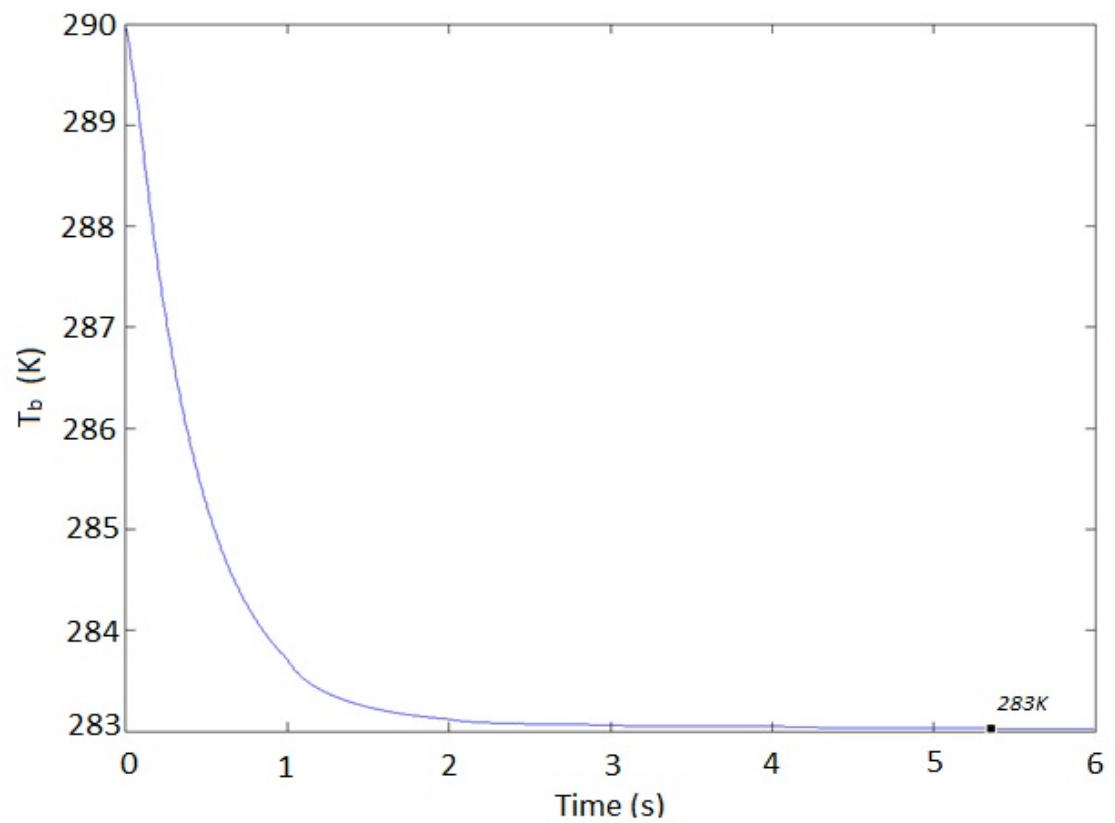


Figure 5-5: Temperature evolution in the booster chamber over time with supply temperature set lower than booster temperature

This shows that the temperature drops to approximately the temperature of the supply air within 2 seconds (approximately 95% of change).

SIMULATION 2:

The following is simulation to show the evolution of the temperature of the air in the booster chamber with the supply air temperature set higher than the initial temperatures in the chambers.

In this test the same conditions as in the previous simulation were used, except:

- Supply air temperature – 300K
- Atmospheric temperature – 293K

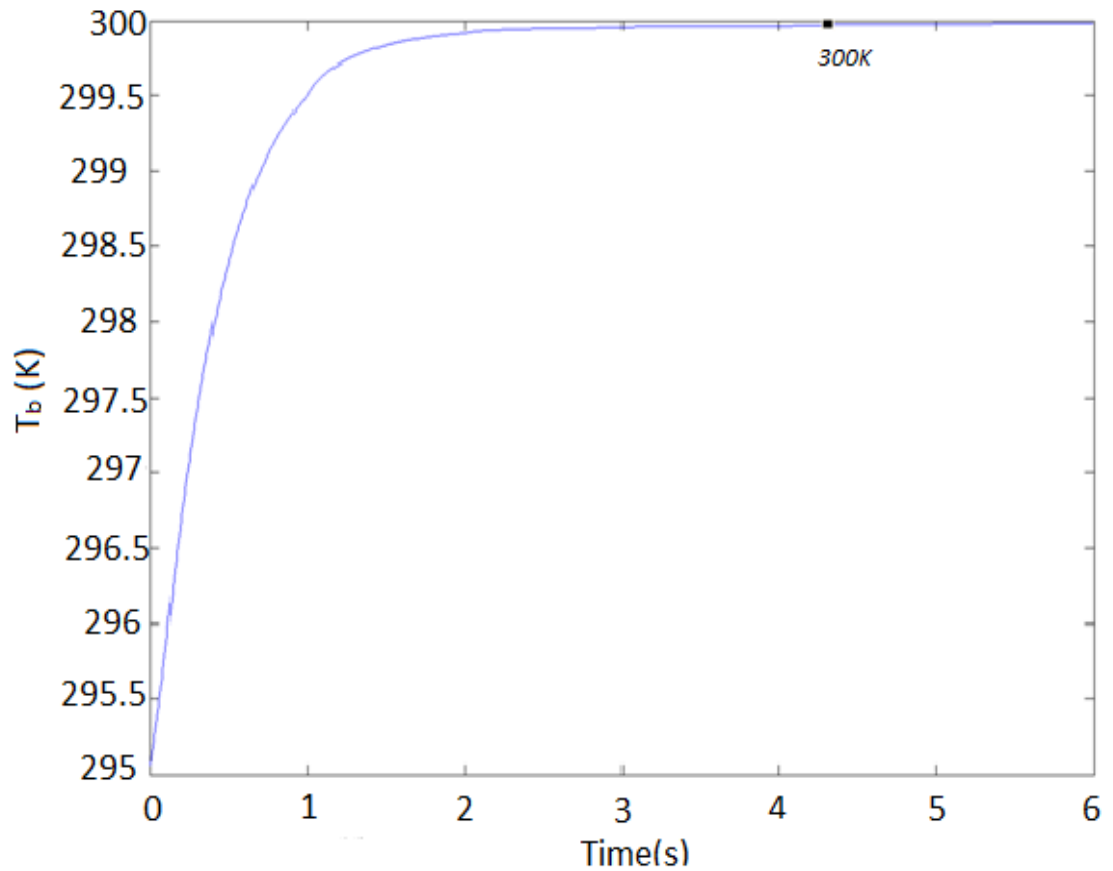


Figure 5-6: Simulation showing the temperature evolution in the booster chamber with supply temperature set higher than booster temperature

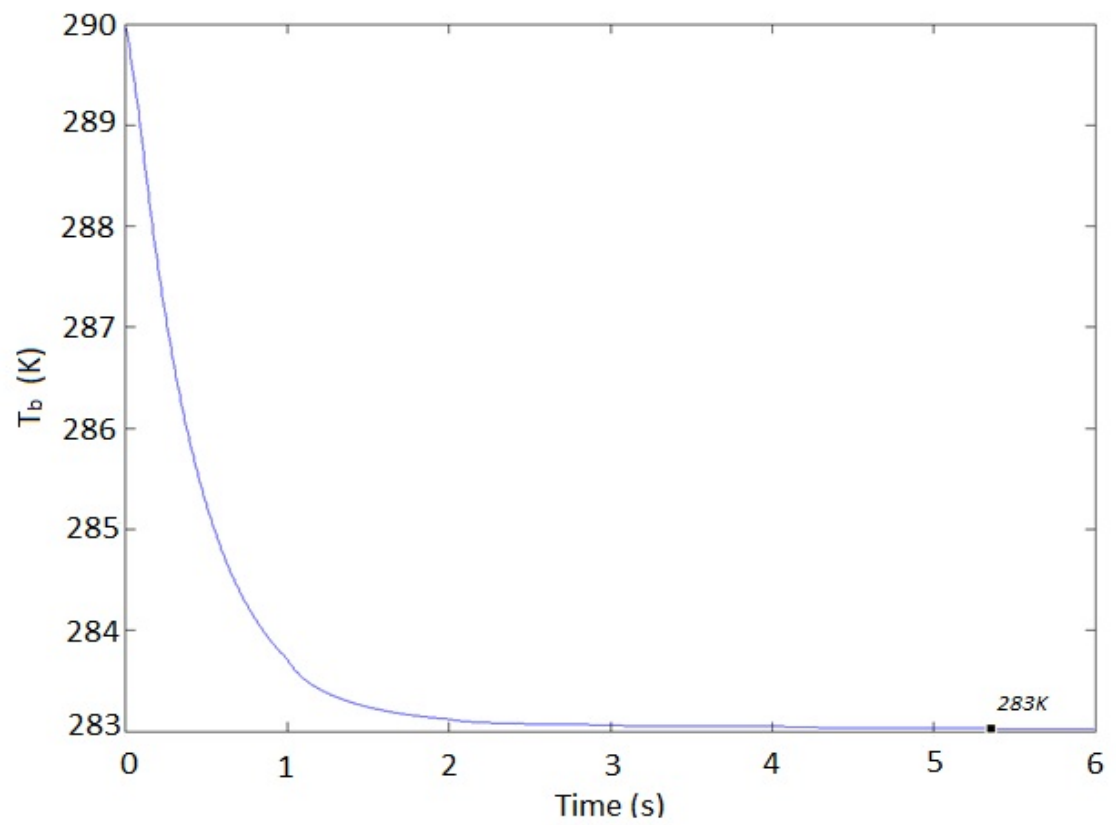


Figure 5-7: Temperature evolution in the booster chamber over time with supply temperature set lower than booster temperature

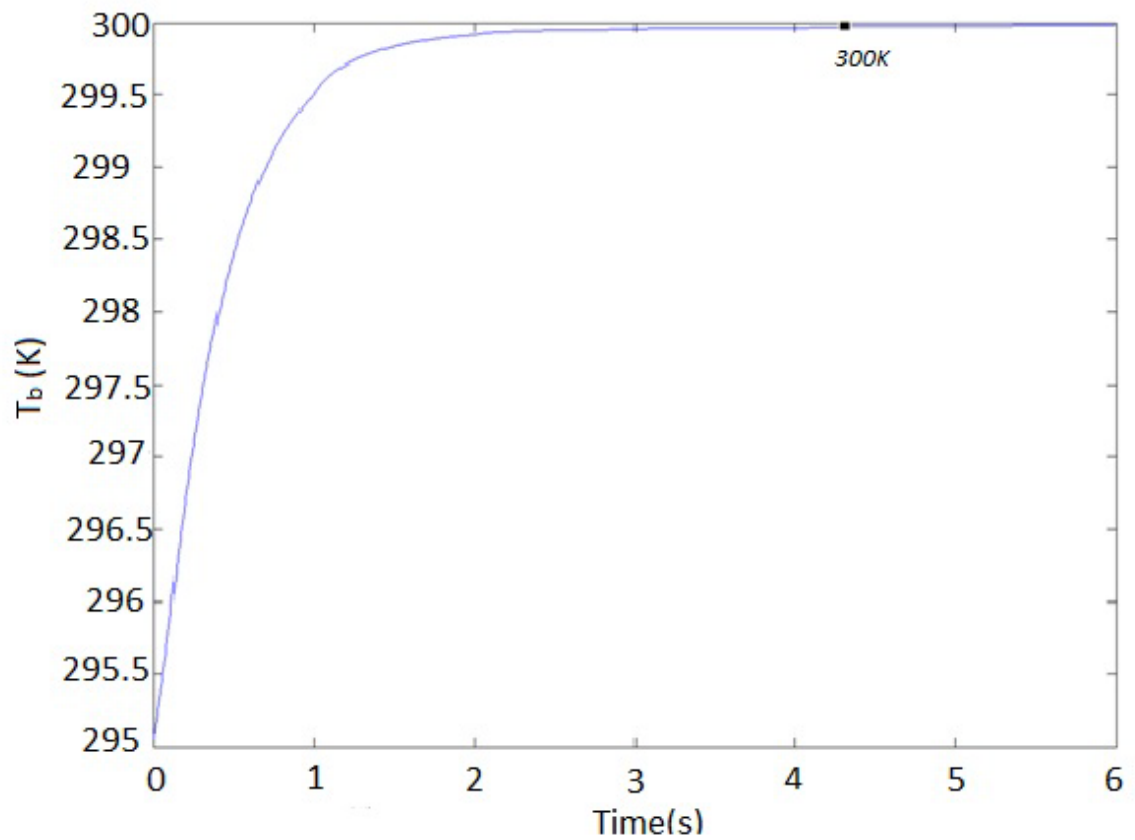


Figure 5-8: Simulation showing the temperature evolution in the booster chamber with supply temperature set higher than booster temperature.

From Figure 5-7 and figure 5-8, it shown that the temperature within the booster chamber changes within two seconds to reach approximately the same level as the supply air temperature.

6. IDENTIFICATION OF CAUSES OF UNWANTED VARIATION

6.1. Introduction

The current I/P converters are known to suffer from non-linearity at low current and permanent changes in output pressures at zero input current after thermal cycles. Orientation and vibration also affect the performance of the I/P converters. In this section the causes of unwanted performances are investigated.

6.2. Non-linearity at Low current & variation with temperature change

Non-linearity at low current ($<5\text{mA}$) was observed from experiments carried out on a few samples and the effects present at 0mA input current seem to be indicative of variations with temperature. The experiment was carried out at set temperature range (between -40°C to $+85^{\circ}\text{C}$, which is the specified operating range of the device) and by using the following step input currents: 0mA , 1mA , 2mA , 4mA , 10mA and 20mA , both the booster volume pressure and the control volume pressure were recorded by means of pressure transducers.

The following schematic shows the test configuration.

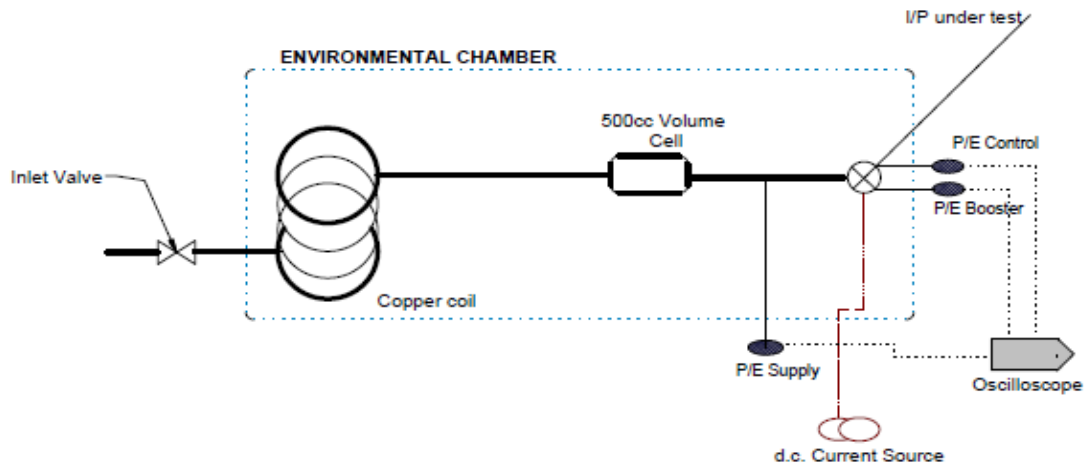


Figure 6-1: Test Setup configuration

A copper coil-tube was used to improve the thermal transfer from the environmental chamber to the supply air. To stabilise the inlet supply pressure to the test unit, a 500cc volumetric cell was used and the supply pressure was also monitored by means of a Pressure transducer (P/E). The inlet valve was adjusted such that a supply pressure of 5bar gauge was obtained. All pressure transducers used were 0-10 bar and were connected to an oscilloscope; the control chamber pressure and the booster chamber were logged from the oscilloscope. The input signal to the test I/P converter was controlled via the d.c. current source; this was programmed in the following sequence:

- 1mA
- 2mA
- 4mA
- 10mA
- 20mA

The input currents were ramped at 10s interval to allow a consistent logging time of the pressures and a sweep value of 0.1s was used to minimise overshooting of the output pressures.

A k-type thermocouple was also used to verify the temperature of the chamber and the test units were allowed to soak at the set temperatures for one hour before any readings were recorded.

The following tables list the processed value of the gains for each test unit:

Test Unit 1

T (°C)	Gain P/I (bar/A) at specified current				
	I=1mA	I=2mA	I=4mA	I=10mA	I=20mA
-40	298.5	242.3	217.1	194.3	165.4
-20	274.5	229.9	210.3	189.3	165.5
0	277.9	231.6	211.0	188.9	165.4
25	290.5	233.9	205.0	182.3	162.9
40	275.9	226.6	206.0	185.7	165.1
85	327.2	248.9	209.3	182.3	164.4

Table 6-1: Measured gain for test unit 1

Test Unit 2

Gain P/I (bar/A) at specified current					
T (°C)	I=1mA	I=2mA	I=4mA	I=10mA	I=20mA
-40	219.9	191.6	181.5	168.1	153.8
-20	246.5	209.6	196.1	179.7	164.8
0	269.2	223.6	202.6	181.6	164.7
20.4	281.2	226.6	203.6	180.5	164.3
40	296.5	232.9	201.8	179.2	164.2
85	317.9	241.3	202.5	173.1	161.9

Table 6-2: Measured gain for test unit 2

Test Unit 3

Gain P/I (bar/A) at specified current					
T (°C)	I=1mA	I=2mA	I=4mA	I=10mA	I=20mA
-40	1153.9	657.9	411.6	199.5	104.7
-20	1171.9	665.6	413.1	238.7	130.1
0	1202.5	680.9	420.5	265.5	159.9
20	1225.2	691.9	425.3	265.3	163.4
85	1301.2	753.3	455.1	275.7	165.2

Table 6-3: Measured gain for test unit 3

Test Unit 4

Gain P/I (bar/A) at specified current					
T (°C)	I=1mA	I=2mA	I=4mA	I=10mA	I=20mA
-40	277.2	236.6	216.6	201.1	164.6
-20	241.9	207.9	198.3	192.1	164.7
0	242.5	200.6	196.8	191.0	164.6
17.9	211.9	181.6	183.1	183.9	164.7
40	227.9	198.3	189.3	184.7	163.9
85	277.2	222.3	198.1	177.5	163.0

Table 6-4: Measure gain for test unit 4

Plotting the overall gain of the control volume pressure with temperature variation at different input current the following graphs were obtained:

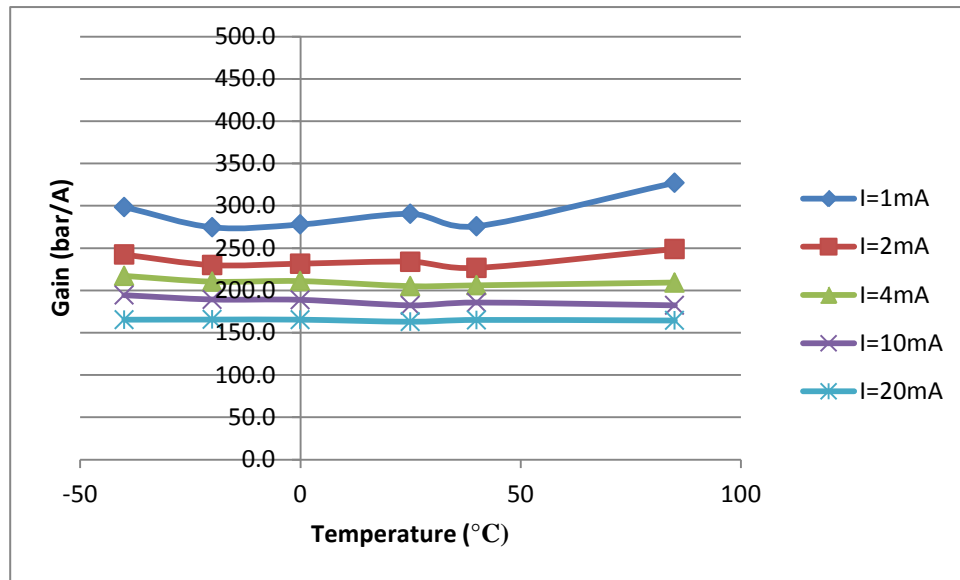


Figure 6-2: Overall gain variation of unit 1

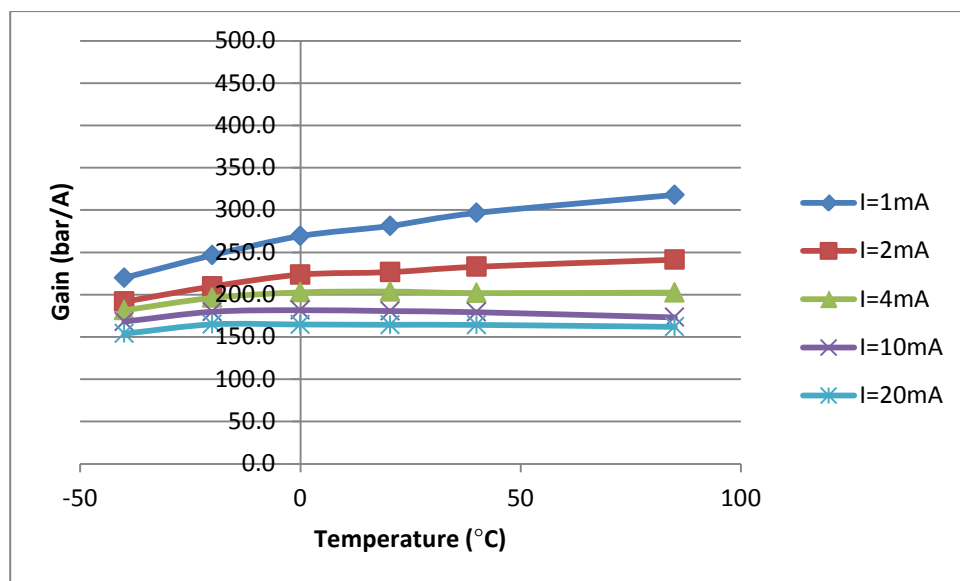


Figure 6-3: Overall gain variation of unit 2

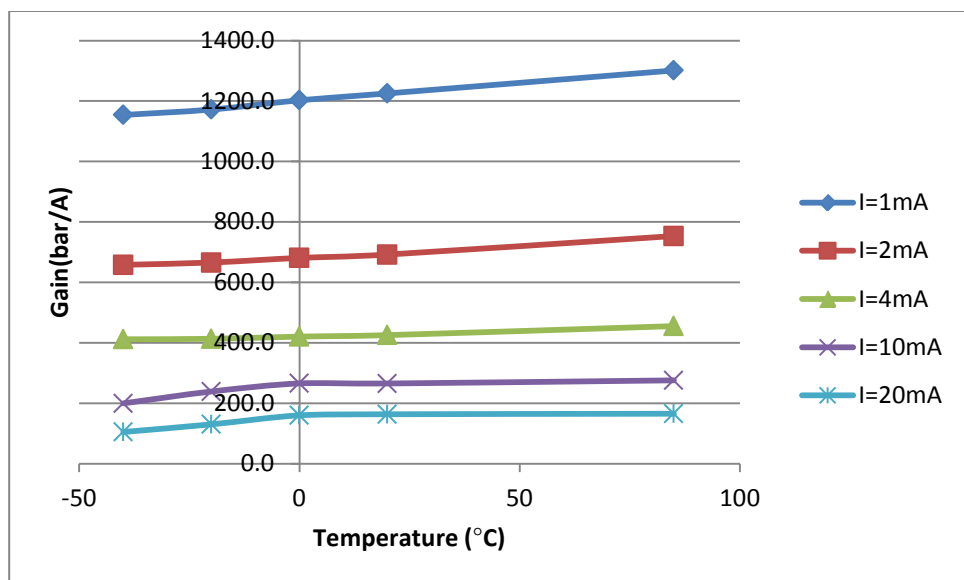


Figure 6-4: Overall gain variation of unit 3

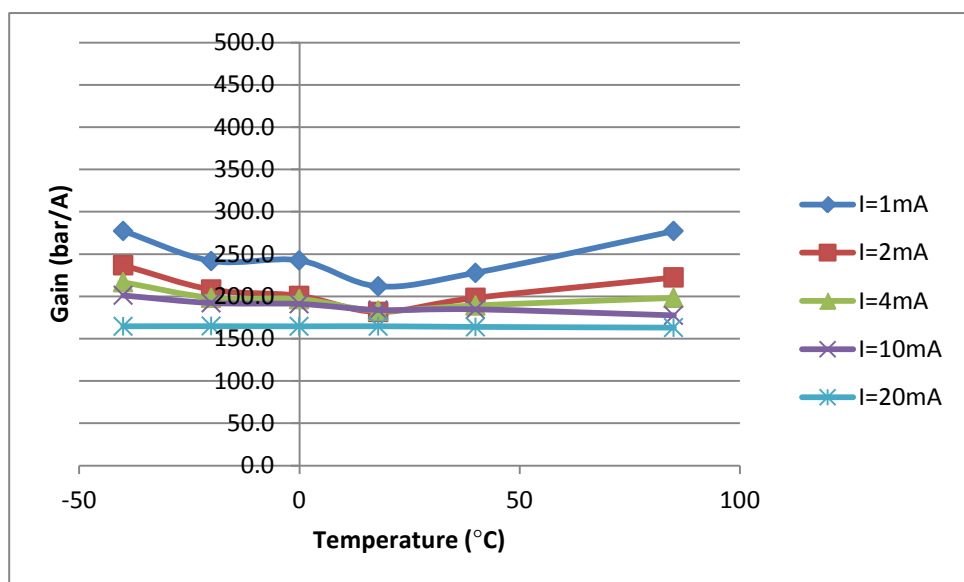


Figure 6-5: Overall gain variation of unit 4

Ideally the overall gain for each input current should be constant and have minimal variations over the full temperature range.

From the graphs, it can be seen that the control volume pressures are generally stable and linear at high current ($>10\text{mA}$), however slight inconsistencies are noted at temperatures below -20°C on some samples.

Test Unit 3 shows quite a different behaviour which appears to be explained by the fact that the nozzle had been wrongly adjusted.

6.3. Theoretical explanation of pressure variations

To better understand the root cause of the observed variation, an analysis of the output pressure at zero current is required. This is because greatest variation is seen at low currents, and this seems to be linked to the output at zero current.

The following section details the derivation of control pressure at zero current (**Note:** *this follows the work in [64]*)

By considering Bernouilli's equation (which is valid at the low pressure differences), the equivalent mass flow rate due to this pressure difference through the orifice disc is given by

$$\dot{m} = \sqrt{2 \Delta P \rho_b} A_{hole} C D_{hole} \quad (6-1)$$

Where A_{hole} is area of the hole in the orifice disc, ρ_B is the density of the fluid in the booster volume and $C D_{hole}$ is the coefficient of discharge of the orifice disc.

This mass flow rate should be same as the control volume mass flow rate, and the time constant, τ (rise-rate of the unit) can be expressed as follows

$$\tau = \frac{\rho_c V_c}{\sqrt{2 \Delta P \rho_b} A_{hole} C D_{hole}}, \quad (6-2)$$

Where ρ_c is the density of the fluid in the control volume, V_c is the control volume. This comes from the contained mass divided by the mass flow rate.

Applying conservation of mass, the mass flow rate from the booster volume should be equal to that of the control volume and eventually that mass flow rate has to exit through the nozzle-flexure opening.

The mass flow rate through the gap from the flexure and nozzle is given by (based on Bernouilli's eq.):

$$\dot{m} = \sqrt{2 P_c \rho_c} CD_{nozzle} 2\pi r_{nozzle} x \quad (6-3)$$

Where x is the gap between the flexure and the nozzle, r_{nozzle} is the radius of the nozzle,

P_c is the pressure in the control volume and CD_{nozzle} is the discharge coefficient between the nozzle and the flexure gap.

Hence, equating the mass flow rates gives

$$\sqrt{2 P_c \rho_c} CD_{nozzle} 2\pi r_{nozzle} x = \sqrt{2 \Delta P \rho_b} A_{hole} CD_{hole} \quad (6-4)$$

Making x the subject of formula

$$x = \frac{\sqrt{2 \Delta P \rho_b} A_{hole} CD_{hole}}{\sqrt{2 P_c \rho_c} CD_{nozzle} 2\pi r_{nozzle}} \quad (6-5)$$

Considering the force balance at the flexure to be in equilibrium at zero current,

$$P_c \pi r_{eff}^2 = k (x - x_0) \quad (6-6)$$

Where k is the stiffness of the flexure, r_{eff} is the effective radius through which the fluid flow in the nozzle and x_0 is the gap between the nozzle and the flexure.

Considering equation (6-5) and equation (6-6), the control pressure can be expressed as follows (with x eliminated):

$$P_c = \frac{k}{\pi r_{eff}^2} \left[\frac{\sqrt{2 \Delta P \rho_b} A_{hole} CD_{hole}}{\sqrt{2 P_c \rho_c} 2\pi r_{nozzle} CD_{nozzle}} - x_0 \right] \quad (6-7)$$

This expression can be simplified since $\Delta P = \frac{F_{spring}}{A_{diaphragm}}$, and for the case when $x_0=0$, to:

$$P_c \approx \left[\frac{k A_{hole} \sqrt{F_{spring} \rho_b} CD_{hole}}{\sqrt{2 \rho_c} 2\pi^2 r_{eff}^2 r_{nozzle} \sqrt{A_{diaphragm}} CD_{nozzle}} \right]^{\frac{2}{3}} \quad (6-8)$$

Also for convenience, the densities can be cancelled as the pressure difference

is only around 60mbar. This should not significantly impact on the accuracy of the result (by a factor of 1.04).

$$P_c \approx \left[\frac{k A_{hole} \sqrt{F_{spring}} CD_{hole}}{\sqrt{2} 2\pi^2 r_{eff}^2 r_{nozzle} \sqrt{A_{diaphragm}} CD_{nozzle}} \right]^{\frac{2}{3}} \quad (6-9)$$

Using typical values for the device in equation (6-11): $k=1000\text{N/m}$; $A_{hole}=1.96\text{e-}7 \text{ m}^2$; $F_{spring}=3\text{N}$; $r_{eff}=0.00045\text{m}$; $r_{nozzle}=0.0005\text{m}$; $A_{diaphragm}=4\text{e-}4\text{m}^2$; discharge coefficients for orifice hole is 0.3 and that of the nozzle is 0.6. P_c is around 0.208 bar which is commonly seen on existing products. This indicates the cause of variations with temperature as the spring/ diaphragm force (F_{spring}) varies with temperature around 10% over 60°C [65], it also varies with load (considering that the ball valve needs to open) and also varies from unit to unit (as shown in Figure 3-4). All of these will result in variation at zero input current and this variation will tend to be less significant as the input current is increased; the force from the current overcomes the force on the flexure (caused by the pressure) at around 5mA. Reducing the effects of this spring force should reduce variability in proportion, and also will potentially allow the improvement of the stability at low current.

Thermal effects will cause variations in some parameters. The stiffness of flexure, force of the control spring/ rubber diaphragm and coefficients of discharge are all likely to be affected by thermal variations.

From equation (6-9) it can be seen that the control chamber pressure at zero current is dependent on parameters of the flexure, orifice disc, control spring, nozzle and rubber diaphragm. Altering any of these identified parameters will impact on the control pressure.

6.4. Orientation and Vibration effects

The mass of the flexure/ coil assembly has some influence on the overall performance of the I/P converter as shown by equation 3-13. The flexure acts as a structure which supports the flapper and the coil but considering the current design, the masses of the coil and the flapper are not balanced. In following schematics the interactions of the forces on the flapper at various orientations (electromagnetic forces have been neglected) are represented.

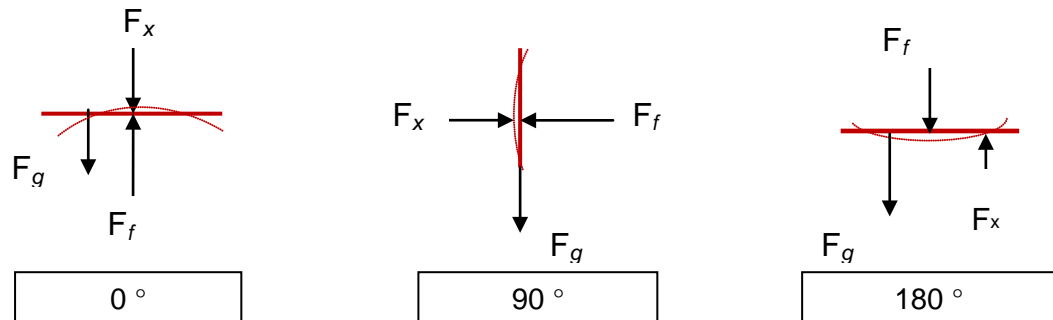


Figure 6-6: Interaction of forces on flexure under various orientation conditions

In the upright position, the gravitational force (F_g) on the mass of the coil/flexure and elastic force (F_x) of the flexure oppose the fluidic force (F_f).

When the I/P converter is oriented on its side at 90°, the gravitational force due to the mass of the coil/ flexure act in a vertical axis and will not influence the forces which are acting horizontally. This results in the interaction of only the elastic force and the fluidic force.

In a 180° tilt, the elastic force will act in an upward direction as the flexure will deform downwards.

Assuming equilibrium condition, the interactions of the fluid force for the different orientations can be represented by the following equations:

$$0^\circ \quad F_f = F_x + F_g \quad (6-10)$$

$$90^\circ \quad F_f = F_x \quad (6-11)$$

$$180^\circ \quad F_f = F_x - F_g \quad (6-12)$$

Based on Equation (6-10), Equation (6-11) and Equation (6-12) the resultant force when a current is applied will be different for each orientation and hence since the output pressure is a function of this resultant force, a pressure variation will be seen at each orientation.

Vibration of the system will also affect the output pressure as the mass of the coil/ flapper is not balanced. The I/P converter can encounter vibration when in operation; it can be used on oil and gas pipeline where small vibrations are often seen or it can be used in applications which are critical even in the event of an earthquake whereby the magnitude of vibration can be quite considerable.

Taking into account the effect of vibration the resulting control pressure (P_c) from equation (3-13) is modified to

$$(P_c - P_0) = \frac{d.I - k(x_2 - x_{20}) - mg - mA_{external}}{\pi r_{eff}^2}, \quad (6-13)$$

where $A_{external}$ is the acceleration due to external vibration, m is the mass of the combined flexure- coil assembly.

6.5. Summary

In this chapter, the observed non-linearity at low currents and the variations with temperature change have been investigated. A theoretical explanation of the observed pressure variations has been carried out by finding the control pressure at zero input current to be reflective of the parameters of influential components. By using typical values in this derived expression for the control pressure, it is found that the theoretical value for the control pressure at zero input matches the experimental value. The last part of this chapter is mainly focused on how the control pressures can be affected by the orientation and vibration of the device.

7. OPTIMISATION

7.1. Introduction

This chapter is a follow-up of the theoretical investigation carried out in earlier chapters; it investigates how changing some of the identified parameters can improve the overall performance of the I/P converter. Ideally the optimised I/P converter should have better stability with temperature change, better linearity at low current and be more immune to vibration than the current TR140 I/P converter.

7.2. Potential improvements

Based on the effects of identified parameters on the output at zero current input, the significance of optimising any of these parameters can be estimated.

$$P_c \approx \left[\frac{k A_{hole} \sqrt{F_{spring}} CD_{hole}}{\sqrt{2} 2\pi^2 r_{eff}^2 r_{nozzle} \sqrt{A_{diaphragm}} CD_{nozzle}} \right]^{\frac{2}{3}} \quad (7-1)$$

Ideally P_c should be zero at zero input current. A low magnitude of P_c could be expected by reducing any values of parameters in the numerator and likewise increasing the values of parameters in the denominator will have similar effect. However certain changes will have some impact on performance, for example reducing the orifice disc hole size will reduce the slew rate and increase the tendency to block.

The effects that give a non-zero output pressure at zero current affect the output (to a reduced degree) at low currents and seem likely to be key to an improved design, because it is at low currents where the gain variation is greatest.

From the analysis of the equation 7-1 some practical solutions to improve the zero current output are listed below:

- Reduce the spring force

- Reduce the flexure stiffness
- Decrease the orifice hole
- Increase the area of the rubber diaphragm
- Increase the nozzle area

Other improvements in form of correction control can be considered:

- **Use of an Open-loop current correction**

This method could compensate for the output pressure shift due to the effect of the spring force, especially at low current.

- **Use of an Open-loop current correction with temperature sensor**

By making use of a temperature sensor, the input current to the coil is adjusted accordingly to compensate for known shifts in the output pressure with temperature.

- **Use of an electronic Closed-loop control**

A closed-loop control method could make use of a pressure transducer which will sense the output pressure and adjust the input signal (current to the coil) to give an ideal output pressure. The performance of the overall I/P will be dependent on the pressure transducer; any anomalies seen by the transducer will be reflected in the output pressure. An additional consideration is powering the transducer and control circuit, which must be able to run off the small control current, often only a milli-amp or so.

- **Others:** Mechanical compensation- novel way of flexure design (further discussed in next section)

The following table assesses the practicability of these solutions

Solution	Strength	Weakness	Threat
Reduce spring force	Easy replacement	Affects start-up pressure (response time).	Still affected by temperature
Reduce flexure stiffness	Fairly easy to implement	Design and material limitations. Possible breakage.	Still affected by temperature. Potential vibration issues. Might affect durability.
Reduce orifice hole	Fairly easy to implement	Susceptible to blockage. Will increase response time.	Debris in flow might be an issue. Discharge coefficient will change.
Increase area of diaphragm		An increase of 10x is required for same effect of 10x reduction in force. Slew rate is affected.	Increase in overall size of device (approximately three-fold increase in width).
Increase nozzle area	Quick replacement	Pressure per current (gain) is reduced in proportion to radius squared.	
Open loop control	Compensates for effects of spring force. Can bring additional features to device.	Temperature dependence (viscosity of air and stiffness of springs and rubber).	Can be subject to inaccuracy due to variation in booster spring forces.
Open loop control with temperature sensor	Compensates for effects of spring force taking as temperature changes. Can allow the monitoring of temperature.	Requires powering	Inaccuracy due to variation in booster spring forces.

Closed-loop	Improved performance and compensates for temperature changes and variability from device to device.	Depends on how good the pressure sensor is.	Increased cost and problem in powering the device at low input currents (as it cannot have a separate power supply)
-------------	---	---	---

Table 7-1: SWOT analysis of identified potential solutions to improve the performance of the I/P converter at zero current input

7.3. Mechanical compensator – New Flexure Design

A careful study of the mechanism of the actual flexure-nozzle design gives a better understanding of the effects caused by the stiffness of the flexure.

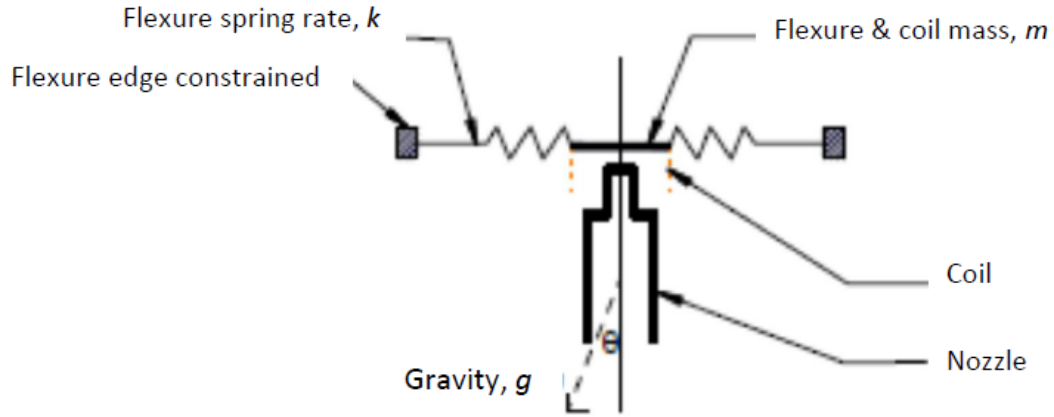


Figure 7-1: Schematic of current flexure-nozzle arrangement

P_c can be expressed as (considering a simple balance of forces);

$$P_c = \frac{Id + k(x - x_0) + mg \cos(\theta_1) + mA_{external}}{\pi r_{eff}^2}, \quad (7-2)$$

Where d is the force per unit current from the coil (in the magnet configuration), k the stiffness of flexure, m is the mass of the suspended part of the flexure, g is the acceleration due to gravity, θ_1 is the angle between the direction of gravity and the axis of the nozzle, and $A_{external}$ is the externally induced acceleration (caused by vibration). r_{eff} is the effective radius through which the fluid flows.

However, what is desired is

$$P_c = \frac{Id}{\pi r_{eff}^2} \quad (7-3)$$

Implying the ideal design would be one without

$k(x - x_0)$, $mg\cos(\theta_1)$ and $mA_{external}$.

The first term, $k(x - x_0)$ is due to the force required to deflect the flexure as its circumferential edge is clamped. It should be noted that the value of k is quite considerable when compared to the other parameters. Also the force to deflect the flexure is dependent upon temperature, load and booster-to-booster variation.

The $mg\cos(\theta_1)$ term is the force required to support the mass. When the device is tilted by over 90° , it would cause a change of approximately 0.1bar for a 1mm diameter nozzle (this has been confirmed by experiments).

The last term, $mA_{external}$ represents the force arising from external vibration.

7.4. Balance Beam

The balance beam configuration proves to be the most suitable solution which in theory can eliminate all the unwanted causes of variation. The system is shown as follows:

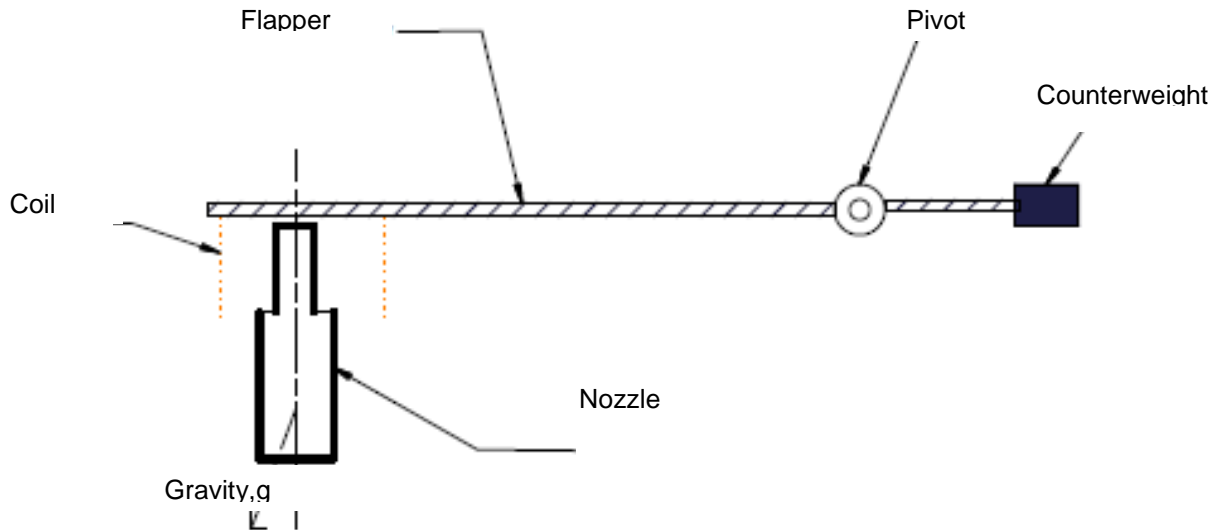


Figure 7-2: Schematic of balance beam-nozzle arrangement

This new configuration will only lead to a change in the flexure design and have additional features such as hinge support, counterweight and a pivot.

The electromagnetic force on the flapper brings it down against the nozzle where it is counteracted by the fluid force which is proportional to the pressure. In theory, the output pressure is

$$P_c = \frac{I \cdot d}{\pi r_{eff}^2}$$

This is desired since the following conditions have been satisfied:

Since the structure does not have any stiffness element which directly affect the operation of I/P converter $k(x - x_0)$ has been eliminated. This in turn removes any dependence on the temperature, load and booster mechanism variations.

By using a counterweight, the second element of $mg\cos(\theta_1)$, the component of force resulting from the mass of the flexure and coil cancels out. This stands true only if the centre of gravity of left and right sides lie on the same axis as the centre of the hinge.

Finally the force created from external vibration $mA_{external}$, can also be terminated with this new design; the counterweigh balance will keep the beam in equilibrium and hence any external acceleration will not have any effects on the system. This is only valid if the flexure remains straight and flat.

However, rotational acceleration about the hinge would have an effect on the output pressure, though this is considered to be a less frequent mode of vibration.

7.4.1. Design and Component sizing

The sizing of the components with regards to their weight is a very important criterion for this concept. For a suitable sizing exercise of the components, the torque exerted by flapper and the coil under static condition is considered.

Based on the fact that the five holes featuring in the current flexure have been designed to allow the exhaust air from the nozzle to escape easily, these features have been retained for the new design.

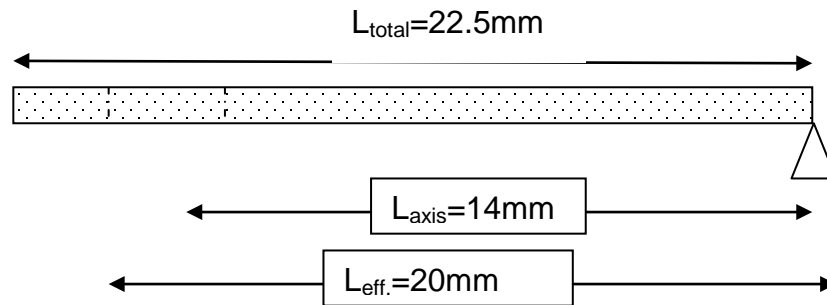


Figure 7-3 shows the schematic of the flapper and the pivot with corresponding lengths.

The beam being of non-uniform shape due to the five holes as illustrated in figure 7-4, the effective length (L_{eff}) of the beam having uniform weight distribution is estimated as 20mm.

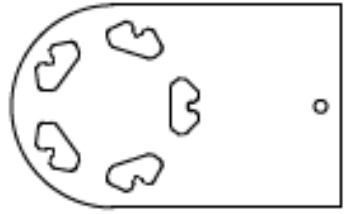


Figure 7-4: Top view of flapper showing 5 holes

The flapper has a thickness (t) of 0.156mm, a width (w) of 12.5mm and the distance from the nozzle axis to the pivot point is estimated at 14mm. The density of material (ρ_{copper}) used for the flapper is based on Beryllium Copper alloy [66] as taken as 8500kg/m³.

The mass per unit length (M_L) of the beam is given by

$$M_L = w \times t \times \rho_{copper} \quad (7-4)$$

$$= 12.5 \times 10^{-3} [m] \times 0.156 \times 10^{-3} [m] \times 8500 [kg/m^3]$$

$$= 0.016 kg/m$$

Hence the torque from the weight of the flapper ($\tau_{flapper}$) is given by

$$\tau_{flapper}$$

= distance along flapper length \times mass per unit length of flapper \times gravity

$$\tau_{flapper\ eff.} = g \int_{x=0}^{x=14mm} 0.016x \cdot dx$$

$$= \frac{0.016g [x^2]_0^{0.014}}{2}$$

$$= 1.61 \times 10^{-5} Nm$$

Adding the torque from the weight of the coil (τ_{coil}):

The mass of the coil is typically 0.45g,

$$\tau_{coil} = \text{distance from pivot} \times \text{mass of coil} \times \text{gravity}$$

$$\tau_{coil} = 14 \times 10^{-3} [m] \times 0.45 \times 10^{-3} [kg] \times 9.81 [m^{-2}]$$

$$= 6.18 \times 10^{-5} Nm$$

The total torque resulting from the combined weight of the flapper and coil (τ_{total}) is

$$\tau_{total} = 6.18 \times 10^{-5} Nm + 1.62 \times 10^{-5} Nm$$

$$= 7.8 \times 10^{-5} Nm$$

From this torque value, the counterbalance mechanism can be sized. The following method outlines calculation for the counterbalance mechanism which consists of a rod and nut(s). The nut gives the flexibility of adjusting the torque. Both the rod and the nut are made out of brass and the length of the rod is L .

The torque resulting from the weight of the rod is given by:

$$\tau_{rod} = g \int_0^L \rho_{brass} \frac{\pi D^2}{4} L \cdot dL \quad (7-5)$$

$$\tau_{rod} = g \left[\rho_{brass} \frac{\pi D^2}{8} L \right]_0^L$$

Including the effect of the nut, the total torque for the counterbalance mechanism ($\tau_{counterbalance}$) is given by:

$$\tau_{counterbalance} = g \left[\rho_{brass} \frac{\pi D^2}{8} L \right]_0^L + \# m_{nut} g L \quad (7-6)$$

Where $\#$ is the number of nuts, m_{nut} is the mass of the nut and g is gravity.

For a perfectly balanced status, $\tau_{counterbalance}$ should be equal to τ_{total} (which is the combined torque of the coil and flapper).

7.4.2. Prototype I

Prototype I was built to demonstrate the basic working principle of the balance beam concept. The main components used in this version consist of a machined flapper (150 μ m thick), a coil of approximately 250 Ω , a pivot (made out of a 1mm drill bit), a 25mm long brass rod (2mm diameter) and an M2 brass nut (as counterbalance).

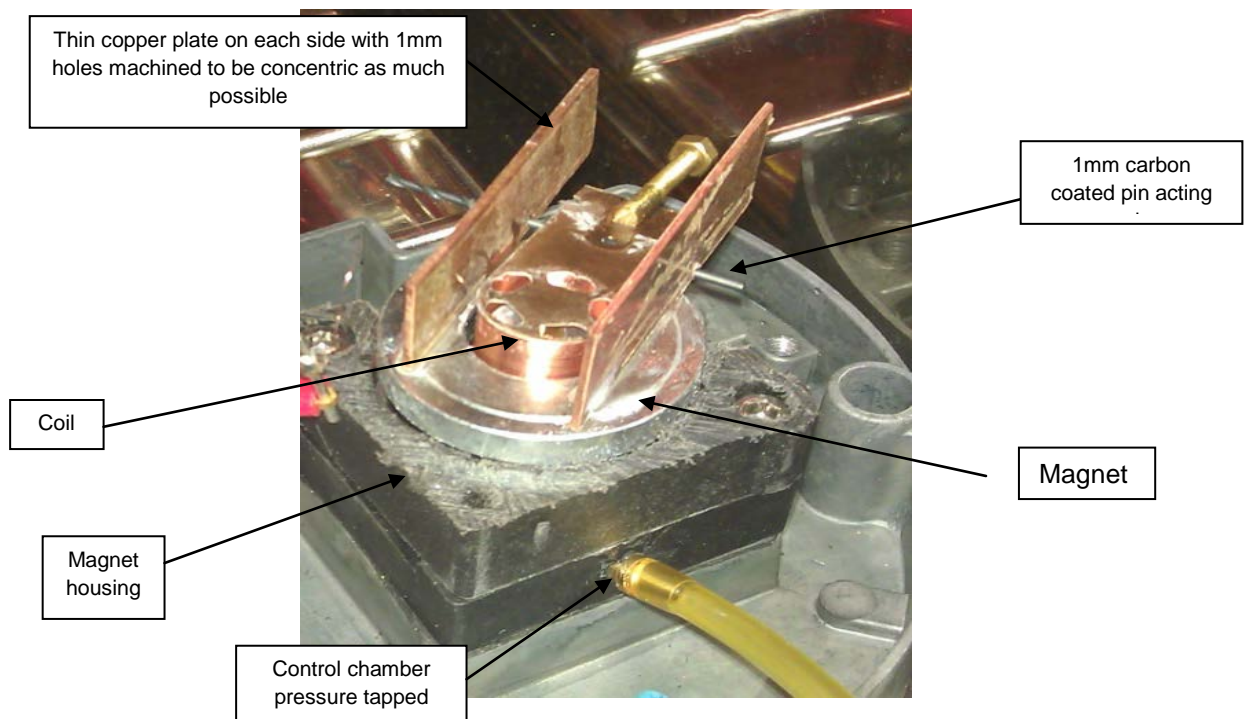


Figure 7-5: Prototype I with components

A test was carried to evaluate the effect of the counterbalance mechanism on the overall gain performance.

	Without Counterweight	With Counterweight	Without Counterweight	With Counterweight
Input signal (mA)	Output Pressure (bar g)	Output Pressure (bar g)	Gain (bar/A)	Gain (bar/A)
0	0.107	0.007	-	-
1	0.266	0.174	266	174
2	0.463	0.360	232	180
3	0.627	0.538	209	179
4	0.782	0.710	196	178
5	0.956	0.901	191	180
6	1.113	1.071	186	179
7	1.256	1.234	179	176
8	1.393	1.396	174	175
9	1.523	1.557	169	173
10	1.694	1.709	169	171
15	2.500	2.487	167	166
20	3.347	3.240	167	162

Table 7-2: Measured output pressures from unit

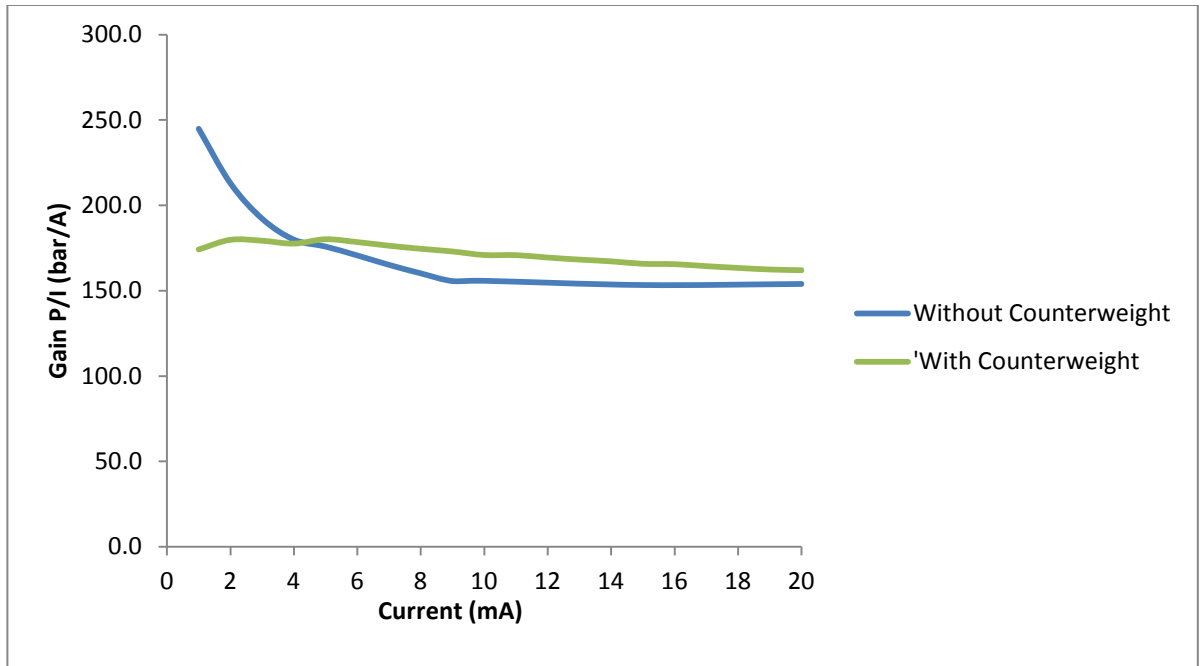


Figure 7-6: Graph of gain with regards to input current for unit with counterweight and without counterweight

Without the counterweight as shown in Figure 7-6, the overall gain flattens down at around 7-8mA, this is mainly due to the fact that the torque provided by the electromagnetic attraction is much more significant than the torque resulting from the counterweight.

With the counterweight adjusted such that it was providing a torque of approximately $7 \times 10^{-5} Nm$, the overall gain became more uniform. The output pressure at zero current dropped to 7mbar from around 140mbar, this was caused by the absence of a spring stiffness, and the counterweight compensating for the weight of the flapper and coil.

7.4.3. Prototype II

Prototype II was built to show the repeatability and to evaluate the performance of the balance beam concept when manufactured. Five units were built and tested.

This prototype consisted of an aluminium beam (1mm thick on the coil end), 2mm diameter threaded copper rod, 2x M2 copper nuts, 2x PTFE coated steel rods which act as the pivot and a brass ring support which accommodates the hinge. The treaded copper rod and the nuts act as counterweight.

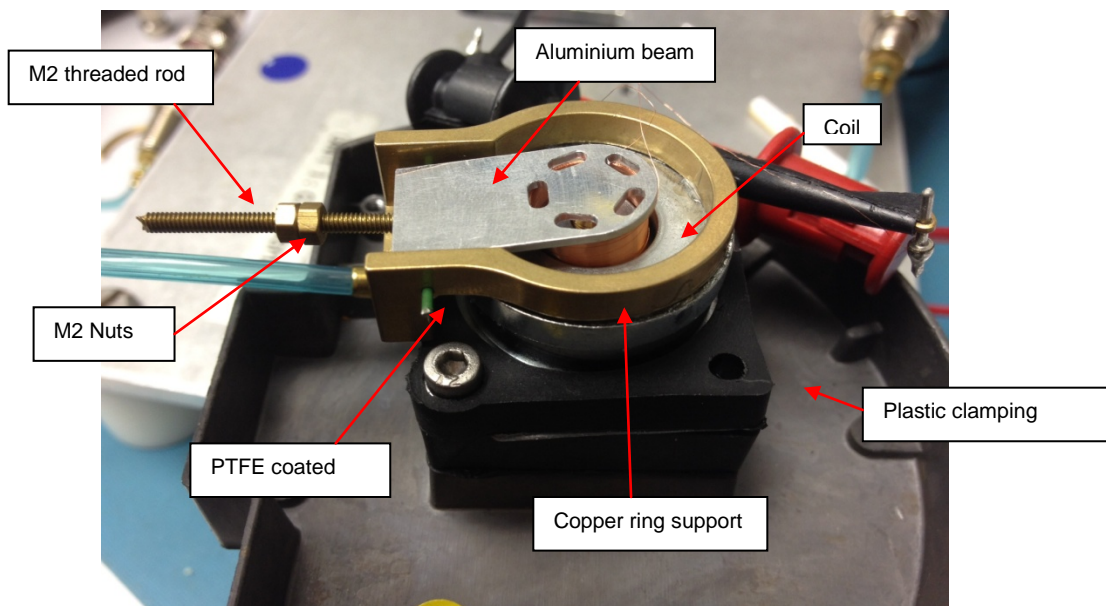


Figure 7-7: Prototype II with various components

A test was carried out on a unit of Prototype II to evaluate the performance in relation to the type of balancing of the counterweight. The following graph shows the responses for the pilot:

- Neutral or mechanical balance (balanced with air supply off)
- Balanced at 1mA (balanced in a way that the gain at 1mA is same as 20mA)
- Unbalanced (without counterweight)

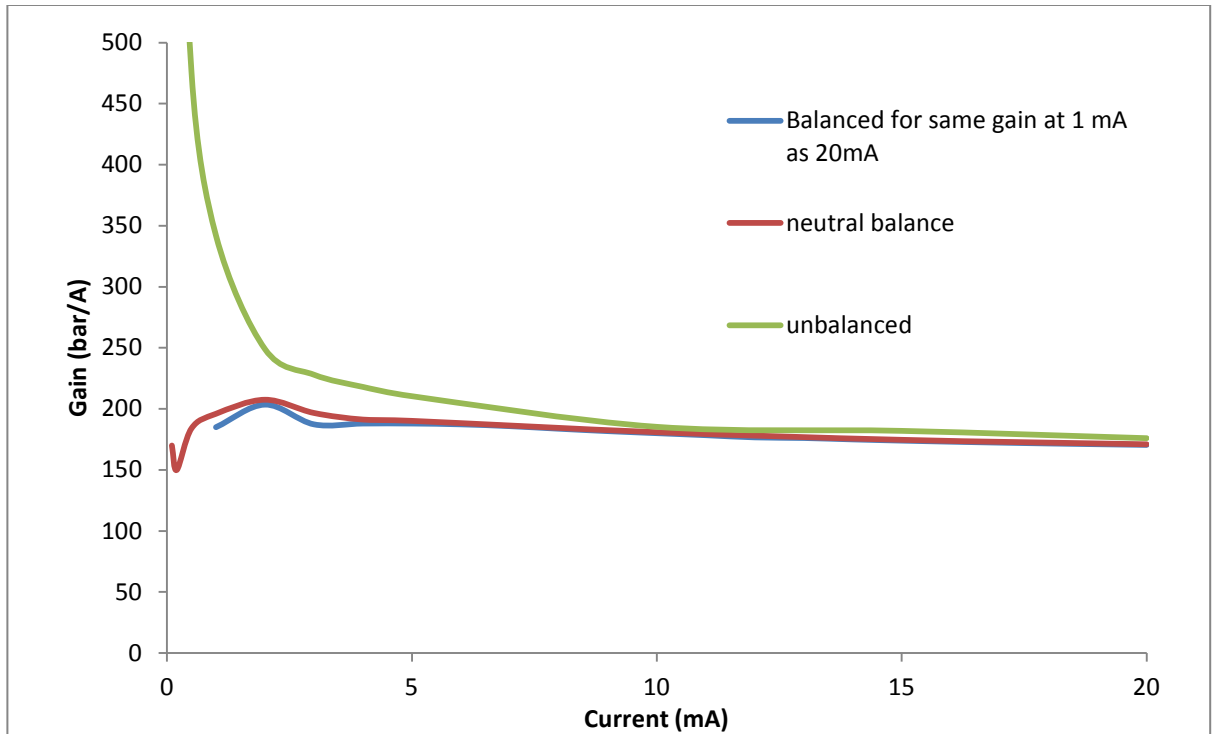


Figure 7-8: Graph showing comparison between neutral balance, 1mA balanced and unbalanced

With the unit balanced at 1mA, the gain tends to be slightly more linear at the low current than when the unit is neutrally balanced. It should be noted that the rise at low currents ($<0.5\text{mA}$) is due to the remaining output pressure at zero input current.

The following graph shows the results of the overall gain for the five units subjected to test.

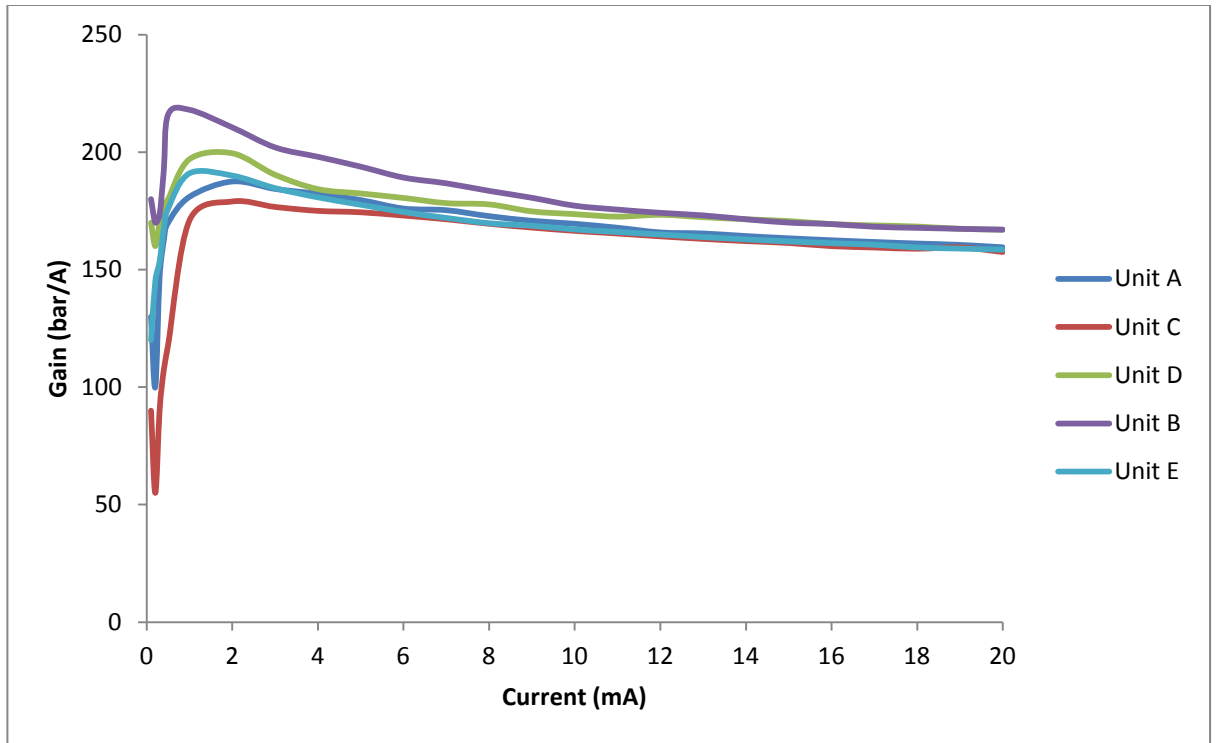


Figure 7-9: Graphs of gain for measured Prototype II units

It can be seen from Figure 7-9 that the measured gains for the five units are very similar in comparison to a similar test on the original unit.

Three units were subjected to thermal tests to see how the overall gains vary with temperature change. The following graphs show the results obtained from the test.

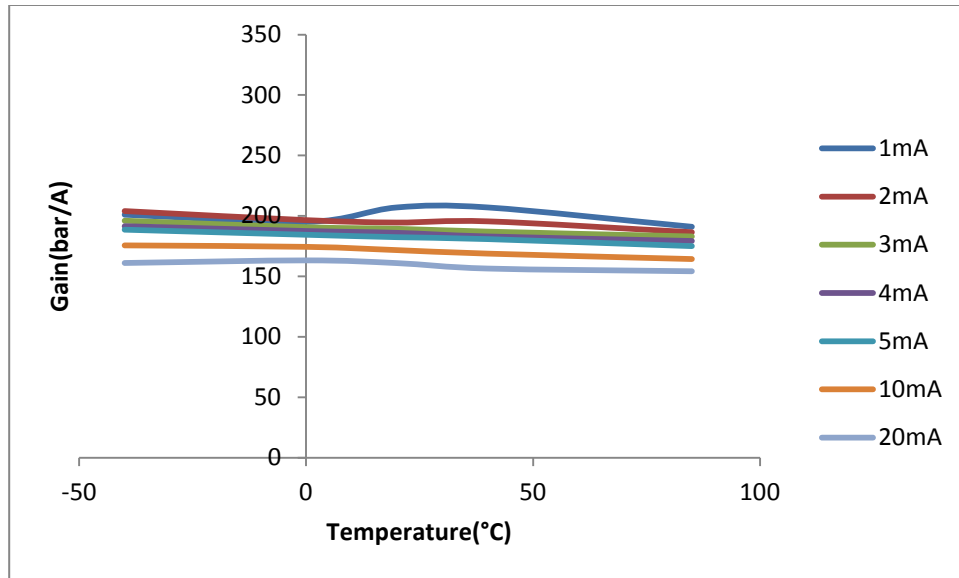


Figure 7-10: Overall gain distribution over -40°C to +85°C for unit C

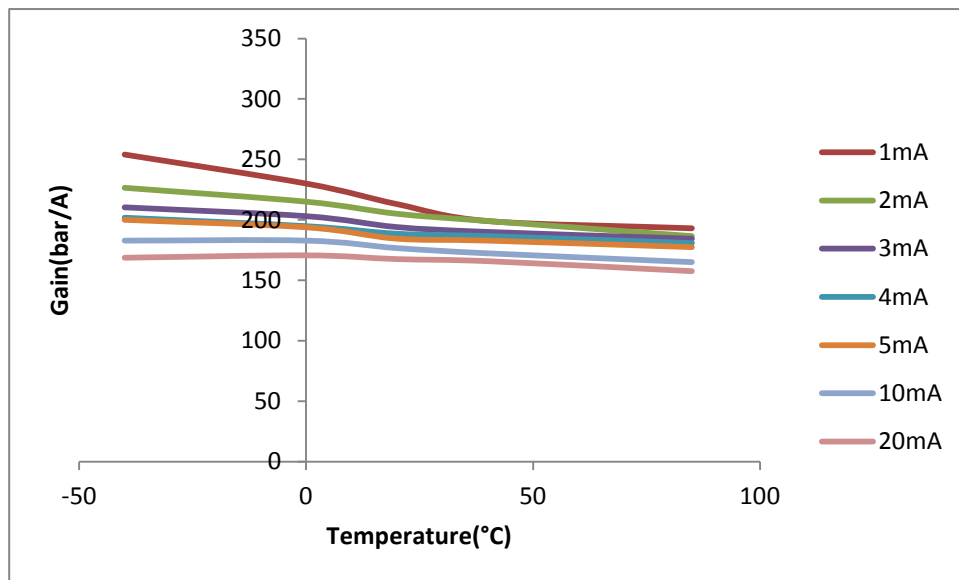


Figure 7-11: Overall gain distribution over -40°C to +85°C for unit D

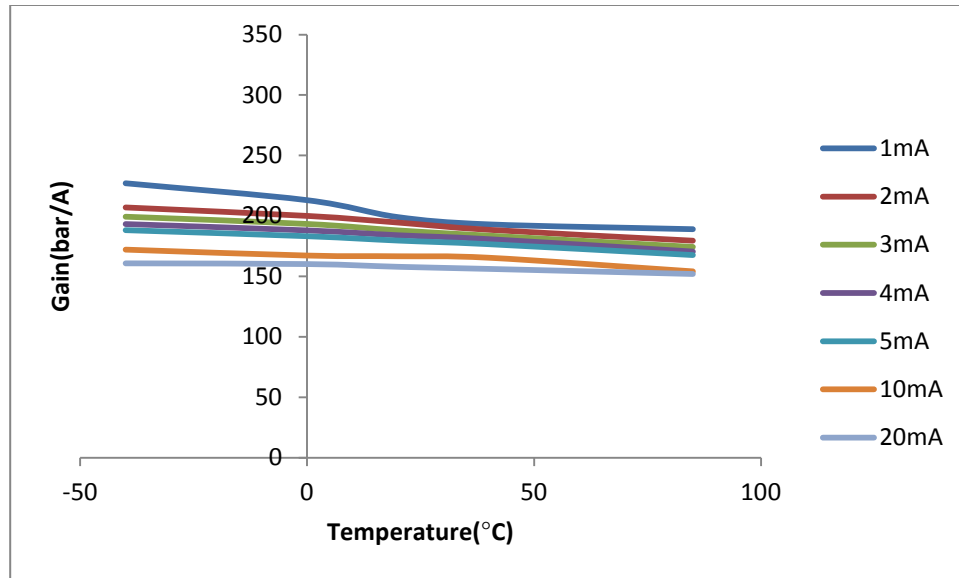


Figure 7-12: Overall gain distribution over -40°C to +85°C for unit E

From Figure 7-10, Figure 7-11 and Figure 7-12 it can be seen that the overall gain distributions for the units under thermal test are considerably uniform over the temperature of -40°C to +85°C.

The small variation in overall gains at low current (1mA) can be attributed to the fact that the nuts moved along the threaded rod during the test. This particular movement affected the torque of the counterweight mechanism.

The pivot (PTFE coated rod) was also noticed to be free to move axially and this led to either the coil rubbing against the magnet, or else the beam to rub against the copper ring support.

How freely the pivot can rotate in the holes (situated in the copper ring support) will influence the hysteresis performance of the unit because of frictional forces in the bearings. The following graph shows the measured hysteresis error (%) based on a simple 21 points test (i.e. the output pressures were recorded at 10% intervals from 0% - 100% of input signal and from 100% - 0% of input signal). These hysteresis errors are relative based on the unit measured span.

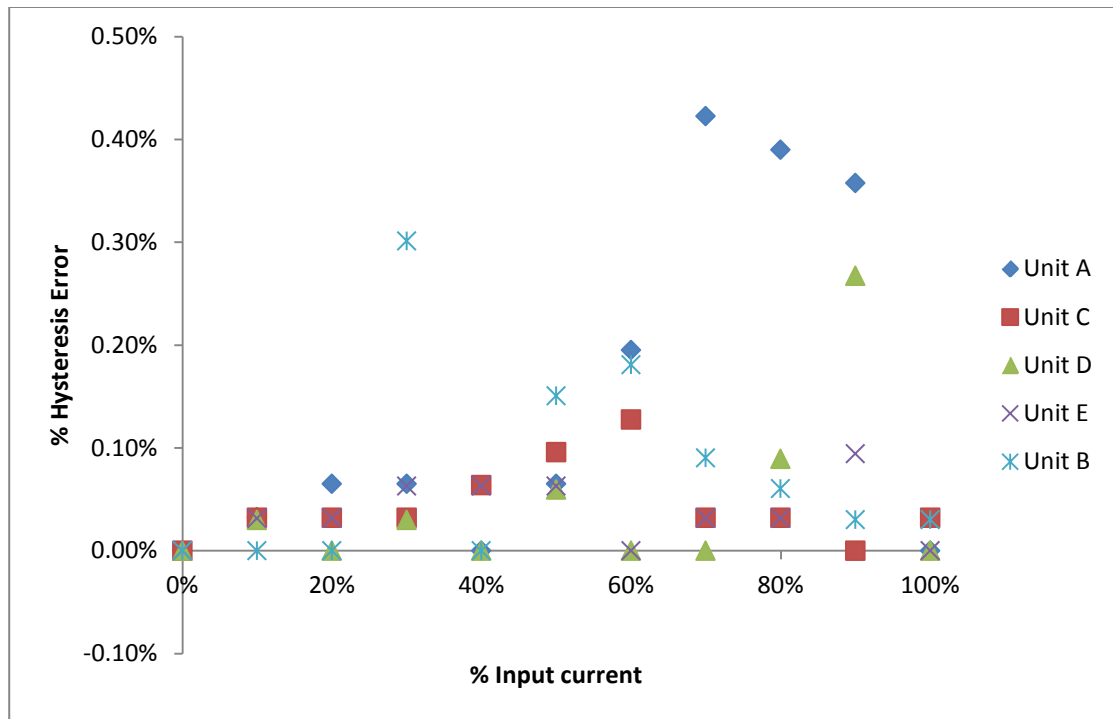


Figure 7-13: Hysteresis errors of Prototype II units

It can be seen from the above figure that the hysteresis errors are significant, with the highest level reaching around 0.4% of measured span. This led to the next prototype – prototype III.

7.4.4. Prototype III

The bearings used in prototype II were considered likely to be the source of the observed hysteresis. The friction coefficient between the PTFE surface of the pivot and the brass holes in the supporting ring is estimated to be around 0.04 [67]. Lowering this value should improve the hysteresis behaviour of the system. Ball bearings were chosen due to their low friction values (between 0.001 - 0.0015) [68,69].

The new prototype design was improved to take into account the robustness of the overall mechanism (by providing a secured positioning of the pivot and reliable counterbalance mechanism). The following picture shows a Prototype III unit.

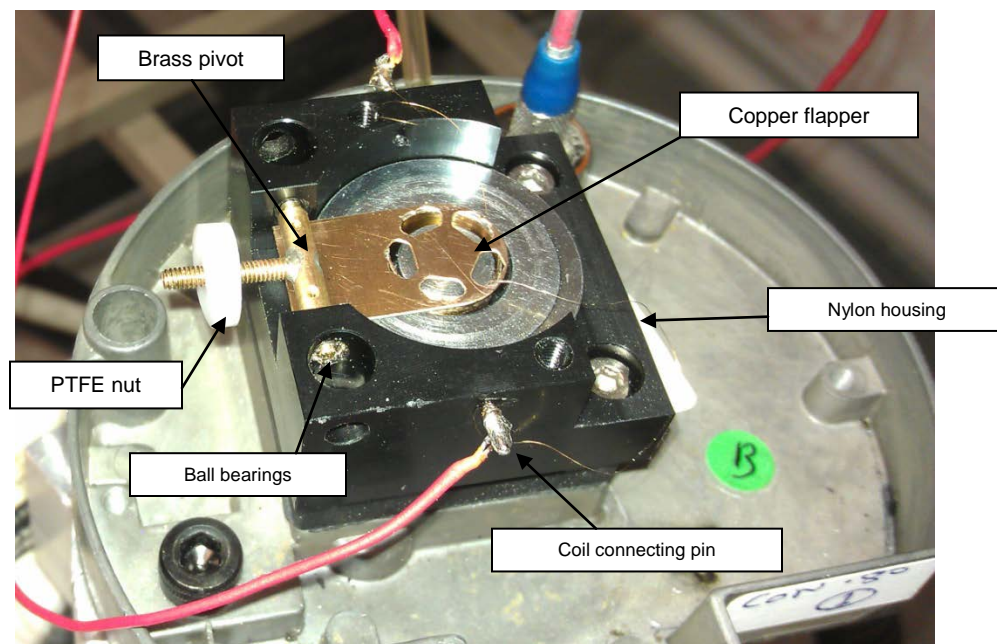


Figure 7-14: Prototype III with constituent components

To demonstrate the improvement in performance by using the ball bearings, a 21 points test was carried on four units of Prototype III and the hysteresis errors (%) are shown in the following graph. The errors are based on the units' measured span.

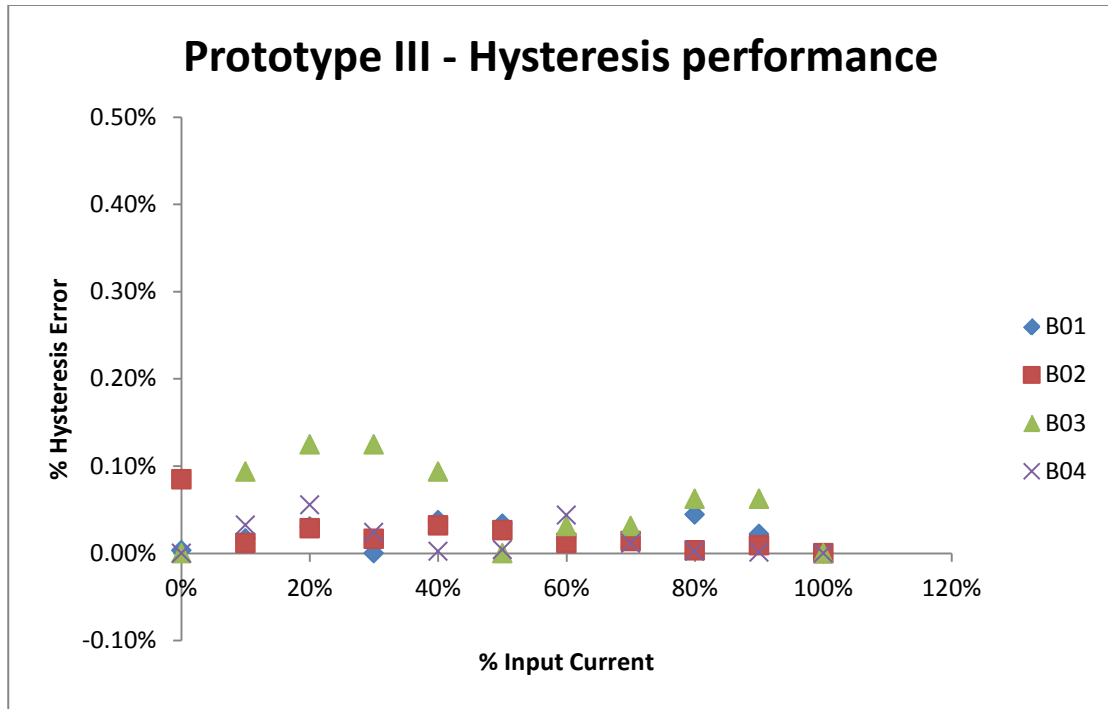


Figure 7-15: Hysteresis error of Prototype III units

Comparing the results from Figure 7-13 and Figure 7-15, it can be seen that the hysteresis errors are much lower for Prototype III units than Prototype II.

With the Prototype III the overall hysteresis errors have been lower when compared to Prototype II. The maximum hysteresis error on Prototype III is around 0.10% of measured span, almost an improvement of 3 fold from Prototype II. As discussed earlier, this seems to be a result of lower friction bearings.

7.5. Testing and performance comparison

This section discusses the tests which have been carried out on actual TR140 I/P converters and prototypes of the optimised version. These tests were carried out to evaluate and to compare the performance.

To evaluate the performance of the balance beam I/P converter the following tests were carried out:

- Gain performance at room conditions
- Gain performance with varied temperature
- Response under vibration

These tests were also carried out on the original TR140 I/P converters to provide data for comparison.

7.5.1. Testing to investigate the overall gain of the I/P converters

For comparison purposes, the overall gains of the balance beam prototype and the original voice coil I/P converter are shown. This comparison acts as a good platform to distinguish the performance of each.

A test to find the output pressures on a sample of 4 of each I/P converter configuration was carried out. The output pressure (from the pilot) was monitored and recorded. The tests were carried out at room ambient conditions and the supply pressure was kept uniform at 5 bar gauge.

The following graph shows the overall gain of four samples of the original I/P converter (voice coil) and four samples of the balance beam I/P converter (prototype III). At low currents the gains for the 'original' I/P converters are very high and are non-linear until around 3 - 4mA. The main causes of this observed behaviour have been discussed in Chapter 6 (Identification of root causes of unwanted variations). The overall gains for the balance beam follow a more linear trend which starts at currents inputs as low as 1mA.

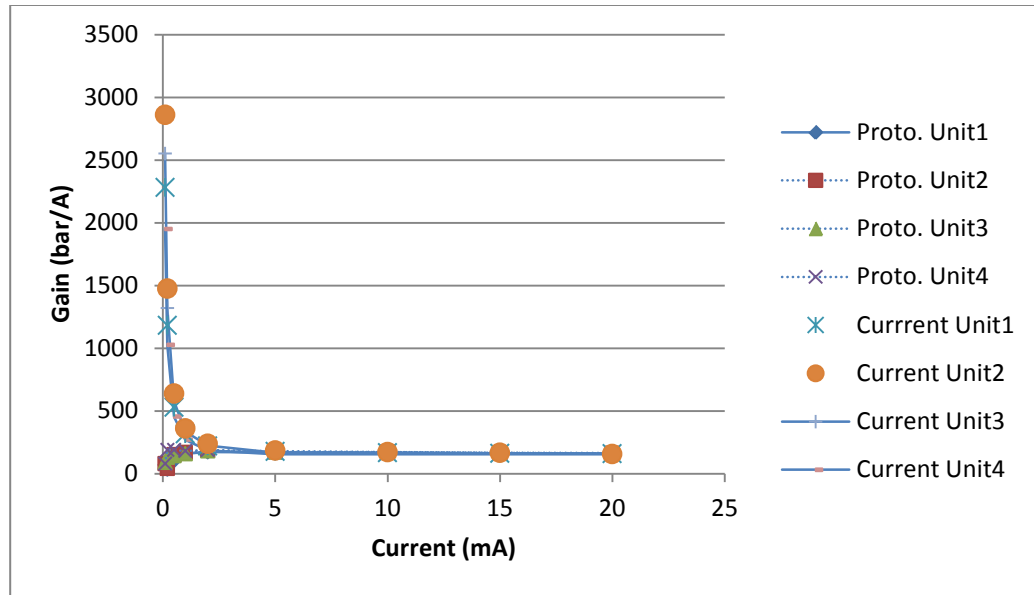


Figure 7-16: Overall gain comparison of Prototype III (balance beam) and original I/P (voice coil) over input current range of 0-20mA.

For a better comparison of the gain at low currents of each I/P converter, a graph with the overall gains starting from 2mA has been plotted. From this graph it can be seen that there is less variation with the new balance beam configuration when compared to the original voice coil I/P converter (the closer together the lines are implies that there is less variation in output pressures from unit to unit).

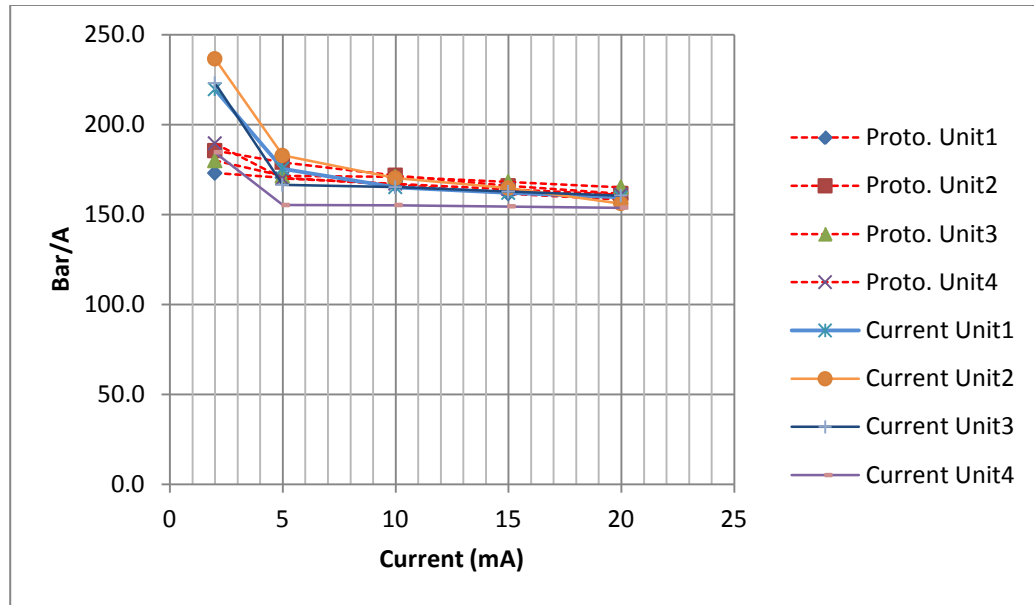


Figure 7-17: Gain comparison of Prototype III and original I/Ps over input current range of 2-20mA.

7.5.2. Temperature variation

The performance of the balance beam with regards to temperature variations has been demonstrated with previous version (prototype II); hence this test has been carried out on two units of Prototype III just to confirm similar performance.

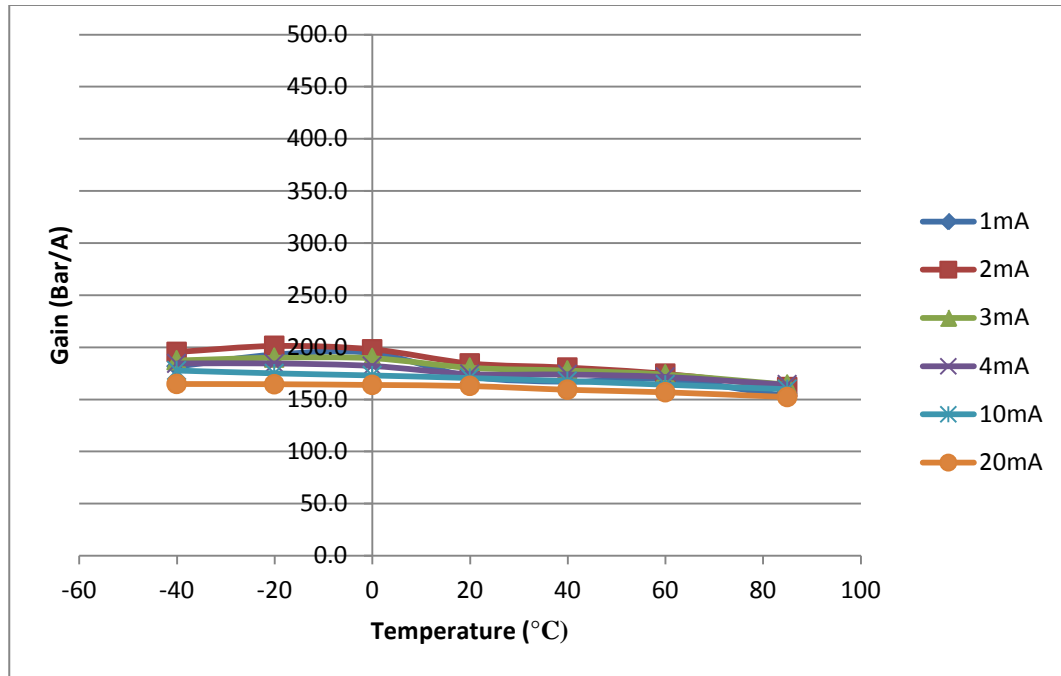


Figure 7-18: Overall gain variation of prototype III - unit1

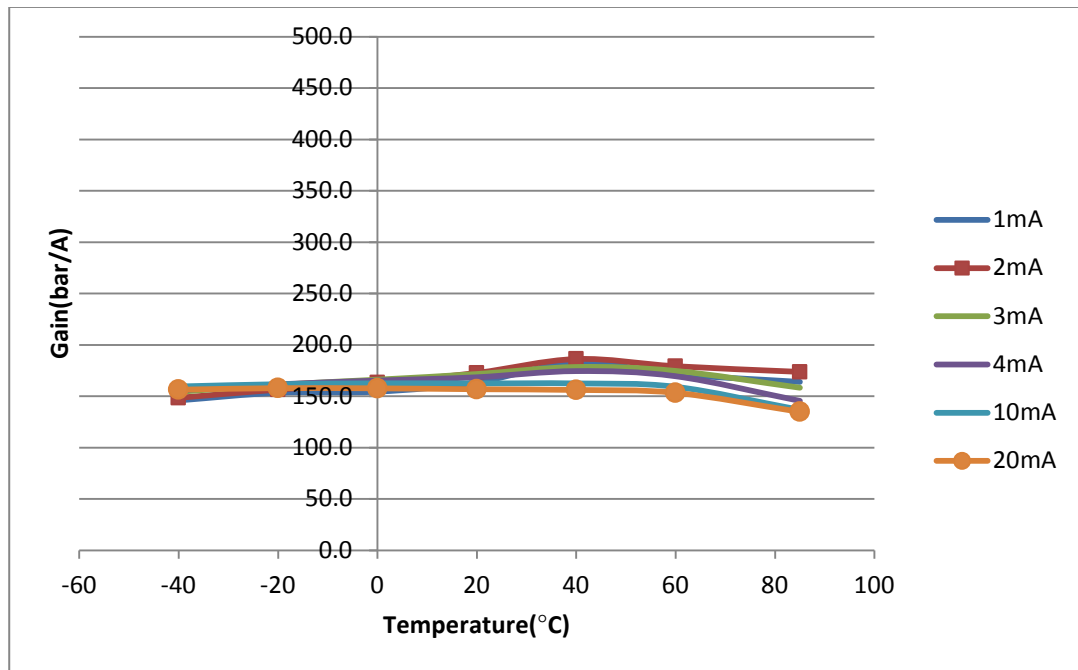


Figure 7-19: Overall gain distribution of prototype III - unit 2

From the above graphs it can be seen that the gain distribution over the full temperature range is considerably reduced, with far less variation than was seen on the voice coil I/Ps (see *graphs in chapter 6: Identification of root causes of unwanted variations*).

7.5.3. Vibration test

Testing was carried to verify how the performance of the balance beam I/P is affected by vibration. The frequency of vibration was made to vary under controlled conditions and the amplitude of oscillation was kept constant at each run.

This test is important as many I/P converters are used in conditions where the vibrations from ancillary components such pipelines, or even from actuating movements such as a valve closing brusquely.

The following figure shows a unit set-up on the vibrating jig.

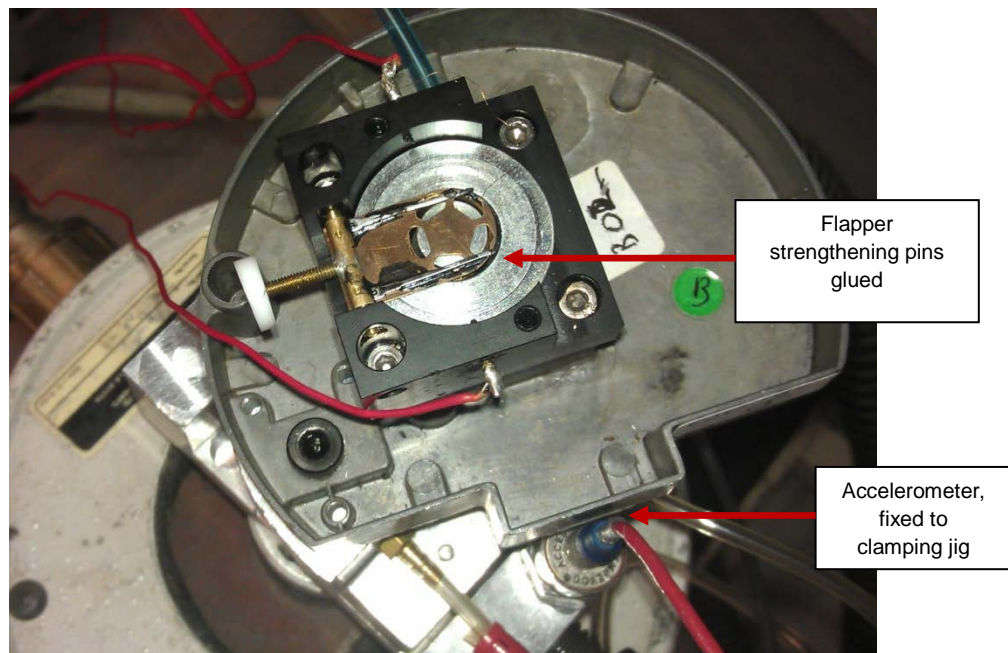


Figure 7-20: Balance Beam Prototype III unit on vibrating jig.

The output pressure was measured and recorded using an oscilloscope.

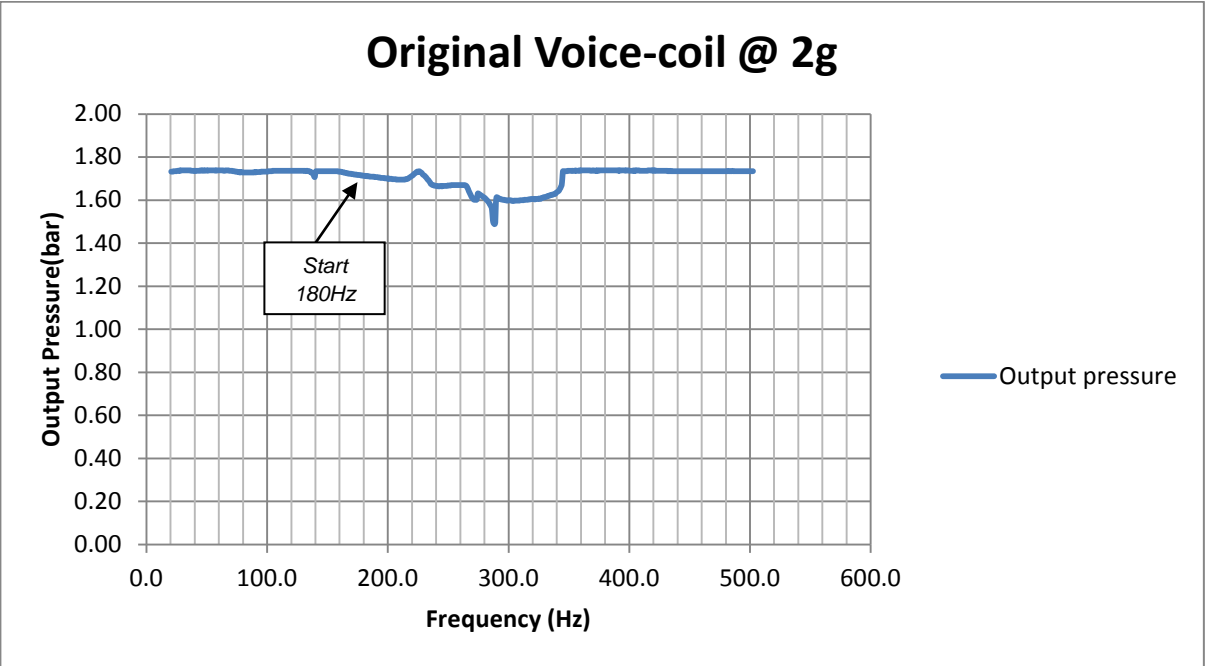


Figure 7-21: Vibration performance of the voice coil I/P converter at 2g acceleration over 20-500Hz range.

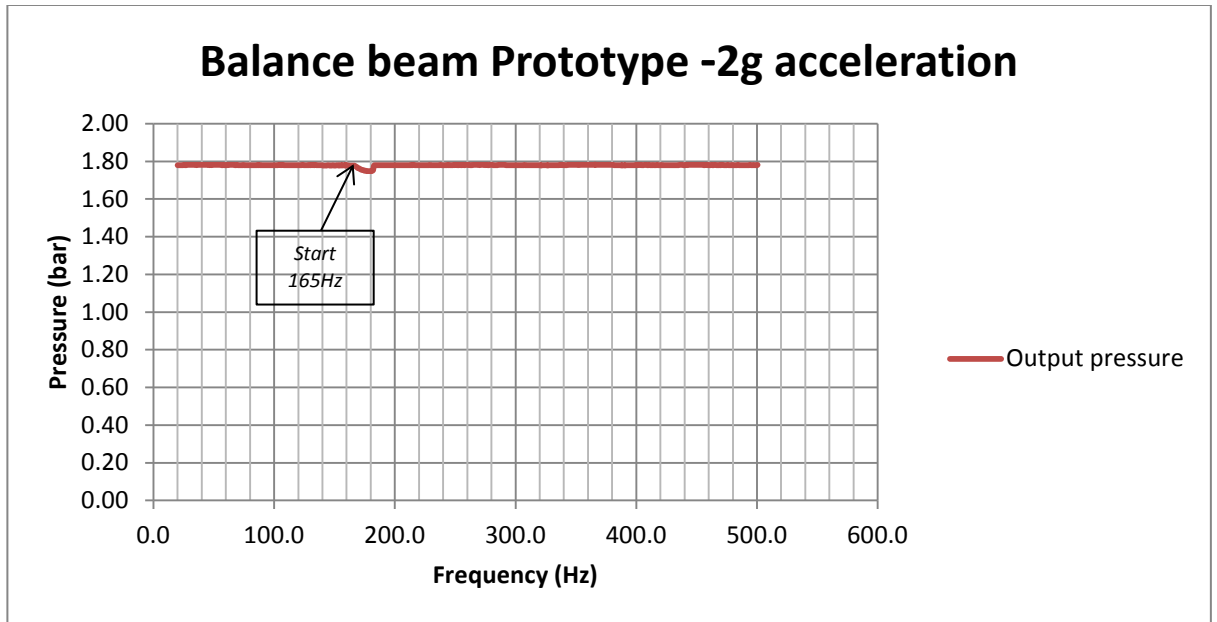


Figure 7-22: Vibration performance of the balance beam I/P converter (prototype III) at 2g acceleration over 20 - 500Hz range.

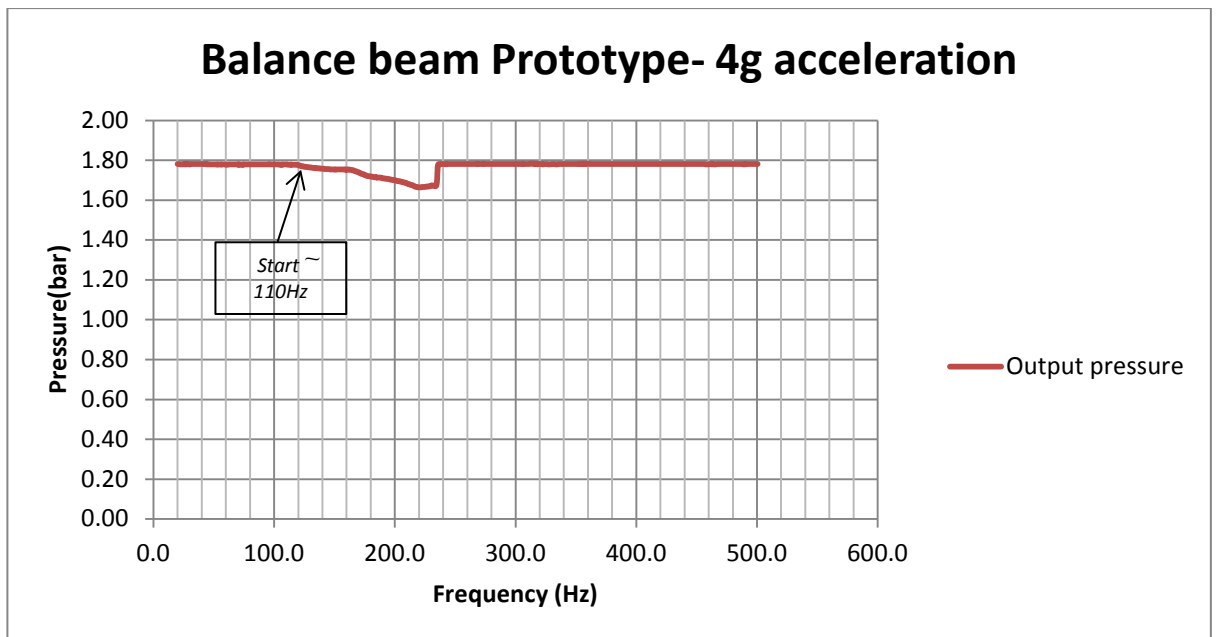


Figure 7-23: Vibration performance of the balance beam I/P converter (prototype III) at 4g acceleration over 20 - 500Hz.

At 2g acceleration: The maximum shift in output pressure seen in the original voice coil unit is around 250mbar and the main drop occurs at a frequency of oscillation at 285Hz. The maximum shift in output pressure seen with the balance beam I/P is around 30mbar with the main drop in pressure occurring at a frequency of oscillation of 180Hz.

At 4g acceleration - the maximum shift in output pressure seen from the balance beam I/P (prototype III) is around 150mbar and this occurs at a frequency of around 220Hz.

Note: The prototype III – balance beam unit which was used for vibration had been modified to be more rigid, as under harsh vibration mode, the thin flapper would flex considerably. This was achieved by adding two rigid pins along the sides of the flapper. Rigidity of the flapper was found essential for good vibration resistance.

7.6. Summary

In this chapter, the potential options which could improve the performance of the I/P converter, based around reducing the magnitude of P_c at zero input signal, were discussed. It was found that the balance beam configuration is a much improved mechanical compensator mechanism which reduces the relationship of the control pressure (P_c) to be dependent only upon the electromagnetic force and the fluid force. An initial sizing of the main components to be used in the balance beam was carried out and Prototype I was built to verify the performance. With Prototype I it was shown that the control pressure (P_c) dropped to 7mbar when the input signal is zero. This is possible as the spring stiffness is nearly zero, and the flapper's mass is balanced by the counterweight.

Prototype II was designed and manufactured to demonstrate the repeatability of performance and also to investigate if temperature changes have an effect on the performance of the I/P converters. Thermal tests were carried out and it was

shown that this design is not as much as affected by temperature as the current voice coil design. However, it was noted that the roller bearings used in Prototype II units were giving poor hysteresis levels (reaching as high as 0.4% of measured span).

Prototype III was designed to mainly address the issues of hysteresis – ball bearings were used in this new generation and it was demonstrated that the hysteresis performances were significantly improved, with the maximum error reaching around 0.1% of measured span.

Finally, tests were carried out on Prototype III units and on original voice coil I/P converters to compare their performance. It was shown that the gains of the balance beam prototypes were much lower than the voice coil I/Ps at low input currents. This showed that the balance beam mechanism is more linear at low current than the original voice coil I/Ps. It was also shown that the performances with regards to temperature variations were similar to Prototype II. A vibration test was carried out on each of the I/P converter configuration and it was found that at 2g acceleration the shift in output pressure from the original voice coil I/P was around 220mbar more than the prototype balance beam I/P converter. However it was found that the major shift in output pressure for the balance beam occurs at a lower frequency (180Hz) than the original I/P converter (which occurs at around 285Hz). This is likely to be due to the different natural frequency of the flapper structure.

7.7. Discussion

Limitations of experimental measurements – The flexure used in the TR140 I/P converter plays a very critical role in controlling the pressure. The stiffness of this component is an important parameter as it dictates the amount of force required to move it up or down, and this affects the output pressure. Measurements carried out in Chapter 4 (Determination of parameters) showed that quite inconsistent readings for the stiffness of the flexure were obtained by using the force gauge; there are a number of explanations for this observed inconsistency: the force gauge used might have backlash in its mechanism; also ensuring that the touch probe was exactly in contact at the centre of the flexure is very difficult and this could have caused inconsistent deformations and finally, although as much care was taken in ensuring that human errors were not introduced in the measurement process, it is possible that some errors were introduced while the gauge was moved. Measurement of the stiffness of the flexure using the USB microscope is a more accurate technique, but due to time limitation, only three measurements were carried out. Both of these measurements required contact with the flexure and it is quite likely that the dynamics would be affected.

Fluidic forces and Computational fluid dynamics- As the flexure moves in relation to the nozzle the discharge coefficient of this aperture is likely to vary with the gap separation. Currently this discharge coefficient has been approximated as **0.6**. The use of CFD to establish the relationship between the discharge coefficient and the nozzle-flexure gap could be made and this information could also be included in the simulation model to improve its accuracy.

Optimisation – The chapter on optimisation presented potential improvements which could be made to the zero current output pressure of the existing TR140 I/P converter by careful analysis of the equation:

$$P_c \approx \left[\frac{k A_{hole} \sqrt{F_{spring}} CD_{hole}}{\sqrt{2} 2\pi^2 r_{eff}^2 r_{nozzle} \sqrt{A_{diaphragm}} CD_{nozzle}} \right]^{\frac{2}{3}}$$

The main practical solutions identified were:

- **Reduction of spring force:** The zero current output pressure is roughly proportional to a one third power of the spring force. Replacing the spring with a less stiff one will affect the start-up pressure and response. Also, this change is unlikely to improve the system thermal stability.
- **Reduction of the flexure stiffness:** This can be achieved by using a thinner flexure or by making the flexure legs longer. However, the side effects of this change are that temperature will still affect the performance; vibration stability will tend to worsen as the suspension provided to the coil is less rigid. The durability of this part could be affected with this change.
- **Reduction of the size of the orifice hole:** Reducing the size of the hole in the orifice disc will improve the output pressure at low current, however the response time will be affected and risk of blockage due to debris will increase.

- **Increase in area of the rubber diaphragm:** An increase of 10 fold is required to give a reduction of around 10 fold in force. Such a change will result in a considerably larger product.
- **Increase in the nozzle diameter:** This will lower the output pressure at zero current and improve linearity, but the pressure per unit current of the unit (gain) will reduce.

It was also shown that the balance beam I/P converter compared to the original converter has improved performance in the following areas:

- Linearity at low current, this is shown by the gain comparison graph (Overall gain comparison of Prototype III (balance beam) and the original I/P over input current range of 0-20mA.)
- Thermal stability, as shown by graphs of overall gain distribution (Figure 7.5, Figure 7.2) comparing these figures with the original I/Ps shown in Chapter 6 (Identification of root causes of unwanted variations). A comparison of the thermal stability at low currents is discussed in the next section.
- It was found that the zero current output pressure of the original I/P converter was around 140mbar whereas on the balance beam unit, this output pressure (from the booster chamber) is around 60mbar. Most of this 60mbar is due to the designed-in pressure difference between control and booster chambers. To offset the 140mbar pressure, a 'reversed' arrangement of spring and rubber diaphragm is normally used in the booster amplifier section of the valve. To provide the offset of 60mbar (when using the balance beam unit) a significantly lower stiffness spring is required. This lower stiffness spring is likely to be less affected by temperature variations than the stronger spring, effectively making the overall valve more stable with temperature changes.

It was found that the bearings play a very important role in the performance of the Balance beam I/P concept. By providing low friction, they ensure that the hysteresis performance is kept low. The proposed type of ball bearings is

shielded thus minimising the risk of dust contaminations – dust contamination could eventually impact on the hysteresis performance. The improved linearity at low current and thermal stability of the Balance beam concept is due to the pivot mechanism - which essentially removes the spring stiffness present in the flexure component (in the original design).

8.CONCLUSION AND RECOMMENDATION

8.1. Conclusion

The governing equation which gives the output pressure of the original I/P converter, combining the essential fluid force, electromagnetic force, elastic force and gravitational force was derived in Chapter 3 (Investigation of operation of TR140 I/P converter).

The non-linear behaviour of the original I/P converter was investigated in Chapter 6 (Identification of root causes of unwanted variations) and an expression which shows the relationship of the components' parameters on the output pressure at zero input current has been derived. This equation also helped in understanding how some of these parameters might change with temperature variations and eventually affect the output pressure particularly at low input currents. In addition, it was shown by Equation 7-2 , that in the original design the mass of the coil and flexure and their arrangement can cause shifts in output pressure when the unit is exposed to vibrations.

The desired output from an ideal I/P converter was determined to be $P_c = \frac{Id}{\pi r_{eff}^2}$; this would ensure a linear relationship between the current signal and the fluid force. A design which would allow this behaviour is the balance beam and it was demonstrated that balancing the beam ensures consistent overall gain, as shown in Figure 7- (Graph of gain with regards to input current for unit with counterweight and without counterweight).Through several experiments carried out, it was shown that the balance beam concept exhibits a more linear behaviour over the full range of input current. It was also shown that the balance beam is more thermally stable than the original I/P converter. The following graphs shows the performance at low currents (with thermal variation) of 3 units of the balance beam I/P converter compared to 3 units of the original I/P converter.

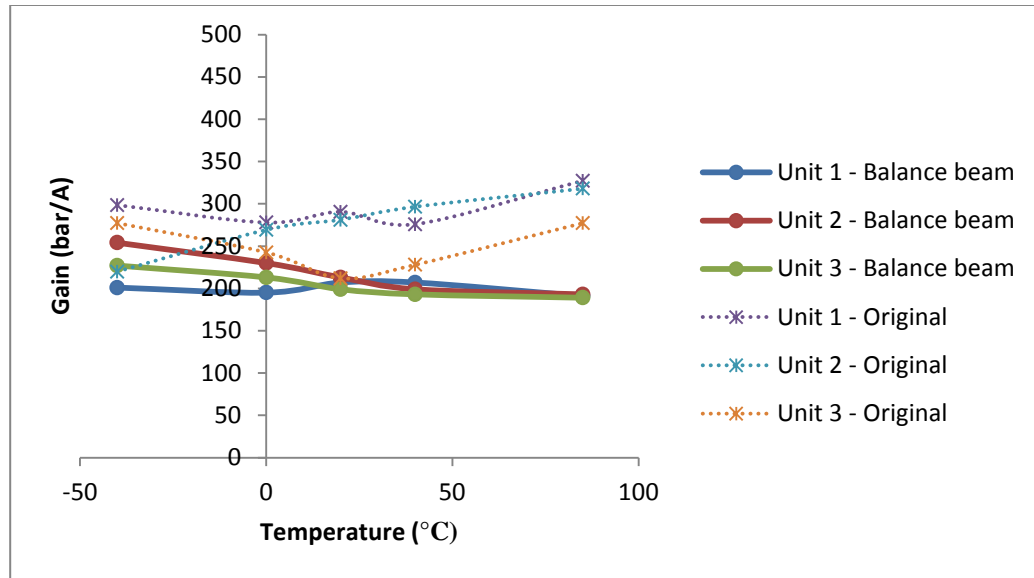


Figure 8.1: Performance comparison of Balance beam units and Original units at 1mA input current with temperature variation

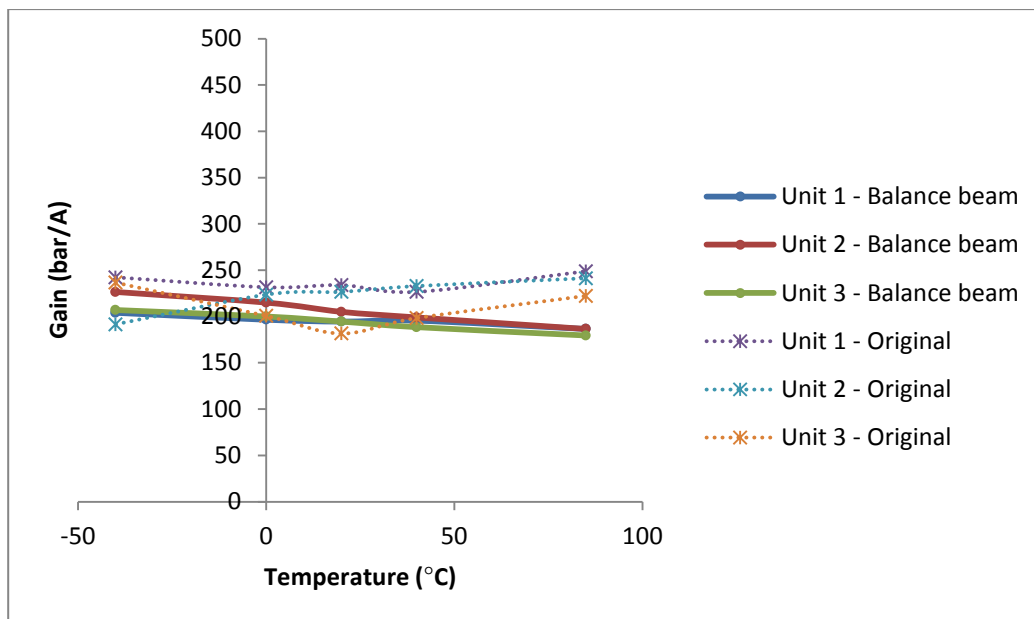


Figure 8.2: Performance comparison of Balance beam units and Original units at 2mA input current with temperature variation

It can be seen from Figure 8.1, that the performance of the original I/P converter suffers from unpredictable variation and the magnitude of which is more than which is seen on the balance beam I/P converters.

A measure of the percentage shift at 1mA and 2mA for both I/P converters as a measure of the measured span (based on normalised gain at 20mA) was carried out and the results are shown in the following table.

	Balance Beam I/P converters			Original I/P converters		
	Unit1	Unit2	Unit3	Unit1	Unit2	Unit3
Normalised gain at 20mA	159	166	157	165	162	164
% shift at 1mA	1.5%	2.7%	2.2%	4.9%	4.8%	3.0%
% shift at 2mA	1.4%	1.8%	1.6%	2.6%	2.5%	2.2%

Table 8-1 : % shift of measured span at 1mA and 2mA input current for both balance beam units and original units

From the above table it can be seen that at 1mA input current the Original I/P converters suffers from more variation with the worst performance of 4.9% whereas the worst performance observed on the Balance beam batch is 2.7%. However at 2mA input current the Original I/P performances are improved but still unmatched to the Balance beam I/Ps.

8.2. Recommendations for further work

Measurement of the flexure displacement in dynamic conditions could provide with useful information of the nozzle-flexure gap. This information could then be used to further validate the simulation model.

From the optimisation section it was found that the balance beam I/P converters tend to have slightly higher gain at low current (<2mA). An experiment was carried out on Prototype III to investigate the gain variation with gap distance from nozzle and flapper. A thin wire of negligible mass was fixed onto the flapper and a USB microscope was made to focus on the thin wire.

Experiment data are as follow and Table 8-2 shows the readings obtained:

Supply pressure: 5.00 bar gauge

Magnification: 316.7x

Estimated screen accuracy: $\pm 2\text{mm}$

Equivalent measurement accuracy: $\pm 6\mu\text{m}$

I/mA	x/ μm	P/ bar g	Gain (bar g/A)
20	28	3.16	158
10	32	1.68	168
5	47	0.84	168
4	51	0.74	185
2	66	0.57	285

Table 8-2: Flapper-Nozzle gap measurement in dynamic condition

The following graphs show the relationship of the gap distance with current variation and of gain with current variation respectively, error bars of $\pm 6\mu\text{m}$ have been estimated on the gap-current graph.

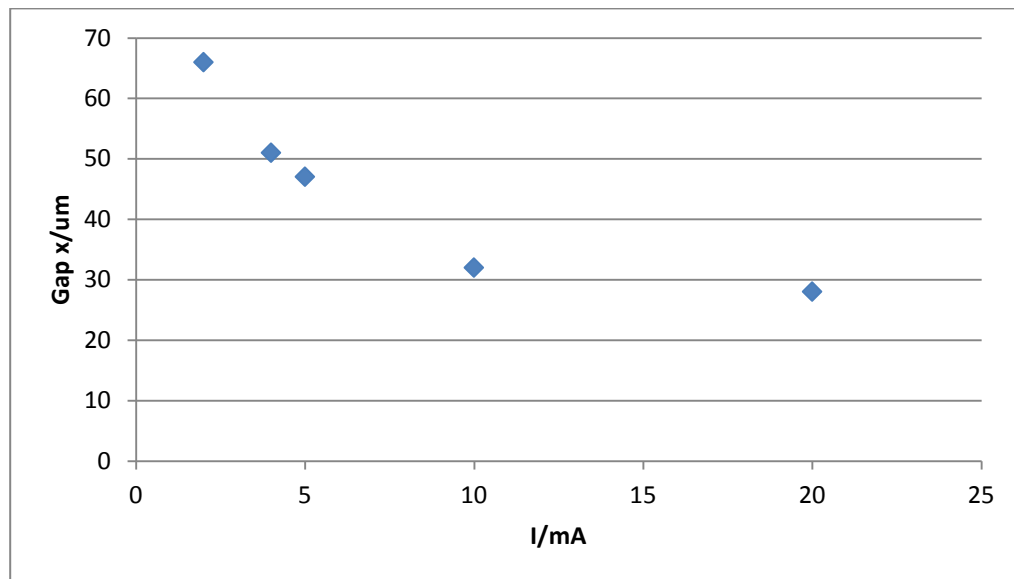


Figure 8.3: Flapper-nozzle gap variations with current

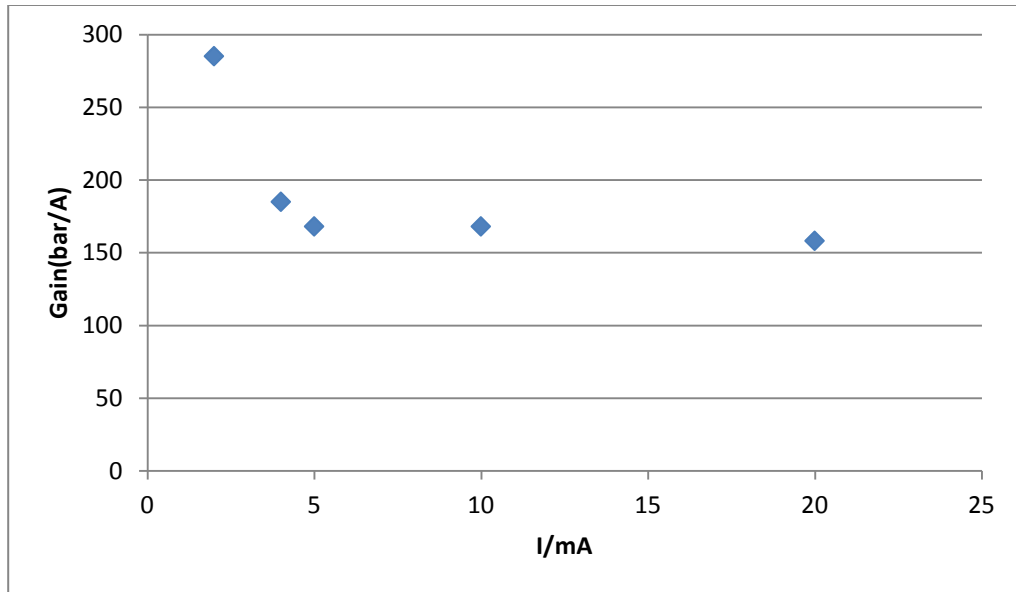


Figure 8.4: Deduced gain variation with input current

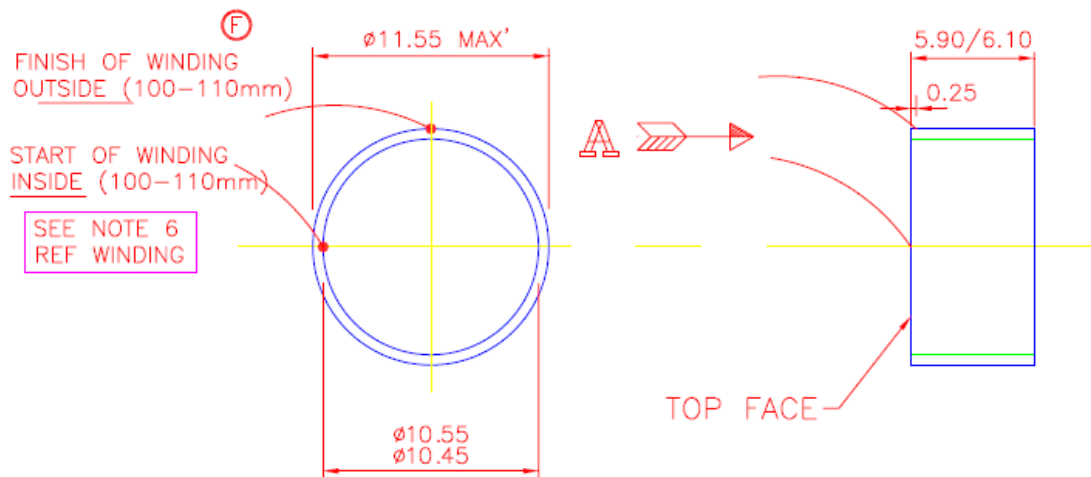
From the two graphs it can be seen that there is a similitude in characteristics of the gain and the gap variation, i.e. as the gap increases the gain also increases and this particular behaviour occurs at low current. This suggests that a higher pressure than expected is needed at wide gaps to balance against the electromagnetic force. A more detailed CFD analysis can be carried out to further investigate this behavior, especially how the air flow rate past the flapper-nozzle gap affects this behaviour.

In addition to the above investigation, the use of CFD in design optimisation of the flapper and/ or the nozzle could help in better understanding the effect of the shape and structure of these two components on the overall performance of the I/P converter.


To improve the understanding of heat transfer and its effect on components present in the I/P converters, a study by means of CFD could be carried out. Such a study should allow a better approximation of the overall heat transfer coefficients (used in the modelling and simulation section); especially when heat is transferred between fluid and solid bodies.

Appendix I – Coil drawing

DO NOT SCALE DRAWING. IF IN DOUBT ASK.



MANUFACTURING NOTES :

1. WIRE SPECIFICATION : $\phi 0.05$ mm NOMINAL CONDUCTOR.
SOLDERABLE SELF-BOND TO IEC 317 – 36, GRADE 1B (GREEN)
TEMP' INDEX 20,000 HOURS TO IEC 172, @ 181°C
MIN' RESOFTENING TEMPERATURE 170°C
2. NUMBER OF TURNS : 650 – 710.
3. NUMBER OF LAYERS: NOMINALLY 6
4. COIL RESISTANCE/INDUCTANCE : 200 – 250 Ω
4.50 – 5.50mH in air.
5. MAXIMUM L/R RATIO OF 27.5 μ H/ Ω TO BE TESTED BY
MAXIMUM Q FACTOR OF 0.17 AT 1 kHz.
6. LEADS TO SUIT TERMINATION ARRANGEMENT + POLARITY LENGTH + POSTION.
ANTI – CLOCKWISE WIND FROM DIRECTION 

Appendix II – Initial Matlab simulation model

```
clear
hold off
%constants/estimated parameters
pi=3.1415926535;
%initial gap of ball valve(m)
a0=1e-6;
%initial gap of diaphragm to nozzle
x20=10e-6;
%stiffness of Flexure N/m
k=550;
%effective radius of nozzle(m)
rp=0.5e-3;
%force from solenoid per unit current (N/A)
d=12.;
%effective circumference of ball opening (m)
a=6.13e-3;
%movement of diaphragm per unit pressure (m/Pa)
b=3.5e-7;
%area of hole in diaphragm
Ah=pi*(.0005*.0005)/4;
%initial values
%supply
Ps=3e5+1.e5; %3bar gauge pressure
Pb=1e5;
Pc=1e5;
%atmospheric pressure, temperatures, densities
P0=1e5;
Ts=293;
Tb=293;
Tc=293;
rhos=Ps/(287*Ts);
rhob=Pb/(287*Tb);
rhoc=Pc/(287*Tc);
%volumes :1cc for booster, 1/4cc for control
Vb=3.74e-7;
Vc=4.0e-8;
%initialise x2- gap from flexure to nozzle
x2=x20;
%gas constant
R=287;
gamma=1.40;
%initial flow rate out (drawn from device)
Mdot=0.
%initial control current
ic=0e-3;
%time stepping:
dt=0.2e-5;
t=0
```

```

%number of time steps
nmax=400000
%plotting controls: store and later plot once every 'nout'
nout=500;
%initialise arrays
PbmPc(nmax/nout+1)=0;
Pbarr(nmax/nout+1)=0;
Pcarr(nmax/nout+1)=0;
tarr(nmax/nout+1)=0;
%opening of pipe-diaphragm
x2arr(nmax/nout+1)=0;
%opening of ball valve
xarr(nmax/nout+1)=0;
for i=1:nmax
    t=t+dt;
    %set changes with time
    icchange=1;%1 for on (i.e. do changes in current), 0 for off
    if (icchange==1)
        if (t>0.1)
            ic=1e-3;
        end
        if (t>0.2)
            ic=2e-3;
        end
        if(t>0.3)
            ic=3e-3;
        end
    end

    imChange=1;%1 for allow changes to mass dtawn from device, 0 for
don't change
    if (imChange==1)
        if (t>.5)
            Mdot=2e-6;
        end
        if(t>.6)
            %would drop at 4e-6 unless supply pressure increases or
inlet
            %ball larger
            %Extreme Test - ramp mass flow rate output
            %Mdot=2e-6+(t-0.6)*20e-6;
        end
    end

    %supply to booster flow
    %first the ball valve opening
    x=b*(Pc-Pb)+a0; % slight offset built in to avoid locking when
Pc=Pb at startup can't be negative
    if (x<0)
        x=0;
    end
    if (x > 0.005)
        x=0.005;
    end
    %*****

```

```

%density of supply
rhos=Ps/(R*Ts);

Area=a*x;
Pu=Ps;
Pd=Pb;
Tu=Ts;
Cd=0.6;%approx worth an investigate
dirn=+1;
diff=Ps-Pb;
if (diff<0)
    Pu=Pb;
    Pd=Ps;
    Tu=Tb;
    dirn=-1;
end
%critical condition
crit = 0;

if((Pd/Pu) <= 0.528)
    crit =1;
end

if(crit ==0)

    z1=Cd*Area*Pu/sqrt(R*Tu);
    z2=(Pd/Pu)^(1.0/gamma);
    z3=((2*gamma)/(gamma-1.0))*(1-(Pd/Pu)^((gamma-1)/gamma))^0.5;

    mdot= z1*z2*z3;
else
    z1=Cd*Area*Pu/sqrt(R*Tu);
    z2=gamma^0.5;
    z3=(2/(gamma+1))^((gamma+1)/(2*(gamma-1)));
    mdot=z1*z2*z3;
end

%*****

%and get mass flow rate from supply to booster (v1)
v1=dirn*mdot;
%and again for booster-control flow
dirn=+1;
dP=Pb-Pc;
if (dP<0)
    dP=-dP;
    dirn=-1;
end
%again get density
rhob=Pb/(R*Tb);
%and mass flow from booster to control (v2)
v2=dirn*sqrt(2*(dP)/rhob)*Ah*rhob;

```

```

    %update Pc
    %assumed dif eq for x2 to iterate to equilibrium
    % assumed viscous motion constant
    visc=1e-1;
    dx2=dt*((Pc-P0)*pi*rp^2-d*ic-k*(x2-x20))/visc;
    x2=x2+dx2;

    %can't be less than zero seperation:
    if (x2<0)
        x2=0;
    end

    %flow from control past diaphragm
    dirn=+1;
    dP=Pc-P0;
    if (dP<0)
        dP=-dP;
        dirn=-1;
    end
    %flow past diaphragm
    rhoc=Pc/(R*Tc);
    v3=dirn*sqrt(2*(dP)/rhoc)*(2*pi*rp*x2)*rhoc;

    %time step for new pressure in booster, Pb
    dPb=(R*Tb/Vb)*(v1-Mdot-v2);
    Pb=Pb+dPb*dt;
    %time step for pressure in control (Pc)
    dPc=(R*Tc/Vc)*(v2-v3);
    Pc=Pc+dPc*dt;
    %store various values in array

end % end of time stepping loop
legend on
plot (tarr,Pbarr,'-b');
hold on
plot(tarr,Pcarr,'-r')
xlabel('Time(s)');
ylabel('Pressure(Pa)');
legend(['Booster pressure (absolute)','Control Pressure (absolute)'],...
    'Location','SouthEast');
grid on
pause
hold off
plot (tarr,x2arr)
xlabel('Time(s)');
ylabel('Nozzle-Flexure opening (m)');
pause
plot(tarr, xarr)
xlabel('Time (s)');
ylabel('ball valve opening (m)');
pause
plot(tarr, PbmPc)
xlabel('Time (s)');
ylabel('Pb - Pc (Pa)');

```

Appendix III – Heat transfer by conduction

Component	Heat transfer equation
Booster chamber volume	$\left. \frac{dT_b}{dt} \right _{HT} = \frac{1}{M_b C_{air}} [H_{bb1} AREA_{bb1} (T_{b1} - T_b) + H_{bc} AREA_{bc} (T_c - T_b) + H_{bc1} AREA_{bc1} (T_{c1} - T_b)]$
Booster chamber body	$\left. \frac{dT_{b1}}{dt} \right _{HT} = \frac{1}{M_{b1} C_{b1}} [H_{ab1} AREA_{ab1} (T_a - T_{b1}) + H_{bb1} AREA_{bb1} (T_b - T_{b1}) + H_{c1b1} AREA_{c1b1} (T_{c1} - T_{b1})]$
Control chamber volume	$\left. \frac{dT_c}{dt} \right _{HT} = \frac{1}{M_c C_{air}} [H_{bc} AREA_{bc} (T_b - T_c) + H_{cc1} AREA_{cc1} (T_{c1} - T_c) + H_{ce} AREA_{ce} (T_e - T_c)]$
Control chamber body	$\left. \frac{dT_{c1}}{dt} \right _{HT} = \frac{1}{M_{c1} C_{c1}} [H_{ac1} AREA_{ac1} (T_a - T_{c1}) + H_{bc1} AREA_{cc1} (T_b - T_{c1}) + H_{c1d} AREA_{c1d} (T_d - T_{c1}) + H_{cc1} AREA_{cc1} (T_c - T_{c1}) + H_{c1b1} AREA_{c1b1} (T_{b1} - T_{c1})]$
Magnet	$\left. \frac{dT_d}{dt} \right _{HT} = \frac{1}{M_d C_d} [H_{ad} AREA_{ad} (T_a - T_d) + H_{c1d} AREA_{c1d} (T_{c1} - T_d) + H_{de} AREA_{de} (T_e - T_d)]$
Nozzle	$\left. \frac{dT_e}{dt} \right _{HT} = \frac{1}{M_e C_e} [H_{ce} AREA_{ce} (T_c - T_e) + H_{ae} AREA_{ae} (T_a - T_e) + H_{de} AREA_{de} (T_d - T_e)]$
Flexure	$\left. \frac{dT_f}{dt} \right _{HT} = \frac{1}{M_f C_f} [H_{af} AREA_{af} (T_a - T_f)]$

REFERENCES

- [1] Carey, D.C., "Electric-To-Pressure converters", *U.S. Patent 5,906,218*, May 25, 1999
- [2] Carey, D.C, Product Training, *Watson Smith internal document*, 2005
- [3] Timings, R.L., "Chapter 5 - Power Transmission". *Newnes Mechanical Engineer's Pocket Book*, Third Edition. Newnes. 2006. Books24x7.
<http://common.books24x7.com.ezproxy.imeche.org/toc.as19px?bookid=17889> (accessed April 5, 2013)
- [4] Parr, A., Table 1.1, *Hydraulics & Pneumatics*, 2nd edition B/Heinemann,.
- [5] Driskell, Control-Valve Selection and Sizing, ISA, 1983.
Process/Industrial Instruments and Controls Handbook, 5th ed., McGraw-Hill, 1999.
- [6] Perry, R. H., and Don W.G. (eds). "Section 8 - Process Control". *Perry's Chemical Engineers' Handbook*, 8th Edition. McGraw-Hill Engineering. 2008.
<http://common.books24x7.com.ezproxy.imeche.org/toc.aspx?bookid=15238> (accessed April 4, 2013)
- [7] Bode, H.W., "Feedback – The history of an Idea," in *Selected Papers on Mathematical Trends in Control Theory*, Dover, New York, 1964, pp.106 - 123
- [8] Black, H.S., "Inventing the Negative Feedback Amplifier," *IEEE Spectrum*, December 1977, pp.55, 60
- [9] Brittain, J.E., Turning Points in American Electrical History, *IEEE Press*, New York, 1977.
- [10] Fagen, M.D., A History of Engineering and Science in the Bell System, Bell Telephone Laboratories, *The Laboratories*, New York, 1975
- [11] Newton, G, Gould, L., and Kaise, J., *Analytical Design of Linear Feedback Control*, John Wiley & Sons, New York, 1957.
- [12] Bode, H. W., "Feedback—The History of an Idea," in *Selected Papers on Mathematical Trends in Control Theory*, Dover, New York, 1964, pp. 106–123.

-
- [13] Huber, J.E., Fleck, N.A. and Ashby, M.F., The selection of mechanical actuators based on performance indices, *Department of Engineering, Cambridge University. Proc. R. Soc. Lond. A* (1997)
 - [14] Jiang, Y., Valdiero, A.C., Andrighetto, P.L., Chong, W., Bortolaia, L., A., Analysis of Pneumatic Directional Proportional Valve with CFX Mesh Motion Technique. *ABCM Symposium Series in Mechatronics – Vol.3* – pp.510-518, 2008
 - [15] Edge, K. A. The control of fluid power systems – responding to the challenge. *Proc. Instn Mech. Engrs, Part I, Journal of Systems and Control Engineering*, 211 (12), 91-110, 1997
 - [16] Barrett, R. Active Plate and wing research using EDAP elements. *Smart Material Structures*. 1, 214 – 226, 1992
 - [17] Crawley, E.F. & De Luis, J, Use of piezoelectric actuators as elements of intelligent structures. *AIAA JI25*, 1373 – 1385, 1987
 - [18] McMillan, G. K., and Douglas M. C. (eds). "Section 9 - VALVES, SERVOS, MOTORS, AND ROBOTS". *Process/Industrial Instruments and Controls Handbook*, 5th Edition. McGraw-Hill Engineering. <http://common.books24x7.com.ezproxy.imeche.org/toc.aspx?bookid=15253> (accessed July 29, 2013)
 - [19] Sharif, M.A., Grosvenor, R.I., Sensor-based performance monitoring of a control valve unit, *Proc. Instn. Mech. Engrs, Part E, Journal of Process Mechanical Engineering* 213:71, 1999
 - [20] Sanecharaun, T., Thompson, D., Robertson, M., Olley, P., Day, A., *Modelling and Experimental Investigation of a Current-to-Pressure Converter*. UKACC Int. Conf. On Control, 574-578, 2012
 - [21] Linsley, D., Power-Plant control and instrumentation – the control of boilers and HRSG systems, *The institution of Electrical Engineers*, London, pg168 ,2005
 - [22] Auer, L., *Current-to-Pressure Transducers for Control-Valve Actuation*, Rosemount Inc., Eden Prairie
 - [23] Choi, S.B., Yoo, J.K., Pressure control of a pneumatic valve system using a piezoceramic flapper, *Proc. Instn. Mech. Engrs., Part C: Journal of Mechanical Engineering Science*, 218:83, 2004

-
- [24] Motoshige Ikehata, Katsuhiko Odajima, "Electropneumatic transducer", U.S. Patent 4 898 200A, Feb 6, 1990.
- [25] Frick, R.I. "Current to pressure converter apparatus", U.S. Patent 4 325 399, Apr.20, 1982
- [26] Gunther Roth, "Electro-pneumatic converter", U.S. Patent 4 595 029A, Jun.17, 1986
- [27] Stratton, Julius Adam, *Electromagnetic Theory*, Wiley-IEEE Press, 2007
- [28] George T. –C. Chiu, R.H. Bishop, Mechatronics Systems, Sensors, and Actuators, *Electromechanical Actuators*, 21-3:5, 2008
- [29] Kaplan, Steven M., *Permanent Magnet*, Wiley Electrical and Electronics Engineering dictionary, IEEE Press, John Wiley & Sons, pg564, 2004
- [30] Trevor Linsley, *Chapter 1- Health and Safety and Electrical Principles*, Advanced Electrical Installation Work, Fourth Edition, Taylor and Francis, 2006
- [31] Brauer, John R., *Magnetic Actuators and Sensors*, 'Chapter 5 – Permanent magnets' IEEE Wiley Interscience, John Wiley & Sons publication, pg64, 2006
- [32] Michael J. Barber and editors of the Trade & Technical Press Limited, *Handbook of Power Cylinders, Valves and Controls*, 1st Edition, pg165, 1986
- [33] Willoughby, David A., R. Dodge Woodson, Rick Sutherland. "Chap.3 – Fluid Flow", Plastic Piping Handbook. McGraw-Hill Engineering, 2002
- [34] Massey, B.S, *Mechanics of Fluids*, 8th Edition, revised by John Ward-Smith, pg162, 2006
- [35] Welty,J.R., Wicks, C.E, and Wilson R.E., *Fundamentals of Momentum, Heat, and Mass Transfer*, 3rd ed., John Wiley & Sons, New York,NY, 1984.
- [36] CRC Handbook, 85th Edition, 6-201
- [37] D.J Tritton , *Equations of motion*, Physical Fluid Dynamics 2nd edit, Oxford Science Publications, pg68, 1988

-
- [38] Douglas, J.F., Matthews, R.D., Bernouilli's for compressible flow, *Solving problems in Fluid Mechanics vol.2*, 3rd edition, pg72-85, 1996
 - [39] Bhaskaran, R., Collins, L., *Introduction to CFD basics*, pg15, Jan.2003
 - [40] Hardisty, H., Can, M., An experimental investigation into the effect of changes in the geometry of a slot nozzle on the heat transfer characteristics of an impinging air jet, *Proc. Inst. Mech. Engrs. Part C Journal of Mech. Engineering Science*, 1983
 - [41] Colter, L. Hollingshead, Discharge coefficient performance of Venturi standard concentric orifice plate, V-cone, and Wedge flow meters at small Reynolds numbers. *All Graduate Theses and Dissertation. Paper 869*, 2011
 - [42] Cohen, I. M., and Pijush, K.K. "Chapter 1 - Introduction". *Fluid Mechanics, Fourth Edition*. Elsevier Science and Technology Books, Inc.. <http://common.books24x7.com.ezproxy.imeche.org/toc.aspx?bookid=28260> (accessed August 4, 2013)
 - [43] Kraus, A.D., Chap.1 Basic concepts- Heat transfer fundamental, John Wiley & Sons, 2003
 - [44] Long, C. A., *Essential Heat Transfer*, pg34, 1999
 - [45] MIT lecture notes, Introduction to Engineering Heat Transfer – Part 3
 - [46] Kielkowski, R.M., *SPICE: Practical Device Modeling*, McGraw-Hill, 1995
 - [47] Leong, S.K., *Extracting MOSFET RF SPICE models*, <http://www.polyfet.com/MTT98.pdf> (accessed July 20, 2013)
 - [48] The Mosis Service, <http://www.mosis.edu>(accessed July 20, 2013)
 - [49] Hazem I., Ali, S.B.B. Mohd., Noor, S.M., Bashi, M.H., Marhaban, *Mathematical and intelligent modelling of electropneumatic servo actuator systems*, Australian Journal of Basic and Applied Sciences, 3(4): 3662 – 3670, 2009
 - [50] Mark, K. and Nariman,S. QFT synthesis of a position controller for a pneumatic actuator in the presence f worst-case persistent disturbances, *Proc. Of the Americal Control Conference*, 3158-3163, 2006
 - [51] Bergada, J.M., Watton, J., A direct solution for flow rate and force along a cone seated poppet valve for laminar flow conditions. *Proc. Of Inst.*

- [52] Brun, X., Belgharbi, M., Sesmat, S., Thomasset, D., Scavarda, S., Control of an electropneumatic actuator: comparison between some linear and non-linear control laws, *Proc. Of Inst. Mech. Engrs, Part I: Journal of System and Control Engineering*, 213:387, 1999
- [53] Sorli, M., Gastaldi, L., Codina, E., de las Heras, S., Dynamic analysis of pneumatic actuators, *Simulation Practice and Theory* 7, 589 – 602, 1999
- [54] Burrows, C.R., Peckham, R.G., Dynamic characteristics of a pneumatic flapper valve, *Proc. Of Inst. Mech. Engrs, Part C: Journal of Mechanical Engineering Science* 19: 113, 1977
- [55] IMI Watson Smith - Norgren CAD document – TR140 pilot cross section view
- [56] Norton, R. L.. "Chapter 8 - Dynamics of CAM Systems-Modeling Fundamentals". *Cam Design and Manufacturing Handbook*. Industrial Press. 2002.
http://common.books24x7.com/book/id_9014/book.asp (accessed April 26, 2012)
- [57] Tritton, D.J., Physical Fluid Dynamics, 2nd Edition, Oxford Science Publications, Pg34, 1988
- [58] Soni, P.R.. "Chapter 12 - Applications". Mechanical Alloying: Fundamentals and Applications. *Cambridge International Science Publishing Ltd*. 2001. Books24x7.
<http://common.books24x7.com.ezproxy.imeche.org/toc.aspx?bookid=14854> (accessed February 25, 2013)
- [59] <http://www.magnetsales.co.uk/sintered-neodymium-iron-boron-magnets.htm> (accessed February 25, 2013)
- [60] IMI Watson Smith – Norgren presentation of Pilot operation
- [61] Perry, R. H., and Don W. G. "Section 6 - Fluid and Particle Dynamics". *Perry's Chemical Engineers' Handbook*, Eighth Edition. McGraw-Hill Engineering. 2008. Books24x7.

-
- <http://common.books24x7.com.ezproxy.imeche.org/toc.aspx?bookid=15238> (accessed February 23, 2013)
- [62] Heywood B. J., Internal Combustion Engine Fundamentals, P226-227, McGraw Hill
- [63] Values of Overall coefficient of heat transfer obtained from Dr. Pete Olley
- [64] Olley, P. , *Investigation of pressure variation at zero current*, internal document, 2012
- [65] <http://www.spring-makers-resource.net/helical-springs.html>
- [66] MatWeb Material Property Data
<http://www.matweb.com/search/datasheet.aspx?matguid=bbe220809bb144eb9c2f3672da24ccda&ckck=1> (accessed on 5th September, 2012)
- [67] Ashby, M.F. 2003, *Materials Selection In Mechanical Design*. 2nd Edition Butterworth Heinemann.4, 59.
- [68]
http://www.roymech.co.uk/Useful_Tables/Tribology/Bearing%20Friction.html
(accessed on 7th September, 2012)
- [69] <http://www.tribology-abc.com/abc/cof.htm> (accessed on 7th September, 2012)